THESIS FOR THE DEGREE OF DOCTOR OF PHILOSOPHY

Observations of Artificial Radio Sources within the Framework of Geodetic Very Long Baseline Interferometry

GRZEGORZ KLOPOTEK

CHALMERS
UNIVERSITY OF TECHNOLOGY

Department of Space, Earth and Environment
Onsala Space Observatory Division
Chalmers University of Technology

Gothenburg, Sweden 2020

Observations of Artificial Radio Sources within the Framework of Geodetic Very Long Baseline Interferometry
GRZEGORZ KLOPOTEK
ISBN 978-91-7905-275-1

Doktorsavhandlingar vid Chalmers tekniska högskola
Ny serie nr 4742
ISSN 0346-718X

Department of Space, Earth and Environment
Onsala Space Observatory Division
Chalmers University of Technology
SE-412 96 Gothenburg, Sweden
Telephone: +46 (0)31-772 10 00

Cover image:
Natural and artificial radio sources observed with geodetic very long baseline interferometry.
Image credits: Grzegorz Klopotek

Printed by Chalmers Reproservice
Chalmers University of Technology
Gothenburg, Sweden 2020

Observations of Artificial Radio Sources within the Framework of Geodetic Very Long Baseline Interferometry

GRZEGORZ KLOPOTEK
Department of Space, Earth and Environment
Chalmers University of Technology

Abstract

Very long baseline interferometry (VLBI) is a mature and fascinating technique with unique and indisputable applications in radio astronomy, planetary sciences, and space geodesy. The latter discipline is a field of science facilitating our understanding of various global-scale phenomena connected to Earth dynamics. Space geodesy provides, in the microwave regime, accurate and long-term stable celestial and terrestrial reference frames, to which those environmental changes can be properly referenced and their spatio-temporal variability can be subsequently accurately investigated. In order to attain better knowledge on complex, and yet subtle, geodynamical phenomena of scientific and economic importance, there is a need for an improved global geodetic infrastructure and enhanced quality of space-geodetic measurements. The common effort of the geodetic community known as the Global Geodetic Observing System (GGOS) shall address that need and provide the highest possible accuracy of geodetic products and reference frames as well as the high consistency across space-geodetic techniques. The ambitious goals of GGOS necessitate appropriate changes to be made also in the area of geodetic/astrometric VLBI, realized at preset in the form of the VLBI Global Observing System (VGOS), a next-generation system aiming to meet the requirements of GGOS and deliver geodetic products with an unprecedented quality. In order to make VGOS succeed, the key components of this complex system need to be refined, including also new observing concepts and scheduling strategies, in order to fully exploit the enhanced performance that this system can bring. Thanks to its characteristics, VGOS creates also a great opportunity for extending the current VLBI research with new applications, for the benefit of the scientific community and society at large.

The subject of this thesis concerns observations of artificial radio sources within the framework of geodetic VLBI, in connection to both the current VLBI system and VGOS. This includes information on the combination of observations of natural radio sources and satellite/lunar objects as well as benefits and challenges related to the observing strategy and the technical feasibility of the presented concept. The thesis is based mostly on extensive simulation studies concerning objects on the Moon and geodetic Earth-orbiting satellites, but it also includes an analysis of VLBI observations of the lunar lander performed during dedicated experiments and with a global network of radio telescopes. The information content of this thesis may be treated as a further step towards global observations of artificial radio sources with VLBI in the VGOS era and stimulate new observing concepts for space geodesy.

Keywords: space geodesy, geodetic VLBI, VGOS, Monte-Carlo simulations, *c5++*

Obserwacje Sztucznych Radioźródeł w Ramach Geodezyjnej Interferometrii Wielkobazowej

GRZEGORZ KŁOPOTEK
Department of Space, Earth and Environment
Chalmers University of Technology

Streszczenie

Interferometria wielkobazowa (VLBI) to dojrzała i fascynująca technika o unikalnych i niezaprzeczalnych zastosowaniach w radioastronomii, naukach planetarnych oraz geodezji kosmicznej. Ta ostania dyscyplina to nauka ułatwiająca nasze pojmowanie różnych zjawisk o zasięgu globalnym związanych z dynamiką Ziemi. Geodezja kosmiczna zapewnia także, w zakresie częstotliwości radiowych, dokładny i stabilny, w perspektywie długoterminowej, niebieski oraz ziemski układ odniesienia, dzięki którym owe zmiany środowiskowe mogą być w sposób poprawny odniesione a następnie ich zmienność przestrzenno-czasowa dokładnie zbadana. W celu pozyskania lepszej wiedzy o złożonych, a jednocześnie subtelnych, zjawiskach geodynamicznych o znaczeniu naukowym i ekonomicznym, istnieje potrzeba ulepszenia globalnej infrastruktury geodezyjnej oraz poprawy jakości pomiarów w geodezji kosmicznej. Wspólny wysiłek społeczności geodezyjnej znany jako Globalny Geodezyjny System Obserwacyjny (ang. akronim GGOS) uwzględni tę potrzebę, zapewniając także najwyższą możliwą dokładność produktów geodezyjnych oraz wysoką spójność pomiędzy technikami geodezji kosmicznej. Ambitne gole GGOS wymagają odpowiednich zmian również w obszarze geodezyjnego/astrometrycznego VLBI, realizowanych obecnie w formie Globalnego Systemu Obserwacyjnego VLBI (ang. akronim VGOS), systemu następnej generacji mającego na celu spełnienie wymagań GGOS oraz dostarczanie produktów geodezyjnych o niespotykanej dotąd jakości. Aby VGOS odniósł sukces, kluczowe elementy tego złożonego systemu muszą zostać udoskonalone, uwzględniając również nowe koncepcje obserwacji oraz strategie ich planowania, aby móc w pełni wykorzystać zwiększone możliwości jakie ten system może dostarczyć. Dzięki swojej charakterystyce, VGOS stwarza również doskonałą okazję do rozszerzenia obecnych badań wykorzystujących VLBI o nowe zastosowania, z korzyścią dla społeczności naukowej oraz całego społeczeństwa.

Temat niniejszej pracy doktorskiej dotyczy obserwacji sztucznych radioźródeł w ramach geodezyjnego VLBI, w nawiązaniu zarówno do obecnego systemu VLBI, jak i VGOS. Obejmuje to informacje dotyczące kombinacji obserwacji naturalnych radioźródeł i obiektów satelitarnych/księżycowych, a także korzyści oraz wyzwań związanych ze strategią obserwacji oraz wykonalności technicznej przedstawionej koncepcji. Niniejsza praca opiera się w większości na obszernych symulacjach dotyczących obiektów na Księżycu oraz satelitach geodezyjnych poruszających się po orbicie ziemskiej, ale zawiera także analizę obserwacji VLBI lądownika księżycowego przeprowadzonych podczas dedykowanych eksperymentów oraz przy użyciu globalnej sieci radioteleskopów. Treść niniejszej pracy może być traktowana jako kolejny krok w kierunku globalnych obserwacji sztucznych radioźródeł za pomocą VLBI w erze VGOS oraz przyczynić się do pobudzenia nowych koncepcji obserwacyjnych dla geodezji kosmicznej.

"I would rather have questions that can not be answered
than answers that can not be questioned"
R.F.

Acknowledgements

Many thanks to my colleagues at Onsala Space Observatory and Department of Space, Earth and Environment. The helpful attitude and the vibe of this department are extraordinary, it was always a pleasure to work at both venues and hang out with people present there. Starting with the staff at the observatory, people from the lab and workshop, Roger, Yun and Simon as well as the administrative/financial officers: Paula, Camilla, Katarina, Maria and Pia. Thank you all for your help concerning technical and practical aspects of various kinds. The former/present members of the group from "the 4^{th} floor" (in no particular order): Anqi, Albert, Anis, Michael, Joonas, Francesco, Wiebke, Santiago, Erik, Ole Martin, Alexander, Emma, Emil, Robin, Franz, Maciej, Kristell, Yufang, Donal and, last but not least, Paulina, who is always positive and eager to help. The present/former members of the astronomy part of the department (this time in an alphabetical order): Andri, Boy, Daria & Piero, Eskil, Francesco, Jean Baptiste, Joachim, Judit, Lucas, Maryam, Mitra, Niklas, Sandra, and Suzy. Thanks, it was fun !

The Space Geodesy and Geodynamics group, a one-of-a-kind association of people that I spent a great deal of time with. A big thanks goes to my former/present office mates: Johan, Niko, Joakim and Periklis as well as the former/present members of the geo group: Jonas, Hans-Georg, Jan, Maxime, Peter and Gunnar. Thomas Hobiger, my first/second supervisor, for providing me with priceless and solid foundations of C++, GNSS, geodetic VLBI and space geodesy in general. Rüdiger Haas, my second/first supervisor, for sharing with me his immense knowledge and experience concerning geodetic VLBI and space geodesy. I would like to express my sincere gratitude to both my supervisors for their continuous support (and patience) throughout those five years of our cooperation. The huge positive impact on my studies that your presence had cannot be questioned. Finally, I thank family and friends, those who live currently abroad (Bartosz D., Janusz P.) and my good old friends back in Poland. Piotr P. and Barbara P., for sticking with me no matter what, for your friendship lasting until now and for years to come.

Per aspera ad astra, the last five years were full of interesting and exciting events, they passed in the blink of an eye. The lessons learned (also from my own mistakes) and experiences gathered along the way allowed me to bring this thesis to completion. However, nothing ends here, really, as science is an endless search, and every answer yields a number of new questions...

Greg

Research Contributions

This thesis is based on the following contributions, referred to by Roman numerals in the text:

I) **G. Klopotek**, T. Hobiger and R. Haas (2018). **Geodetic VLBI with an artificial radio source on the Moon: a simulation study**. *Journal of Geodesy*, 92 (5), 457–469. doi:10.1007/s00190-017-1072-4.

II) **G. Klopotek**, T. Hobiger, R. Haas, F. Jaron, L. La Porta, A. Nothnagel, Z. Zhang, S. Han, A. Neidhardt and C. Plötz (2019). **Position determination of the Chang'e 3 lander with geodetic VLBI**. *Earth, Planets and Space*, 71 (23). doi:10.1186/s40623-019-1001-2.

III) **G. Klopotek**, T. Hobiger, R. Haas and T. Otsubo (2020). **Geodetic VLBI for precise orbit determination of Earth satellites: A simulation study**. *Journal of Geodesy*, under review.

The author either wrote or contributed to the following publications (not appended):

A) **G. Klopotek**, T. Artz, A. Bellanger, G. Bourda, M. Gerstl, D. Gordon, R. Haas, S. Halsig, G. A. Hjelle, T. Hobiger, U. Hugentobler, A. Iddink, A.-S. Kirkvik, S. Lambert, L. Plank, R. Schmid, F. Shu, O. Titov, F. Tong and G. Wang (2016). **Results from the VLBI Analysis Software Comparison Campaign 2015**. *IVS 2016 General Meeting Proceedings*, International VLBI Service for Geodesy and Astrometry, Johannesburg, 203–207. NASA/CP-2016-219016.

B) **G. Klopotek**, T. Hobiger and R. Haas (2017). **Implementation of VLBI Near-Field Delay Models in the c5++ Analysis Software**. Proceedings of the First International Workshop on VLBI Observations of Near-field Targets, *Schriftenreihe des Inst. f. Geodäsie u. Geoinformation*, 54, Bonn, 29–33. ISSN: 1864-1113.

C) N. Kareinen, **G. Klopotek**, T. Hobiger and R. Haas (2017). **Identifying optimal tag-along station locations for improving VLBI Intensive sessions**. *Earth, Planets and Space*, 69 (16). doi:10.1186/s40623-017-0601-y.

D) **G. Klopotek**, T. Hobiger and R. Haas (2017). **Lunar Observations and Geodetic VLBI – A Simulation Study**. *Proceedings of the 23rd European VLBI Group for Geodesy and Astrometry Working Meeting*, Chalmers University of Technology, Gothenburg, 122–126. ISBN: 978-91-88041-09-8.

Contents

Chapter 1

Introduction

A long time ago in ancient Alexandria a Greek polymath, and a man of many talents, Eratosthenes of Cyrene heard that at noon of the day of the summer solstice (about 21 June every year) the Sun shines directly above a deep well in the city of Syene (present day Aswan, Egypt), without casting any shadows. With this knowledge in mind, Eratosthenes measured, at noon on the summer solstice, the angle of a shadow cast by a vertical rod located in Alexandria. By determining also the the distance between Alexandria and Syene, he could then calculate the circumference of the Earth. One could say that with Eratosthenes' method for deriving Earth's size the science of geodesy was born.

Geodesy is a scientific discipline that deals with measurement and representation of the Earth. Thanks to geodesy we know, for instance, the size and shape of the Earth, its orientation in space, and its distance from the Moon. Throughout the centuries, using stars as reference points as well as accurate clocks, one could reliably determine latitude and longitude so that ships could cross oceans to get where they intended to go. Through land surveying one could create detailed maps of whole countries and map the uncharted territories. With the same height reference surface, rail tunnels could be started on both sides of a mountain and somehow still meet in the middle. Once radio telescopes were invented and satellites were launched to orbit the Earth, geodesy gained a whole new set of tools that could be used to observe the Earth on global scales. Concerning radio telescopes, scientists used primarily several small radio telescopes synthesizing a big one in order to look at very distant galaxies. Soon it was also realized that one could use these natural radio sources (quasars) to determine very accurately the distance between the telescopes and apply this knowledge to Earth observations. Almost at the same time, but a bit earlier, laser measurements to spacecrafts equipped with retroreflectors first occurred, giving rise to the technique commonly known as satellite laser ranging (SLR). That is also how space geodesy was born. Nowadays, numerous satellites are used in different fields such as telecommunication, meteorology or environmental monitoring. The establishment and development of the global positioning system (GPS) by the United States Department of Defence provided a satellite-based radio

navigation system accessible to millions of users around the world since late 1990's, leading to various applications in science and industry. Through the analysis of satellite orbits at different altitudes, one can also learn about our planet's changing size, shape and gravity field. In addition, by making laser measurements from/to or between satellites (SLR, laser altimetry, space gravimetry) one can investigate various geodynamical phenomena, from seasonal and decadal changes in the height and shape of the oceans and ice sheets to deriving global circulation models of various kinds. Moreover, progress in space sciences and a continuous interest in the exploration of the solar system have motivated numerous missions with the aim to study the Moon. The Moon missions in the 1970's left plenty of scientific equipment on the lunar surface, including corner-cube retroreflectors. Highly precise measurements of ranges between an observatory on the Earth and a retroreflector on the Moon are used nowadays for studies concerning the Earth-Moon dynamics, lunar interior or even gravitational physics. Moreover, remotely guided space probes have flown by all the planets of our solar system. Observations of those spacecrafts across the decades contributed to our better knowledge on planets and helped to improve planetary ephemerides. Thanks to space geodesy one can monitor movements of Earth's crust, investigate how long days are and how the Earth wobbles around its axis. Satellite gravimetry, space-geodetic techniques and global reference frames give us a better understanding of global-scale geophysical phenomena such as mass redistribution in the global water cycle, shrinking ice sheets or sea-level rise, topics that are of high importance for society and crucial for revealing the signals of a changing climate.

The technique used in this thesis is geodetic very long baseline interferometry (VLBI), originating from astronomy where VLBI was used first for deriving high-resolution images of very distance objects in the Universe. Dedicated system configurations and continuously revised processing chains enabled however to derive accurate distances between telescopes forming a baseline and thus to use radio interferometry for geodetic applications. Geodetic VLBI is a fascinating but a complex technique relying on knowledge from various fields of science and engineering. It consists of many different elements, which have to work together correctly in order to make this technique useful. Geodetic VLBI has a long tradition of realizing celestial and terrestrial reference systems, and has a unique capability of deriving a full set of Earth orientation parameters (EOP) that relate those two systems. This technique has been recently shifting towards a next-generation system that will provide a significantly improved observation precision and enhanced determination of global geodetic parameters. This epochal shift brings also a necessity of improving the antenna design, data acquisition schemes, calibration systems as well as new scheduling strategies and novel observing concepts. The anticipated enhanced performance of that next-generation system, referred to as the VLBI Global Observing System (VGOS, Petrachenko et al., 2009; Niell et al., 2018), aims to meet the requirements of the Global Geodetic Observing System (GGOS, Plag and Pearlman, 2009). The ambitious goal of the latter is a very stable and millimeter-precise global reference frame, for the benefit of the scientific community and society at large.

The subject of this thesis concerns geodetic VLBI and observations of artificial radio sources within its framework. The basis of this thesis form theoretical and technical aspects of this topic including scheduling, observation, data processing and parameter estimation, also for deriving a set of parameters which were out of scope for geodetic VLBI so far. In the following, a method of utilizing geodetic VLBI for observations of man-made radio objects on the Moon is described. The thesis covers also Earth satellites and precise determination of their orbits using geodetic VLBI. The feasibility of the proposed concepts is validated mainly through simulation studies, but the thesis includes also an analysis of experiments consisting of observations of a lunar lander performed with a global network of radio telescopes. The aim of this dissertation is to provide insights concerning the combination of quasar and lunar or satellite observations, with the purpose of extending the field of geodetic VLBI research with new applications, and pave the way for introducing this technique into the field of satellite geodesy.

1.1 Thesis Structure

First a brief introduction to space geodesy, reference frames and EOP is given in Chapter 2, along with information on the combination of space-geodetic techniques. A comprehensive overview of geodetic VLBI is given in Chapter 3, including delay modelling, scheduling, observation, correlation, data analysis, observations in the VGOS era, and geodetic VLBI simulations. Chapter 4 is dedicated to VLBI observations of artificial radio sources of various kinds. Several aspects are covered including delay modelling, signal structure, and relate technical aspects. In Chapter 5 observations of lunar targets with VLBI are described in detail. This includes observation schemes, correlation, post-correlation analysis and parameter estimation. Chapter 6 is related to Earth satellites and the feasibility of geodetic VLBI for precise orbit determination of their orbits. This chapter comprises general information on satellite geodesy, orbit modeling and several related theoretical considerations. Chapter 7 consists of conclusions and outlook concerning the presented topic. A brief summary of the attached articles forms the final chapter of this thesis.

Chapter 2

Space Geodesy

Space geodesy is a field of science facilitating our understanding of Earth dynamics and is fundamental for providing accurate and stable reference frames, to which global-scale environmental changes and their variability can be properly referenced. Space geodesy encompasses observations of artificial satellites and also extragalactic point-like radio sources in order to measure the Earth's shape, its gravity field as well as quantity of numerous geophysical phenomena (loading effects, crustal dynamics, glacial isostatic adjustment, Earth's interior) in space and time.

Space geodesy relies on observations from various techniques, as illustrated in Fig. 2.1. The backbone of space geodesy form (in no particular order)

- geodetic and astrometric VLBI,
- global navigation satellite systems (GNSS),
- SLR and lunar laser ranging (LLR),
- doppler orbitography and radiopositioning integrated by satellite (DORIS).

Other satellite-based techniques, established for global Earth observations, can be also adopted for geodetic purposes. This includes gravity missions at low altitudes, satellite altimetry or other remote sensing techniques (Bertiger et al., 1994; Visser, 1999; Beckley et al., 2007). Each space-geodetic technique is sensitive to different sets of Earth-based parameters and conducts observations with different spatio-temporal resolution, providing geodetic products with different latency and quality. Therefore, only the utilization of many space-geodetic techniques allows to establish a global observing system and model subtle global-scale phenomena of various kinds.

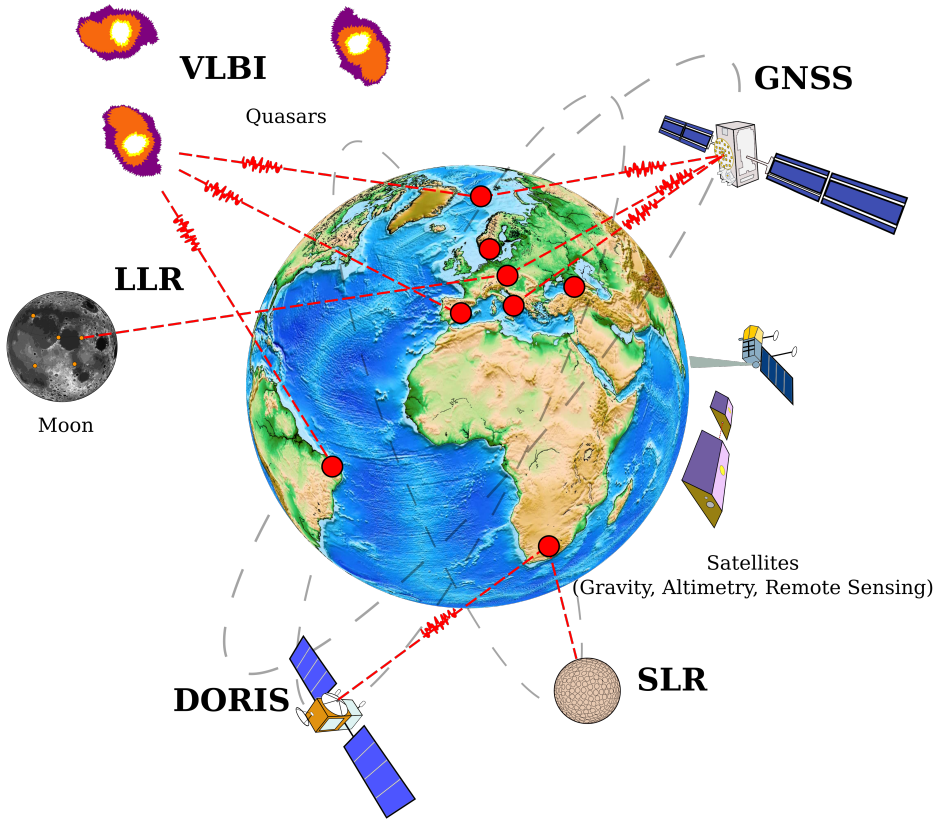

Fig. 2.1 Space-geodetic techniques. Space geodesy requires a holistic approach for global-scale monitoring of the Earth system. This includes utilizing a number of various instruments with different sensitivity and the spatio-temporal resolution.

2.1 Terrestrial and Celestial Reference Systems

Observations from four space-geodetic techniques allow for continuous availability and frequent realization of global reference systems in order to treat all observations in a consistent and homogeneous manner. An access to a reference system is obtained through a set of physical points with precisely determined coordinates. A set of such materialized coordinates constitute a (crust-based) reference frame, which is the realization of a reference system. The latter can be a system that is non-rotating w.r.t. distant celestial objects (fixed to distinct directions in space) or a system co-rotating with the Earth in its diurnal motion in space. In the latter case, a selected number of geodetic stations and a long-term input, in the form of time series of station positions, velocities and, EOP from four space-geodetic techniques (geodetic VLBI, SLR, GNSS and DORIS) is used for providing timely

updates of the International Terrestrial Reference Frame (ITRF), with the latest release designated as ITRF2014 (Altamimi et al., 2016). Each new release of the ITRF is published every three to five years and tends to be superior to the past versions due to the continuously increasing amount of observations as well as improved strategies of the ITRF combination and the submitted solutions. This is also related to the fact that ITRF is attached to the deformable Earth, and frequent updates are necessary to maintain the realization as close to the ideal reference system as possible (Dong et al., 2003). In addition, the spatial relation between reference points of geodetic instruments at the same site are expressed via local surveys and also form an input to the ITRF combination. Technique-specific solutions stem from the combination of the individual analysis centers' solutions of the particular technique and include an entire observation history. A terrestrial reference frame (TRF) realizes a terrestrial reference system (TRS) by establishing its origin (3 parameters), scale (one parameter), and orientation of its axes (3 parameters), including the time evolution of these parameters. The ITRF origin is today defined exclusively via SLR observations. In the case of the scale of the ITRF, it is obtained based on the time series from both VLBI and SLR. The orientation of the ITRF is conventionally aligned to the previous release, implying zero rotations and no rotation rates between two frames at a particular epoch (Petit and Luzum, 2010). The transformation between reference systems is performed, in a least-squares sense, on the basis of 14 parameters, i.e., three translation components T_1, T_2, T_3, one scale factor D, three rotation angles R_1, R_2, R_3 as well as first time derivatives of $T_{1,2,3}$, D and $R_{1,2,3}$.

Observations of distant celestial objects provide the basis for the realization of the celestial reference system, convenient for modelling of satellite orbits, describing the motion of the Earth, planetary orbits or trajectories of spacecrafts. The International Astronomical Union (IAU) defined two coordinate systems (and 4-dimensional transformation between them), differing by the origin definition. The Barycentric Celestial Reference System (BCRS) with the Barycentric Coordinate Time (TCB) and the origin in the solar system barycenter and the Geocentric Celestial Reference System (GCRS) with the Geocentric Coordinate Time (TCG) and referred to the Earth's center (Petit and Luzum, 2010). Conventionally, the axes of both BCRS and GCRS are aligned to those of the International Celestial Reference System (ICRS). Its first realization at radio frequencies (ICRF1) was adopted by the IAU in 1997 and consisted of precise equatorial coordinates (right ascension α, declination δ) of stable and point-like extragalactic radio sources obtained from VLBI measurements at S/X frequencies (Ma et al., 1998). Its successor (ICRF2) was characterized by a more uniform distribution of radio sources and an improved axes stability (Fey et al., 2009). As of 1 January 2019, ICRF3 is the new fundamental celestial reference frame as adopted by the IAU. It comprises 4536 (303 defining) sources (at X band) and incorporates nearly 40 years of VLBI data, resulting with the noise floor, caused by structural instabilities, of 30 μas for individual source coordinates. In addition, ICRF3 improved also source coverage in the southern hemisphere. Unlike previous realizations, ICRF3 includes also higher frequencies (K, Ka) (Malkin et al., 2015) and is expressed at a

particular epoch (2015.0). For the most accurate applications, positions of radio sources have to be propagated for observations away from that epoch, accounting for galactocentric acceleration of 5.8 μas/yr (MacMillan et al., 2019).

The celestial reference system is realized also with the use of optical observations of extragalactic sources. A recent example are measurements carried out by the Gaia spacecraft (Gaia Collaboration, 2016; Gaia Collaboration, 2018a) and used to materialize the Gaia Celestial Reference Frame (Gaia-CRF2). The latter is characterized by a sub-milliarcsecond astrometric precision and sources that are equally distributed in the celestial sky, apart from the areas close to the galactic equator (due to interstellar dust and stars in the plane of the Milky Way). The number of sources in the Gaia-CRF2 is more than one hundred times higher than the quantity of objects in the radio frame. For a common set of objects, the axes of the Gaia-CRF2 and ICRF3 are aligned with an uncertainty on the level between 20 μas and 30 μas, with a similar level of astrometric quality concerning sources forming those frames (Gaia Collaboration, 2018b). The Gaia/VLBI position offsets of individual sources, leading to the misalignment of those two frames, may arise from real offsets between the centres of emission at optical and radio wavelengths, errors in matching VLBI and Gaia objects, the number of common sources, presence of (optical/radio) structure effects or statistical outliers. As the accuracy of VLBI and Gaia measurements continuously improves and amount of data increases, statistically significant differences between radio and optical frames may become even more pronounced in the future.

2.2 Earth Orientation Parameters

The relation between ITRS and GCRS is expressed as a function of time and by means of Earth orientation parameters. The latter are published by the International Earth Rotation and Reference Systems Service (IERS) and provided as predicted, rapid, monthly and long-term data[1]. The IERS is also an organization in charge of maintaining conventions containing models, constants and standards, known as the IERS Conventions, which are recommended for analyses of space-geodetic data and revised as required (Petit and Luzum, 2010). For an arbitrary epoch t, the rotations between these two systems can be expressed as (Petit and Luzum, 2010)

$$\vec{\mathbf{X}}_{GCRS} = \underbrace{Q(t)}_{\substack{\text{precession and} \\ \text{nutation}}} \overbrace{R(t)}^{\substack{\text{Earth} \\ \text{rotation}}} \underbrace{W(t)}_{\substack{\text{polar} \\ \text{motion}}} \vec{\mathbf{X}}_{ITRS}, \tag{2.1}$$

where $Q(t)$, $R(t)$ and $W(t)$ are the transformation matrices (system rotation matrices) referring to the movement of the Celestial Intermediate Pole (CIP) in the GCRS, rotation of the Earth around the axis of the CIP and polar motion (motion of the CIP in the ITRS), respectively. The CIP relates to the transformation strategy based on the IAU-compliant concept of the non-rotating origin (Petit and

[1] www.iers.org/IERS

Luzum, 2010). The latter is referred to as the Celestial Intermediate Origin (CIO) and Terrestrial Intermediate Oorigin (TIO), depending upon the viewing reference system. The CIO-based approach is illustrated in Fig. 2.2.

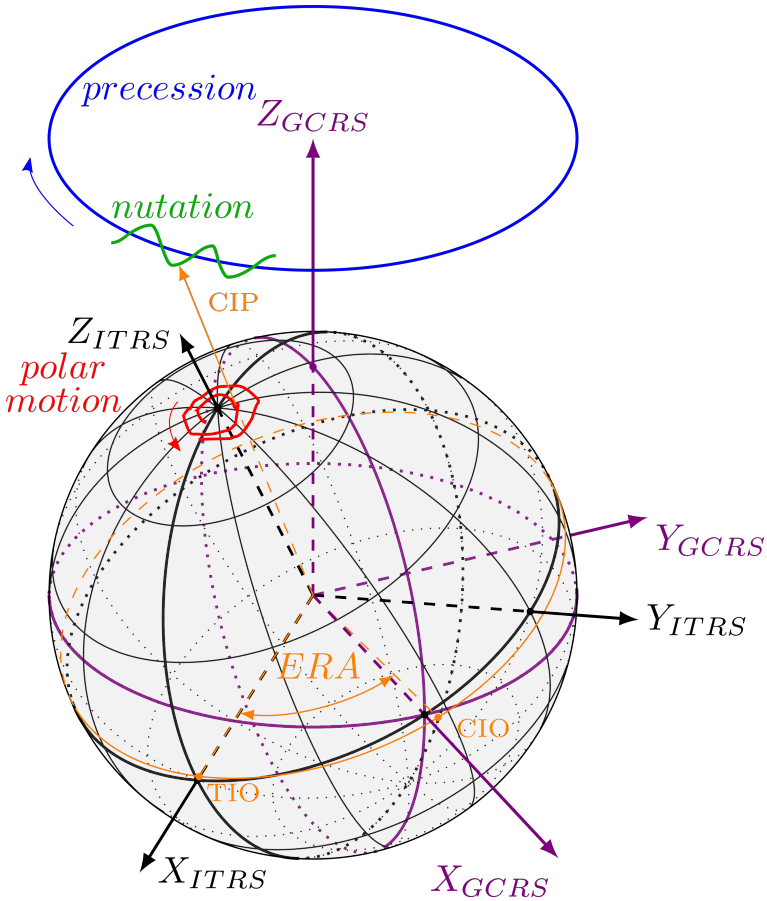

Fig. 2.2 The CIO-based transformation between ITRS and GCRS. EOP (precession-nutation, polar motion, ERA) are determined via space-geodetic techniques. Fig. 2.1 from Klopotek (2017)

The motion of the CIP in the celestial reference system includes the long-term (25,772-year) effect (precession) of the overall response of the Earth to the gravitational attraction of the Sun, Moon and planets, with superimposed periodic components from days up to 18.6 years (nutation). Conventionally, the position of the CIP (celestial pole coordinates) is calculated in a manner consistent with the IAU2006/2000A precession-nutation model (Mathews et al., 2002; Capitaine et al., 2003). Additionally, the CIP motion is complemented with the observed differences w.r.t. the modelled motion, reported by the IERS in the form of so-called celestial pole offsets (dX, dY). The latter are related to the free core nutation

effect emerging from the lack of coincidence between the axes of rotation of Earth's mantle and Earth's core (Mathews et al., 2002).

Polar motion reflects the movement of the CIP in the ITRS and includes short-term changes of pole coordinates (x_p, y_p). Observations of the rotation axis are dependent on the viewing reference frame. As viewed in the ITRS, this includes frequency terms lower than -1.5 cycles per sidereal day (cpsd) or greater than -0.5 cpsd (Petit and Luzum, 2010). On the Earth's surface, changes in x_p and y_p reach several meters. Due to its unpredictable nature, polar motion has to be monitored on a regular basis with the use of space-geodetic techniques. A similar level of unpredictability characterizes the sideral rotation of the Earth, expressed conventionally as the Earth rotation angle (ERA). Its non-uniform movement is caused by numerous effects associated to the redistribution of Earth's mass or to gravitational interactions with the Moon, leading to the rotation of the Earth that is slowing down. At any particular epoch t, the rotation matrix $R(t)$ from Eq. 2.1, is expressed as (Capitaine et al., 2000)

$$R(t) = R_3(-ERA) \tag{2.2}$$

$$ERA(T_u) = 2\pi(0.7790572732640 + 1.00273781191135448\,T_u), \tag{2.3}$$

where T_u= (Julian UT1 date − 2451545.0). $UT1$ is related to the Greenwich Mean Sideral Time (GMST) and describes the direction of the ITRS zero meridian in the GCRS. Earth rotation is usually expressed as the difference between the duration of a day and 86,400 seconds (length of the day) or w.r.t. the coordinated universal time (UTC) in the form of $UT1$-UTC values. Continuous monitoring of Earth rotation is carried out with geodetic VLBI as it is the space-geodetic technique capable of accessing that parameter directly[2] and providing $UT1{-}UTC$ values on a daily basis (Kareinen et al., 2015). However, VLBI-derived $UT1$ estimates are not bias-free and suffer from technique-specific effects such as clock offsets of reference stations (Hobiger et al., 2009b; Himwich et al., 2017). In general, such issues need to be addressed correctly in order to obtain utmost accurate geodetic products, see Sec. 3.5.

2.2.1 High-Frequency EOP Variations

For most accurate applications, short-term variations affecting Earth rotation and polar motion, but not included in the IERS EOP series, have to be calculated at the observation epoch and included in the interpolated EOP values. Such additional components account for daily and subdaily variations caused by mass redistribution within the Earth system (ocean tides) and the impact of gravitational forces of external bodies (mostly luni-solar forces) on the Earth (diurnal and semi-diurnal nutation components, Chao et al., 1991). High-frequency EOP variations ($(\Delta x, \Delta y)_{\text{ocean tides}}$, $(\Delta x, \Delta y)_{\text{libration}}$, $\Delta UT1_{\text{ocean tides}}$, $\Delta UT1_{\text{libration}}$) should be included as these effects are larger than the current uncertainty of the determined polar

[2] acknowledging also the capability of LLR to derive $UT1$ from $UT0$ and variation of latitude (Pavlov, 2020)

motion and $UT1$ estimates. The related corrections can be calculated in accordance to the provided models (Petit and Luzum, 2010; Desai and Sibois, 2016).

2.3 Combination of Space-Geodetic Techniques

A simultaneous use of various space-geodetic techniques has many benefits as it improves the global geometrical coverage, provides better observation density, increases redundancy and helps to reduce correlations between the estimated parameters. Combination of space-geodetic techniques is useful for overcoming the technique-specific limitations as each technique can have a poor, or sometimes lacking, sensitivity for determining certain global geodetic parameters. Examples can be satellite techniques (GNSS, SLR, DORIS) and *UT1-UTC*, GNSS and the scale parameter[3], or geodetic VLBI and Earth's gravity field. On the other hand, an inclusion of SLR observations into the GNSS data analysis can be used, e.g., to transfer geocenter coordinates to the GNSS network (Thaller et al., 2014). The combined use of space-geodetic observations is thus beneficial for making full use of strengths of each technique, assuming that the combination is properly constructed, proper observation weighting is applied, and local ties with sufficient quality are available. The aim of the simultaneous use of the input from several space-geodetic techniques is to derive common parameters of interest, such as EOP or TRF, in a robust and physically consistent fashion in order to provide the highest possible quality and homogeneity of the final products (Rothacher et al., 2011; Artz et al., 2012) as well as independent time series for investigating technique-specific errors (Riddell et al., 2017).

In order to relate independent technique-specific frames in a multi-technique combination, geodetic instruments (*stations*) co-located at an IERS site (*core site*) can be connected by local surveys. Such measurements provide three-dimensional distances between the reference points of the co-located instruments and are commonly referred to as *local ties*. The latter are obtained from surveys performed with different measurement methods and equipment for the horizontal (distance and direction measurements) and vertical (precise leveling) components. Local ties are expressed as a set of coordinates (usually with covariance information) in the current ITRF release and accessible via a dedicated website[4]. Although the local surveys are generally highly precise (on the millimeter level), the tie accuracy varies from site to site and its overall accuracy may reach centimeter level (Ray and Altamimi, 2005; Altamimi et al., 2016). The rather inhomogeneous local ties have been identified as one of the limiting factors for the accuracy of today's ITRS realizations, besides the non-optimal observation network configurations, intra or inter-technique combination approaches (Kotsakis and Chatzinikos, 2017) and the technique-specific error sources (Altamimi et al., 2013). The latter effects contribute also to discrepancies between local ties and distances derived from single-technique solutions (Altamimi et al., 2016; Nothnagel et al., 2019).

[3]GNSS antenna phase center variations are highly correlated with the scale parameter
[4]`http://itrf.ign.fr/`

The combination approach can be extended with Earth-orbiting satellites, which are observed by several techniques. The employed satellites in that case are equipped with technique-specific instruments and vectors between the satellite center of mass (CM) and the reference points of sensors of different space-geodetic techniques are known to a high degree of precision. Such geometrical connections on a satellite level are commonly referred to as *space ties* and can be transferred to each core site via space-geodetic observations. The simultaneous use of space-geodetic techniques in that fashion is currently realized for the multi-technique analysis of space-geodetic data (Thaller et al., 2011; Sośnica et al., 2019) or an independent validation of microwave-based GNSS orbits with SLR observations (Urschl et al., 2005; Montenbruck et al., 2015b). A corresponding co-location satellite is not limited to a certain orbital height and an optimal choice of orbital parameters depends upon many factors, including also the expected outcomes of the undertaken project and available resources (Männel, 2016).

The both aforementioned concepts are illustrated in Fig. 2.3. Local ties and co-location in space (space ties) could be used simultaneously in the future in order to overcome the aforementioned limitations of today's reference frames. This applies also to other observation types such as GNSS data obtained from observations of satellites at low altitudes, SLR tracking to GNSS satellites or observations of Galileo satellites, as they are currently not present in the ITRF solutions. Moreover, the concept of space ties could be potentially extended with geodetic VLBI, see Sec. 6.4. Although not used, all of those observation types have the potential of contributing to future ITRF combinations. Additionally, space-geodetic techniques can be connected at core sites by estimating common parameters related to the atmosphere (*troposphere ties*, Krügel et al., 2007) or the frequency standard (clock) at the core site, known also as *clock ties* (Hobiger and Otsubo, 2014; Hobiger et al., 2015). Deriving a single set of EOP from multi-technique observations realizes in principle the concept of *global ties*, applied for instance in the ITRF combination (Altamimi et al., 2016). In the case of two or more VLBI telescopes located at one site, one can also establish very precise distances between the reference points of those antennas by means of a short-baseline interferometry (Herring, 1992; Halsig et al., 2019), see Sec. 3.6.4.

Based on observations available from different space-geodetic techniques, the common parameters can be derived (typically) in a least-squares adjustment by combining data on the 1) *observation level*, 2) *normal-equation (NEQ) level* or 3) *parameter level* (Seitz, 2015; Männel, 2016). This procedure is conducted under the assumption that these techniques share a set of target parameters (EOP, geocenter), can be related to each other by a mathematical or physical model, or that can be combined with the use of external information such as local ties.

The highest consistency and homogeneity between techniques is ensured in the first approach as one has a direct access to individual observations, which can be augmented with information derived from local ties (Hobiger et al., 2014). Combination on the observation level allows for an epoch-wise estimation of parameters of interest as well as common, and consistent, observation weighting and inter-technique outlier detection based on all observations that are available. In

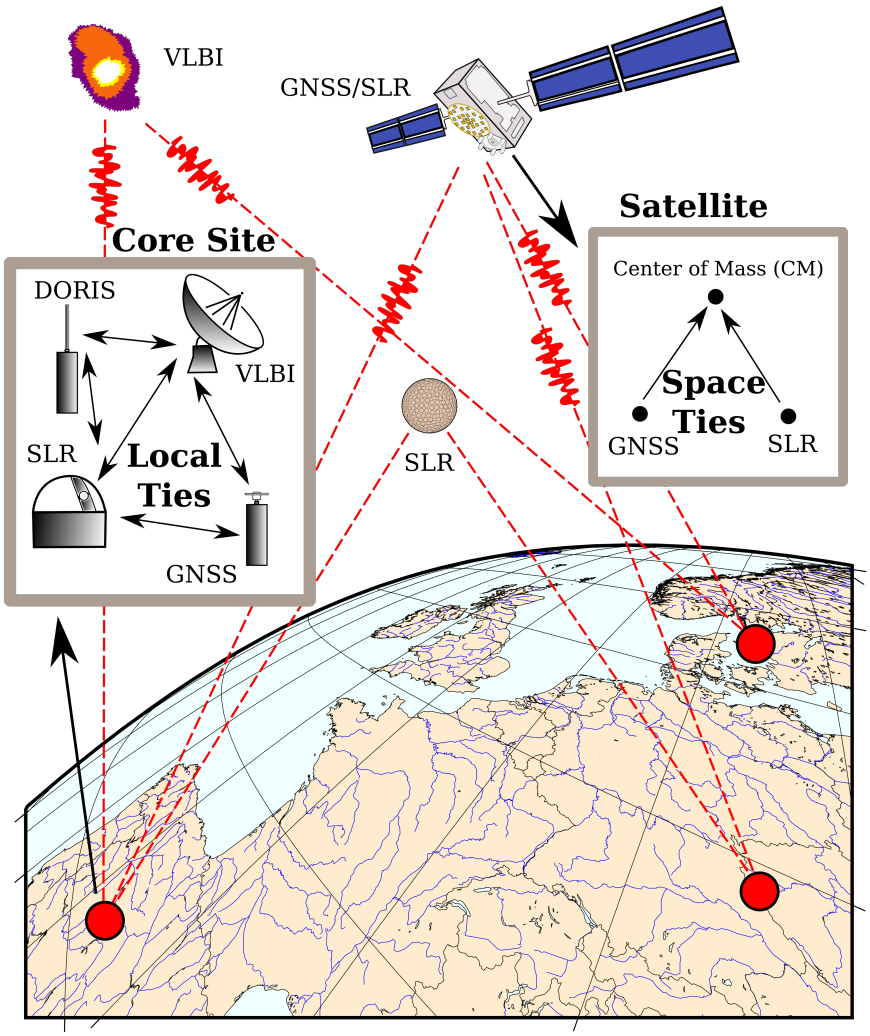

Fig. 2.3 The concept of local ties and co-location in space (space ties)

addition, all correlations between the estimated parameters are also preserved. Using a single software package for this purpose prevents also from discrepancies in the a priori models or in methods for their interpolation at the observation epoch as a lack of consistency in the modelling exhibits itself directly in the estimated parameters.

The second approach is most commonly used in space geodesy. The parameters of interest such as EOP, station coordinates or common troposphere parameters are derived in this case using technique-specific datum-free NEQ systems. The clear benefit of the combination with the use of NEQ systems has already been shown in various studies (Thaller et al., 2007; Fritsche et al., 2014). Combination on the

NEQ level is an effective way of analysing large data sets spanning many years and can reduce the computational load significantly while still being consistent, to high degree, with the combination on the observation level. The lower computational cost is associated to the reduced size of the normal equations obtained at the stage of parameter pre-elimination, in which epoch-wise parameters, that are not relevant for the solution (*nuisance* parameters), can be removed without affecting other solve-for parameters.

In the case of the combination on the parameter level, the target parameters and related variance-covariance matrices from technique-specific solutions are used in an additional least-squares adjustment. Here, the parameters can be interpolated, filtered, averaged and re-weighted to generate the final solution, as in the case of the IERS 14 C04 series[5], related to polar motion, $UT1$ and celestial pole offsets. In terms of the ITRS realization, the methods for combining the input from space-geodetic techniques and the processing strategies may vary (Karbon et al., 2019), but generally include the combination on the parameter level (Altamimi et al., 2002; Altamimi et al., 2005) and on the NEQ level (Seitz et al., 2012).

2.4 The Global Geodetic Observing System

A truly stable and very accurate global geodetic reference frame is of a crucial need for scientific and societal applications. The economic and scientific importance of a global reference frame has been confirmed with the resolution adopted on 26 February 2015 by the General Assembly of the United Nations on the Global Geodetic Reference Frame (GGRF) for Sustainable Development[6]. In order to achieve the requirements put upon the future reference frame as well as attain better knowledge on Earth dynamics, there is a necessity for improving the current global geodetic infrastructure and the quality of current geodetic and gravity measurements. The International Association of Geodesy (IAG) had recognized the need for such an improvement and in the early 2000's proposed the GGOS concept, which became IAG's official component in 2007 with the ambitious goal of integrating geometric and gravimetric aspects of modern space geodesy. The aim of GGOS is to improve the current geodetic infrastructure necessary for monitoring the Earth system with an unprecedented quality and provide a very accurate reference frame, which is crucial for quantifying key global-change processes in space and time. Observations in the GGOS era shall advance our understanding of the geodynamical phenomena that are vital for society such as global trends in the sea-level rise (Beckley et al., 2007; Blewitt et al., 2010), plate tectonics, space weather or mass redistribution in the global water cycle. The goals of GGOS are long-term and accurate monitoring of geodetic parameters and a TRF characterized by 1-mm accuracy of station positions and 0.1-mm/yr accuracy in terms of station velocities. This implies that today's reference frame realization (and satellite orbit determination) concepts need to be revised and improved in many areas including station-network configurations, technique-specific

[5] `ftp://hpiers.obspm.fr/iers/eop/eopc04/`

[6] `http://www.un.org/ga/search/view_doc.asp?symbol=A/69/L.53`

errors, correlations between different parameter groups, integration of diverse sensor systems, applied models or combination approaches. This should pave the way for combining independent Earth observations into a single frame with the highest possible accuracy and assure high consistency across the *three pillars of geodesy* (geometry and kinematics, Earth rotation, and gravity field). The GGOS concept necessitates thus an active cooperation between geodetic, geodynamic and geophysical communities and should also include scientists from other fields in order to address relevant science issues of the 21st century (Plag and Pearlman, 2009).

Chapter 3

Very Long Baseline Interferometry

Very long baseline interferometry (VLBI) and its basic ideas were first demonstrated in the 1960's and early 1970's as a technique using interferometry at radio frequencies and antennas separated by thousands of kilometers (Bare et al., 1967; Broten et al., 1967; Cohen, 1972). Continuous progress made over the subsequent years and decades, including specialized system configurations and dedicated processing chains (Rogers, 1970; Whitney et al., 1976; Rogers et al., 1983) and an ingreasing number of antennas, resulted in significant contributions of VLBI to our understanding of a wide range of astrophysical (Robertson and Carter, 1984; Gwinn et al., 1997) and geophysical (Carter et al., 1985; Herring et al., 1986; Gipson, 1996) phenomena. Applied to astronomy, VLBI provides the highest imaging angular resolution based on observations of radio signals emitted by various objects in the Universe. This allows to map certain parts of the sky in great detail, reveal the nature of objects located there and study physics behind them (Boccardi et al., 2016).

In VLBI, the observed radio signals are digitized, time-tagged and recorded locally. In the next step, the recorded signals are cross-correlated for all pairs of antennas with the goal of producing high-resolution images of objects of interest. VLBI enables to observe radio sources with the angular resolution of λ/D, where λ is the observed wavelength. D refers to the maximum distance (projected onto a plane perpendicular to the source) between two radio telescopes in the array. The enhanced angular resolution is achieved by increasing the distance between telescopes, which are usually separated by hundreds or thousands of kilometers. The basic observable in geodetic and astrometric VLBI is however the time difference of signal reception between two telescopes observing the same source over a relatively short period of time. While in astronomy VLBI focuses on mapping a single object, typical astrometric or geodetic experiments will have several hundred observables per baseline and include multiple radio sources (Fomalont, 1995; Sovers et al., 1998).

3.1 The VLBI Delay Model

Spherical wave fronts emitted by a very distant natural radio source become planary by the time they reach the Earth. Including EOP, the time difference (τ) of the signal reception between two VLBI antennas observing the same source can be expressed in a simplified form as

$$\tau(t_1) = t_2 - t_1 = -\frac{1}{c}\,\hat{\mathbf{k}}\,\vec{\mathbf{b}} = -\frac{1}{c}\,\hat{\mathbf{k}} \quad \underbrace{Q(t_1)}_{\substack{\text{precession and}\\ \text{nutation}}} \quad \overbrace{R(t_1)}^{\substack{\text{Earth}\\ \text{rotation}}} \underbrace{W(t_1)}_{\substack{\text{polar}\\ \text{motion}}} \vec{\mathbf{B}}, \tag{3.1}$$

with c as the speed of light and $\hat{\mathbf{k}}$ as the direction to the radio source expressed in the GCRS as

$$\hat{\mathbf{k}} = \begin{bmatrix} \cos\alpha\cos\delta \\ \sin\alpha\cos\delta \\ \sin\delta \end{bmatrix} \tag{3.2}$$

and calculated with the use of angular coordinates (α, δ) of the radio source. The coordinates are first taken from the ICRF3 catalogue and then accounted for galactocentric acceleration. The GCRS baseline vector $\vec{\mathbf{b}}$ is defined as a difference of the GCRS positions of telescopes forming a baseline ($\vec{\mathbf{x_2}} - \vec{\mathbf{x_1}}$), whereas the ITRS baseline vector is denoted as $\vec{\mathbf{B}}$ and defined in a similar fashion. The relation expressed with Eq. 3.1 provides the basis for accessing various phenomena related to Earth orientation and dynamics. As the Earth rotates, the delay changes depending upon the relative positions of stations forming a baseline and the position (α, δ) of the observed radio source. The arrival time at the reference station, this epoch denoted hereafter with *1* in the subscripts, serves as the reference for computing all scalar and vector quantities of the model. Earth orientation parameters can be derived using corresponding partial derivatives w.r.t. the parameters of interest (Sovers et al., 1998), see also Sec 3.6.5. The VLBI delay model for natural radio sources is illustrated in Fig. 3.1.

In the barycentric frame, the vacuum delay can be formulated as (Petit and Luzum, 2010)

$$T_2 - T_1 = -\frac{1}{c}\,\hat{\mathbf{K}}\,\left(\vec{\mathbf{X}}_2(T_2) - \vec{\mathbf{X}}_1(T_1)\right) + \Delta T_{grav}, \tag{3.3}$$

where $\hat{\mathbf{K}}$ refers in this case to the unit vector from the barycenter to the source in the absence of gravitational or aberrational bending and ΔT_{grav} containing the relativistic terms. The $\vec{\mathbf{X}}_i(T_j)$ quantity refers to the barycentric position of the i^{th} station at time T_j. T_2-T_1 can be related to the geocentric vacuum delay t_{v2}-t_{v1}

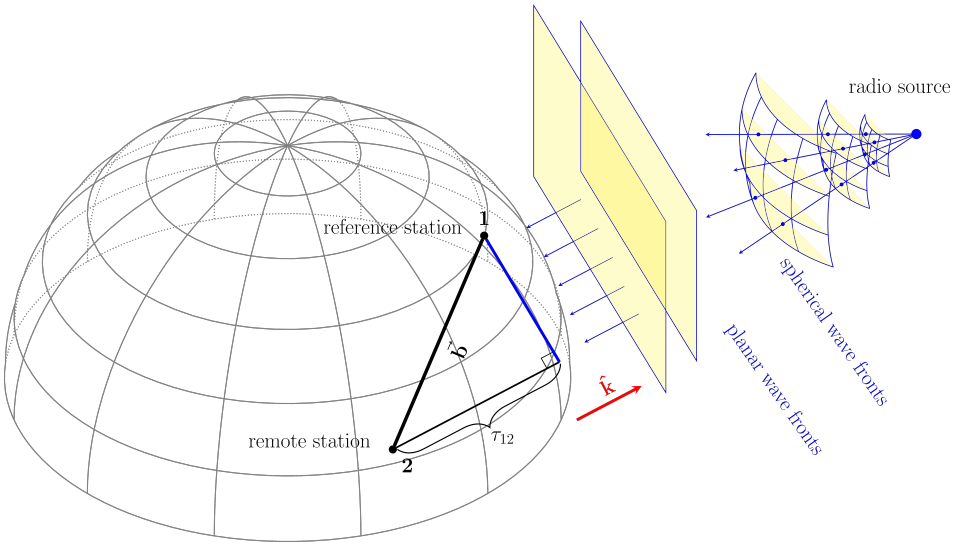

Fig. 3.1 The VLBI delay model for natural radio sources. Fig. 3.1 from Klopotek (2017)

by (Petit and Luzum, 2010)

$$t_{v2} - t_{v1} = \frac{\Delta T_{grav} - \frac{\hat{\mathbf{K}}\,\vec{\mathbf{b}}}{c}\left[1 - \frac{(1+\gamma)\,U}{c^2} - \frac{|\vec{\mathbf{V}}_\oplus|^2}{2c^2} - \frac{\vec{\mathbf{V}}_\oplus\,\vec{\omega}_2}{c^2}\right] - \frac{\vec{\mathbf{V}}_\oplus\,\vec{\mathbf{b}}}{c^2}\left(1 + \hat{\mathbf{K}}\,\frac{\vec{\mathbf{V}}_\oplus}{2c}\right)}{1 + \frac{\hat{\mathbf{K}}\,\left(\vec{\mathbf{V}}_\oplus + \vec{\omega}_2\right)}{c}}. \tag{3.4}$$

The terms in Eq. 3.4 do not include the change in the geometric delay attributed to the atmospheric propagation delay at the reference station. If one considers this effect, the geometric time delay (τ_g) in this form reads as

$$\tau_g = t_{g2} - t_{g1} = t_{v2} - t_{v1} + \delta t_{atm1}\frac{\hat{\mathbf{K}}\,(\vec{\omega}_2 - \vec{\omega}_1)}{c}, \tag{3.5}$$

where δt_{atm1} refers to the atmospheric propagation delay at the reference station (Sovers et al., 1998). The total delay t_2-t_1 is then obtained by including other contributions, also briefly described in the subsequent subsections.

The incoming radio waves are affected by the gravity fields of the Sun and all planets of our solar system. This results in the change of the time delay as well as the direction of the incoming signal. In order to accommodate these effects, VLBI delays contain also relativistic terms accounting for the space-time curvature

$$\Delta T_{grav} = \sum_J \Delta T_{grav,J}, \tag{3.6}$$

where the relativistic delay $\Delta T_{grav,J}$ for the J^{th} gravitating body can be formulated as (Petit and Luzum, 2010)

$$\Delta T_{grav_J} = 2\frac{GM_J}{c^3}\ln\frac{|\vec{\mathbf{R}}_{1_J}| + \hat{\mathbf{K}}\,\vec{\mathbf{R}}_{1_J}}{|\vec{\mathbf{R}}_{2_J}| + \hat{\mathbf{K}}\,\vec{\mathbf{R}}_{2_J}}, \tag{3.7}$$

$$\vec{\mathbf{R}}_{1_J}(t_1) = \vec{\mathbf{X}}_1(t_1) - \vec{\mathbf{X}}_J(t_{1_J}), \tag{3.8}$$

$$\vec{\mathbf{R}}_{2_J}(t_1) = \vec{\mathbf{X}}_2(t_1) - \vec{\mathbf{X}}_J(t_{1_J}) - \frac{\vec{\mathbf{V}}_\oplus}{c}(\hat{\mathbf{K}}\,\vec{\mathbf{b}}), \tag{3.9}$$

$$\vec{\mathbf{X}}_i(t_1) = \vec{\mathbf{X}}_\oplus(t_1) + \vec{\mathbf{x}}_i(t_1), \tag{3.10}$$

where G refers to the gravitational constant, M_J is the rest mass of the J^{th} gravitating body and $\vec{\mathbf{R}}_{i_J}$ describes the vector from the J^{th} gravitating body to the receiver at station i. The $\vec{\mathbf{X}}_\oplus(t_1)$ and $\vec{\mathbf{x}}_i(t_1)$ terms refer to the barycentric position of the Earth and the GCRS radius vector of the i^{th} station at time t_1, respectively.

The gravitational delay associated to the contribution of the Earth, and denoted as $\Delta T_{grav_\oplus}$, can be formulated in a simplified form as (Petit and Luzum, 2010)

$$\Delta T_{grav_\oplus} = 2\frac{GM_\oplus}{c^3}\ln\frac{|\vec{\mathbf{x}}_1| + \hat{\mathbf{K}}\,\vec{\mathbf{x}}_1}{|\vec{\mathbf{x}}_2| + \hat{\mathbf{K}}\,\vec{\mathbf{x}}_2}, \tag{3.11}$$

where $\vec{\mathbf{x}}_i$ is the the GCRS radius vector of the i^{th} receiver. The total gravitational delay, as defined in Eq. 3.6, consists of contributions of all planets of our solar system, including the Sun, Moon and Earth. For observations close to massive bodies or the Sun, the ΔT_{grav} term has to be revised with higher-order relativistic terms (Klioner, 2003; Petit and Luzum, 2010).

3.2 The VLBI Global Observing System

The ambitious goals of GGOS require appropriate changes to be made also in the field of geodetic and astrometric VLBI. This is expected to be achievable in the era of VGOS, the next-generation VLBI system conceived by the International VLBI Service for Geodesy and Astrometry (IVS, Nothnagel et al., 2016) and with its conceptual stage dating back to the early 2000's. The main characteristics of VGOS-type observations are an unprecedented quality of delay observables, reaching few picoseconds, and a major increase in the quantity of observations per session. Ideally, the VGOS concept aims for continuous monitoring of EOP and station positions with a turnaround time to initial geodetic results of less than 24 hours. VGOS should also allow to determine positions of telescopes with a global accuracy reaching 1 mm. VGOS-type observations will thus provide the geodetic community with improved tools for Earth monitoring and significantly contribute to the maintenance of the terrestrial and celestial reference frames.

Various challenges need to be addressed from the technical and theoretical perspective in order to make the VGOS concept succeed. This includes changes made at

the very beginning, from the way how the telescopes are build to modelling of subtle phenomena at the data analysis stage. Such a holistic approach results in ongoing efforts to enhance the data recording schemes, redesign the contemporary signal chain, utilize additional and broader frequency bands, improve the global network coverage, modify scheduling approaches or test new estimation methods or models of various kinds. A visible change, compared to the present geodetic/astrometric VLBI system, is the unified telescope structure (13-m telescope reflectors, fast-slewing antennas, compact design) allowing to better handle gravitational and temperature-driven deformation of telescopes, effects still present in these systems (Lösler et al., 2019) and having a significant impact on the key VLBI products (Sarti et al., 2011). Examples of the VGOS-type and the conventional telescope of the present system, hereafter referred to as the *legacy VLBI* system, are shown in Fig. 3.2. One of the key improvements is also the redesigned VLBI signal chain, a system with broadband characteristics and designed for short-observation scans (see Sec. 3.6.1). In essence, all these improvements shall allow to significantly enhance the observation precision, decrease the measurement noise and better handle instrumental and atmospheric effects, compared to the current S/X-type system (Niell et al., 2006; Cappallo, 2014).

3.3 Microwave Signal Propagation in the Atmosphere

Electromagnetic waves are subject to various propagation effects as they traverse Earth atmosphere. Among other phenomena, signal refraction is of major concern in the analysis of space-geodetic data as it introduces an additional time delay to the observed signal and changes slightly the signal path. This additional contribution to the delay depends on the vertical profile of the atmosphere and the elevation angle of the (natural or artificial) radio source of interest. The refraction effect can be described with the refractive index n representing the ratio of the speed of light and the velocity in the medium. Due to the inhomogeneous nature of the atmosphere, n changes along the signal path. As a result, the signal passing through the ionosphere and troposphere, two major atmospheric layers in this context, is bent, which gives rise to changes of the speed and the direction of travel of the observed signal.

The ionosphere is the upper layer (50–1000 km) of the atmosphere where solar radiation (ultraviolet light and X-rays) drives the production of free electrons and ions. The delay of the signal occurring there is proportional to the slant total electron content (STEC), which is a measure of the electron density along the signal propagation path in that medium. STEC varies with local time, a geographical location of the receiver, the Sun-Earth distance and the solar activity (seasonal variation). The vertical distribution of electrons is also non-homogeneous as various ionospheric layers are subject to the ionization process in different ways (Teunissen and Montenbruck, 2017). Space geodesy allows also to estimate the total electron content (TEC) in the ionosphere based on rudimentary models, which relate slant observations to TEC in the vertical direction (Schaer et al., 1996; Sekido et al., 2003; Hobiger et al., 2006).

(a) **(b)**

Fig. 3.2 Examples of the legacy and next-generation VLBI telescopes. The legacy 26-m telescope (HARTRAO) located at Hartebeesthoek Radio Astronomy Observatory, South Africa **(a)** and the 13-m VGOS-type telescope (ONSA13SW) located at Onsala Space Observatory, Sweden **(b)**

The main property of ionospheric delays is their frequency dependence. As a result, a linear combination of dual-frequency measurements at well-separated frequencies allows to obtain ionosphere-free observables (Kedar et al., 2003) and reduce more than 99.9 % of the total ionospheric delay. With multi-frequency space-geodetic observations, the full correction can be extended to higher-order ionospheric terms. In the case of the legacy geodetic VLBI systems however, the higher-order ionospheric terms can be neglected (Hawarey et al., 2005; Petit and Luzum, 2010). The ionosphere-free VLBI delay τ_0 derived from the linear combination of dual-frequency observables can be expressed as (Hobiger et al., 2006)

$$\tau_0 = \frac{\tau_1 f_1^2 - \tau_2 f_2^2}{f_1^2 - f_2^2}, \tag{3.12}$$

with τ_1, τ_2 as the VLBI delays observed at two distinct frequencies f_1, f_2. In the case of VGOS, the delays are corrected for the ionosphere effect already at the post-correlation analysis stage, in which all used bands are synthesized to produce a single observable (Cappallo, 2014). Compared to the legacy VLBI system, the

residual ionosphere contributions are in this case further reduced (Niell et al., 2018).

Radio signals passing through the lower parts of the atmosphere (troposphere and stratosphere) are affected by refraction effects in the same manner, i.e., irrespective of their center frequency. The tropospheric path delay can be separated into *dry* (hydrostatic) and *wet* components. The hydrostatic delay is related to the refractivity of gases in the troposphere and stratosphere. It accounts for most of the total tropospheric delay and it can be modelled accurately using in situ pressure data. Expressed in the zenith direction, the (zenith) hydrostatic delay (ZHD) can be represented as (Davis et al., 1985; Petit and Luzum, 2010)

$$ZHD = \frac{(0.0022768 \pm 0.0000005)\, P_0}{f_s\,(\phi, H)}, \tag{3.13}$$

$$f_s\,(\phi, H) = 1 - 0.00266\, \cos 2\phi - 0.00000028 H, \tag{3.14}$$

where P_0 is the total atmospheric pressure in hPa at the antenna reference point. H and ϕ refer to the station orthometric height (in meters) and geodetic latitude, respectively.

The wet component accounts only for a minor part of the tropospheric delay. However, it is a quantity rather difficult to model as it depends on the water vapor content, which can change rapidly. In the data analysis, it is common practice to estimate the wet part of the tropospheric delay in the form of the zenith wet delay (ZWD) along with other geodetic parameters. The resulting ZWD is used thus as a a correction to the applied a priori troposperic delay. Mapping functions are used to obtain the total delay along the signal path (Niell, 1996; Petit and Luzum, 2010; Landskron and Böhm, 2018). The wet ($m_w\,(\varepsilon)$) and dry ($m_d\,(\varepsilon)$) mapping functions have identical forms as they are based on the continued fraction expansion of $1/\sin(\varepsilon)$, differing only by the applied coefficients. In order to account for the azimuthal asymmetry, commonly known as tropospheric gradients (GRD), the gradient mapping function ($m_g\,(\varepsilon)$) is usually represented by the $1/(\sin(\varepsilon)\tan(\varepsilon) + 0.0032)$ term (Chen and Herring, 1997). The tropospheric slant delay (TSD) for a given direction can be expressed as (Petit and Luzum, 2010)

$$TSD\,(\varepsilon, \alpha) = m_h\,(\varepsilon)\, ZHD + m_w\,(\varepsilon)\, ZWD + m_g\,(\varepsilon)\,[G_N \cos(\alpha) + G_E \sin(\alpha)]\,, \tag{3.15}$$

where G_N, G_E are the (north/east) horizontal delay gradient coefficients and α refers to the azimuth angle in which the signal is received, measured clockwise from north (Chen and Herring, 1997). The related mapping functions $m_{\{w,d,g\}}\,(\varepsilon)$ are evaluated for a given satellite/quasar elevation angle (ε) of the observation direction in vacuum.

An alternative to in situ atmospheric measurements can be globally valid models of metorological parameters (Landskron and Böhm, 2018). The tropospheric delay computed in that way can be then expressed in the slant direction using empirical mapping functions (Lagler et al., 2013; Landskron and Böhm, 2018). In addition, numerical weather models can be utilized in ray-tracing methods (Hobiger et al., 2008) with the goal of reconstructing the true signal path for the subsequent

slant delay estimation, an alternative to the parameterization of ZHD, ZWD and tropospheric gradients (Hofmeister and Böhm, 2017).

3.4 Station Displacements

Complex processes in the Earth system trigger periodic and secular changes of the Earth surface. This leads to non-linear variations of reference points of geodetic instruments, seen as both vertical and horizontal displacements. Endogenic and exogenic processes, referred to as geodynamical phenomena, are deduced from various geophysical, geodetic and geological measurements as well as based on theoretical considerations. The gravitational attraction of celestial bodies induces tidal variations (Agnew, 2007) of oceans and the solid Earth, giving rise to station displacements on the level of tens of centimeters. Another example is the ocean tidal loading (Scherneck, 2016) with a non-negligible impact on the long-term movement of station positions. Other loading effects should be also taken into account in the analysis of data obtained from space-geodetic techniques for consistent and long-time stable realization of the reference system (Petit and Luzum, 2010). The range of loading effects is wide (Desai, 2002; Ray and Ponte, 2003) and it may also include non-tidal loading series related to atmospheric pressure or oceans (Tregoning and van Dam, 2005; Williams and Penna, 2011).

In most of the station position time series, seasonal signatures with amplitudes of several millimeters are still present (Collilieux et al., 2007; Tesmer et al., 2009). As an example, hydrology loading may have a noticeable impact on the vertical deformations of geodetic reference points (Bevis et al., 2005; Eriksson and MacMillan, 2014). The inclusion of seasonal models into a priori station coordinates in the analysis of space-geodetic observations can be thus beneficial as any remaining, and unwanted, signals can easily alias geodetic products or frame parameters (Malkin, 2013; Krásná et al., 2015).

3.5 Technique-Specific Effects

There are several natural and instrumental sources that introduce unwanted effects to VLBI measurements. Many of that sources (ionosphere, troposphere, station clocks, non-tidal effects) are taken care of at the data analysis stage. When including local ties in the combination of space-geodetic techniques, some of the technique-specific effects however may still be present (Altamimi et al., 2002; Altamimi et al., 2016). Similarly to unmodelled station displacements, those effects can introduce systematic errors to the estimated geodetic parameters, if not accounted for correctly (Sarti et al., 2011).

3.5.1 Telescope Structure

The legacy VLBI system consists of radio telescopes with various mount types (elevation-azimuth, equatorial, or X-Y mounts), dimensions and slew speeds. For some of them, the primary and secondary rotation axes do not intersect. For the

reference (invariant) point on the (primary) rotation axis fixed relative to the Earth (chosen as a conceptual convenience), this results in an axis offset (AO) defined as the projection of the elevation (secondary) axis onto the primary axis. In the data analysis, the AO-related effects are accounted for and treated as an additional contribution to the VLBI delay (Sovers et al., 1998; Nothnagel, 2009). In the case of VGOS-type antennas, no or sub-millimeter axis offsets are expected and thus delays due to to this effect should be negligible.

Thermal expansion of the telescope structure (reflector, antenna tower), caused by variations in the ambient temperature, and gravitational deformation (Nothnagel et al., 2019; Lösler et al., 2019), dependent upon antenna orientation, change the antenna's focal length. This introduces additional delays and results mainly in vertical displacements of the antenna reference point. Similarly to AO, these deformation effects are considered in the data analysis and the related delay contribution is included in the VLBI delay model (Sovers et al., 1998; Nothnagel, 2009).

3.5.2 Radio-Source Structure

The intrinsic structure of radio sources can vary noticeably with frequency and time (Piner et al., 2007; Fomalont et al., 2011). This results in fluctuations in source brightness inducing time-varying changes in the location of radio sources on the celestial sky. As a consequence, radio sources exhibiting significant position variations are excluded from the group of defining sources (Fey et al., 2009). For a stable celestial reference frame, the structure effects should be correctly handled. The errors originating from the source structure are also a big fraction of the total measurement error and have a non-negligible impact on astrometric and geodetic measurements (Cotton, 1995; Sovers et al., 2002; Xu et al., 2017) as non-stationarity of radio sources causes variations of the observed delays. If left uncorrected, the extended source will have an accuracy impact. This problem will be even more pronounced in the VGOS era due to lower measurement noise (Bolotin et al., 2019) as well as more problematic due to the low values of singal-to-noise ratio (SNR) that may be used at the scheduling stage (Anderson and Xu, 2018). Apart from regular and frequent monitoring of changes in the source structure, accounting for this effect, starting from scheduling through post-correlation analysis (Cotton, 1995) to the data analysis stage (Sovers et al., 1998), is of major importance in order to obtain geodetic measurements in the absence of source effects and thus further enhance the performance of geodetic VLBI.

3.6 Data Processing

Geodetic VLBI consists of many stages, at which different sets of products are obtained. The data processing chain, with regard to either legacy or the VGOS-type system, can be divided into three main parts

- level-0: scheduling, observation, data transfer and correlation resulting in *complex visibilities*,

- level-1: amplitude and polarisation calibration, imaging, post-correlation analysis resulting in *geodetic delays*,
- level-2: geodetic data analysis resulting in *geodetic results*.

All begins with *scheduling*, where baseline-based observations are grouped into source-specific scans and created using available a priori information on station/source performance, location and characteristics. VLBI observations are organized in sessions, which differ in length depending upon the session type. During an *observation* stage several radio telescopes are used and many radio sources are observed all over the sky in a rapid sequence. After the session is finished, the recorded (raw) data at each site are transferred to a correlator facility, where *correlation* and *post-correlation analysis* take place to obtain level-0 and level-1 data. Next, *geodetic delays* are made available for the data analysis, where parameters of geodetic and astrometric interest such as EOP, station and source coordinates are derived in a global solution or on a single-session basis. Finally, *geodetic results* can be then used for frame realization or scientific investigations of various kinds.

3.6.1 Scheduling

The basis of geodetic VLBI are simultaneous observations of the same radio source by at least two stations that form a *baseline*. In the case of n radio telescopes simultaneously observing the same radio source, an instant observation geometry consists of $n\,(n-1)/2$ baselines. This set of observations comprises the so-called source *scan*. In the case of global networks, it could happen that different sets of stations participate in different scans simultaneously, realizing the concept of *subnetting*. Before a VLBI experiment takes place, one needs to create an observing plan, which facilitates coordination of observations for each station during the whole experiment. This observing plan, referred to as *schedule*, contains a time-ordered list of scans (sources to track) and stations to use, supplemented with information on station-based observing times, equipment or frequency setup. Due to the complex nature of this task, scheduling is carried out in an automatic fashion with the use of dedicated software packages, e.g., *SKED* (Gipson, 2010) or *VieSched++* (Schartner and Böhm, 2019). The created schedules are then stored as *.skd* and *.vex* files (Whitney et al., 2002), accessible via three primary IVS data center servers[7]. These ASCII files consist of the schedule itself, a complete description of the session and additional information used during scheduling. Each participating station utilizes those files in order to create station-specific procedure files (*.prc* and *.snp* files), which are then used during observations. Routine experiments for geodetic and astrometric VLBI are coordinated by the IVS. For the legacy system, the yearly observing programs consist mostly of the daily 1-hour VLBI *intensive* (INT) sessions as well as 24-hour VLBI observations that are carried out twice a week as so-called *rapid-turnaround* sessions (Nothnagel et al., 2016). IVS sessions

[7] `ftp://cddis.gsfc.nasa.gov/`, `ftp://ivs.bkg.bund.de` and `ftp://ivsopar.obspm.fr`

Tab. 3.1 IVS observing programs. Listed are S/X sessions with various applications. Although global experiments have already been carried out (24-hour VGOS test (VT) sessions) and the network has reached an operationally stable stage, VGOS is not included here due to its still not fully operational status

Session type (Session code)	Frequency	Duration	Purpose
Intensive 1 (IVS-INT1) Intensive 2 (IVS-INT2) Intensive 3 (IVS-INT3)	Weekdays Weekends Mondays	1 hour[a]	$UT1$-UTC determination
Rapid-turnaround 1 (IVS-R1) Rapid-turnaround 4 (IVS-R4)	Mondays Thursdays	24 hours	EOP & TRF determination
Research & development (IVS-RD, IVS-EURD)	Several per year	24 hours	Specific scientific & technical goals
TRF-related (IVS-T2, IVS-OHG)	Several per year	24 hours	TRF improvement
VLBA-related (IVS-RV)	Several per year	24 hours	Various geodetic & astrometric applications
CRF-related (IVS-CRD, IVS-CRF, IVS-AUA)	Several per year	24 hours	Southern hemisphere astrometry programme
Continuous VLBI campaign (CONT)[b]	Every three years	Two weeks	State-of-the-art VLBI data

[a] 2-hour session duration in the case of experiments including VLBA telescopes
[b] CONT17 included three different networks (legacy, VGOS and VLBA) and it is the last campaign representing the concept of two-week measurements

of global coverage are listed in Tab. 3.1. Other experiments cover various purposes including regional network monitoring, system improvement and scientific studies.

A typical 24-hour astrometric/geodetic experiment includes multiple stations and many scans, resulting in several hundred observations per baseline. Numerous aspects of the VLBI system such as the network geometry, observation sequence, local azimuth or elevation angles of the chosen radio sources play a major role in the quality and type of geodetic parameters that can be determined in the data analysis stage. As an example, long east-west baselines are sensitive to Earth rotation ($UT1$-UTC) and therefore are preferable when scheduling INT sessions. In the case of polar motion, a global distribution of VLBI stations is preferable for

a reliable estimation of that parameter (Nothnagel and Schnell, 2008; Nothnagel et al., 2016). Therefore, many factors need to be taken into consideration when attempting to create an optimal schedule. In general, the designed schedule should provide the highest possible quality of the parameters of interest and contain a large number of observations. This implies minimum slewing and idle times between the subsequent source scans. For legacy systems, observing and slew times are highly variable as they depend upon the antenna characteristics (slew speed, antenna sensitivity, cable wrap), whereas a similar design of VGOS antennas should diminish a negative impact of this effect. In the case of radio sources, they should exhibit a compact (point-like) structure and preferably have high flux density to avoid source loss (non-detections of observations). In order to address the estimation of parameters related to the atmosphere, observations are scheduled at different azimuth and elevation angles and telescopes usually sample as much of the sky as possible in a short period of time. The baseline-based observation time should be also long enough in order to achieve a proper SNR, which is inversely proportional to the precision of the group delay (Takahashi et al., 2000). The minimum observation time per telescope is usually chosen (with some margin) to match a predefined baseline SNR. For natural radio sources and the legacy S/X systems, SNR targets per each band are set between 15 and 25. For VGOS, those quantities are expected to be smaller in order to obtain observations after shorter integration times (Petrachenko et al., 2009). For an interferometric observation for a given band and signals sampled with the Nyquist rate, SNR can be expressed as (Shaffer, 2000)

$$\mathrm{SNR} = \frac{\eta_c \, S_f}{\sqrt{\mathrm{SEFD}_1 \, \mathrm{SEFD}_2}} \sqrt{2 \, B_{ch} \, N_{ch} \, T_{int}}, \tag{3.16}$$

$$\mathrm{SEFD}_i = \frac{2k \, T_{S_i}}{A_{e_i}} = \frac{8k \, T_{S_i}}{\eta_A \, \pi \, D^2}, \; i = \{1, 2\}, \tag{3.17}$$

where η_c (0.5 – 1) is the efficiency factor that is related to the effects due to digital sampling and correlation. S_f is the flux density of an observed radio source and is expressed in Jansky (1 Jy = $10^{-26}\,\mathrm{Wm}^{-2}\mathrm{Hz}^{-1}$). The channel bandwidth B_{ch} and the number of used channels N_{ch} are chosen at the scheduling step, both dependent upon the station hardware. T_{int} refers to the integration (observation) time and defines the scan length. The system equivalent flux density (SEFD) of an observing system (station) describes the combined sensitivity of both the antenna and receiving system (signal chain) and is associated to Boltzmann's constant k, system temperature T_{S_i} and A_{e_i} as an antenna effective area. The η_A term denotes the antenna efficiency. Low SEFD has a positive impact on scheduling and observations in general, whereas high S_f implies that a particular radio source is strong, which is preferable. Different levels of SEFD (hundreds to few thousand Jy) characterize legacy VLBI systems, whereas VGOS-type systems are expected to reach SEFDs of about 2500 Jy (Niell et al., 2018).

Besides the predefined SNR targets, additional criteria are used during scheduling in order to obtain the most optimal schedule. This is achieved by investigating

certain aspects of a scan and choose the most beneficial sequence of scans from a very large number of possible scan combinations. Based on some initial conditions that scans need to fulfill (e.g. minimum number of participating stations in the scan, minimum angular distance between adjacent radio sources, how often a particular source has to be observed), all possible scans are generated and then evaluated based upon several criteria. Among many others this can include, e.g., sky coverage, results from the covariance analysis, scan duration, number of observations or idle time. Such optimization criteria are used to assign a score to the generated and potentially usable scans, i.e., all possible successive scans are calculated and evaluated. The total score for the validated scan is the weighted sum of the subscores and the scan with the highest total score among the possible scans is then selected as the next scan and included in the schedule. This scan-selection procedure is repeated until the session end time is reached. Additional operations on the generated schedules (diminishing the idle times, optimization for target parameters) allow to further improve the observation geometry (Gipson, 2010; Gipson and Baver, 2016; Schartner and Böhm, 2019). In an alternative approach, impact factors derived based upon singular value decomposition of the design matrix can be applied as selection criteria of the VLBI observations and creation of an optimal schedule (Vennebusch et al., 2009; Leek et al., 2015).

3.6.2 Observation

Large reflector antennas with diameters (D) on the order of tens of meters have two major properties that are important in VLBI observations at millimeter or centimeter wavelengths (λ). Parabolic antennas allow to monitor only very small parts of the sky, where the target radio source is present (antenna half-power beamwidth can be approximated as $70° \cdot \lambda/D$), and significantly amplify the incoming signal (electromagnetic radiation) from distant radio sources (Baars, 2007). After being reflected by the antenna main reflector and subreflector (if present), the radio signal is focused into the feed horn. Most legacy VLBI telescopes are equipped with circularly polarized feed horns, whereas in VGOS dual linear polarization (horizontal (H) and vertical (V)) is a necessity in order to maintain high aperture efficiency over wide frequency ranges (Petrachenko et al., 2009). In the feed, the collected radiation is converted into an electrical voltage signal and then amplified by the Low-Noise Amplifiers (LNAs). At this stage (front-end) and throughout the course of observations, the phase calibration (*phase-cal*) tones (distinct tones separated by a few MHz) are continuously injected into the signal chain. In addition, a noise calibration (*noise-cal*) signal is also used between observations. Phase-cal and noise-cal are of major importance for the VLBI system. Although the implementation of the phase-cal system in S/X and VGOS differ (Niell et al., 2018), phase-cal tones are in principle used to correct for phase and delay errors introduced by various elements of the VLBI signal chain, at the part between the feed and a digitizer (Cotton, 1995). The instrumental delays differ among channels, bands, and polarizations. This is handled at the post-correlation analysis stage, in which the phases of the tones are extracted and proper calibration

is made, see Sec. 3.6.4. Typically, the phase-cal pulses are separated by 1 MHz across all channels (Whitney, 2000), whereas the VGOS system tend to have either 5-MHz or 10-MHz spacing of the tones (Niell et al., 2018) in order to avoid the risk of signal saturation. The role of the noise-cal generator is to provide a stable noise signal, which is introduced between the feed and LNA. Based on this additional signal source, accurate SEFD measurements can be obtained and correct values for the correlated flux densities of the radio sources can be derived (Thompson et al., 2017). Although the exact signal processing stages may vary between currently used VLBI receiving system solutions, the RF signal needs to undergo further modifications in order to be compatible with the VLBI standards and usable at the correlation stage. Typically, the RF signals coming from the LNAs are converted to intermediate-frequency (IF) signals, either before the digitial back-end (DBE) or inside, and then digitized and sampled inside the DBE. Several different DBEs with slightly different architecture exist, e.g., the European DBBC family (Digital BaseBand Converter, Tuccari et al., 2010; Tuccari et al., 2014; Tuccari et al., 2018), the Japanese K-type systems (Koyama, 2013), the American Reconfigrable Open Architecture Computing Hardware (ROACH) Digital BackEnd (RDBE, Niell et al., 2010), the Russian Multifunctional Digital BackEnd (MDBE, Nosov et al., 2018) or the Chinese VLBI Data Acquisition System (CDAS, Zhu et al., 2016). At the DBE stage, usually 8-bit sampling produces the digital version of the IF signals, which are further processed. In short, this includes separation of each IF signal into a predefined set of frequency channels, reduction to a 1-bit or 2-bit representation (only 2-bit quantization for VGOS), time-tagging based on the 1-pps (pulse-per-second) signal from a hydrogen maser (H-maser) and formatting using dedicated VLBI formats such as Mark 4, Mark 5B, Mark 6, K5 or the VLBI Data Interchange Format (VDIF, Whitney et al., 2010). In the last stage, the formatted (*baseband*) data are stored locally or streamed directly to a correlator facility (Whitney, 2004; Whitney et al., 2004; Whitney et al., 2014; Salminen, 2015).

Legacy (S/X) VLBI telescopes are used as dual-frequency systems capable of observing at S band (2.2 – 2.4 GHz) and X band (8.1 – 8.9 GHz). The frequency setup is usually arranged as 8 X-band channels and 6 S-band channels with 8-bit sampling, which is then reduced to 1-bit or 2-bit representation. Although higher quantization levels can improve SNR (Thompson et al., 2017), they cause the problem of a need for an increased recording space[8]. Therefore, more beneficial in geodetic and astrometric VLBI is to increase the spanned bandwidth in order to compensate for the reduced SNR, rather than increasing sample representation, see Sec. 3.6.4. Depending upon the session type and station hardware, the channel width in S/X systems usually varies from 4 to 16 MHz and recording rate is chosen typically between 128 Mbps and 1 Gbps.

VGOS is a four-band system using a broadband feed to cover the frequency range between 2 and 14 GHz[9] with the use of 1-GHz bands (Fukuzaki et al., 2015;

[8] recording rate = sampling frequency × number of bits × number of channels

[9] An initial assumption made at the conceptual stage of VGOS. The lower boundary may vary as radio-frequency interference is very problematic at lower bands (2–3 GHz). The upper

Niell et al., 2018; Haas et al., 2019) and with 2-bit representation, similarly to S/X systems. The sampled signal can be channelized with up to 16 channels of 32-MHz bandwidth (Niell et al., 2018) or alternatively one can also sample the RF signal directly (Sekido et al., 2016; Kondo and Takefuji, 2016; Tuccari et al., 2018). VGOS requirements result in data rates on the level of several Gbps, often 8 Gbps, but with the goal of using 16 Gbps or 32 Gbps, as anticipated at the conceptual stage of VGOS (Petrachenko et al., 2009; Niell et al., 2018; Haas et al., 2019).

Antenna motion and temperature changes cause stretching and twisting of the cable delivering reference signals from the H-maser to the phase-cal generator. This leads to additional systematic delay errors, which need to be handled in a proper manner as any variation correlated with the antenna orientation will introduce a systematic error (offset or variation) in the site position estimate. This issue has a similar effect in all bands (and polarizations) and is addressed with a dedicated cable measurement system, referred to as *cable-cal* and *cable-delay measurement system* (CDMS) for S/X systems and VGOS, respectively. Cable-delay measurements are carried out between scans. An additional short cable is also attached to the signal path before and right after the experiment in order to determine the cable sign (sense). The latter is needed to convert the cable-cal data to the corresponding group-delay contribution, which is included later at the data analysis stage. This helps to reduce both elevation- and azimuth-dependent cable-delay errors. Apart from the cable sense, a similar approach is used in the VGOS systems employing CDMS (Niell et al., 2018).

VLBI relies on two UTC-related reference signals, one provided by GPS and the other based upon the H-maser, a crucial component at each VLBI site. The GPS clock receiver allows to establish, with an accuracy on the level of up to one hundred ns, the time at each VLBI site relative to UTC. The much more precise and stable output from the H-maser is used to drive (synchronize) the 1-pps of the DBE (such as DBBC or RDBE) and results in data time tags of a H-maser stability. The same reference frequency signal is also common to all components of the signal chain (phase-cal, cable-cal) in order to maintain phase stability throughout the whole VLBI signal chain. The stability of the reference frequency should prevent from significant losses of coherence, on short time scales of a scan, and be sufficient enough to not introduce any significant noise into the obtained delays (Thompson et al., 2017; Niell et al., 2018).

Data acquisition at each station is controlled and carried out automatically by the field system (FS, Himwich, 2000). Based on the station-specific schedule (*.prc* and *.snp* files), FS communicates with various elements of the VLBI system, and the associated sensors, as well as steers the antenna with the use of commands sent to the antenna control unit. In addition, FS provides a set of tools that allow to carry out additional actions such as determining pointing corrections or measuring the antenna gain. During an experiment, a sequence of commands (*preob*, *midob* and *postob*) related to tracking, recording and calibration are performed for each scan and a set of related parameters is stored in a station-specific log-file. The auxiliary information from these files is used during data correlation and data analysis stages.

boundary may also be shifted towards higher frequencies

Among others, this data includes meteorological readings (temperature, pressure, wind speed and direction, relative humidity), derived system temperatures, cable-delay data and measurements of the time difference between the GPS time and the time standard provided by the H-maser.

3.6.3 Correlation

Once the experiment ends, the recorded and properly formatted data are transferred to a correlator facility for processing. Station-based signals, which are always wideband white Gaussian noise, are cross-correlated by finding the maximum of the cross-correlation function (Nothnagel, 2019) in order to obtain, as a function of time, the delay ($\tau_{ij}(t)$) in signal reception between two stations (i and j) forming a baseline. For a given observing frequency (ν), an interferometer measures precisely the relative phase ($\phi_{ij} = 2\pi\,\nu\,\tau_{ij}(t)$) of the signals at two stations in units of the observed wavelength. The correlation result is a set of such interferometric phases and correlation amplitudes, derived for a wide range of frequencies at different observation times. The fundamental observable of geodetic and astrometric VLBI is then obtained, in the subsequent stage (Sec. 3.6.4), by measuring the change in the phase over the utilized frequencies. In the case of legacy systems, one correlation product is needed, whereas for VGOS one correlates all polarization products (HH, HV, VH and VV) and then combines them coherently at the subsequent stage (Niell et al., 2018). It is also possible to use legacy and VGOS antennas simultaneously in so-called *mixed-mode* observations and then cross-correlate data streams from those two systems (Cappallo, 2014; Marknäs, 2019). The baseband data can be nowadays correlated with FX-style correlators such as the Distributed FX (DiFX, Deller et al., 2007; Tingay et al., 2009; Deller et al., 2011) software correlator, SFXC software correlator (Keimpema et al., 2015) or K-type software correlators (Koyama, 2013), which are embedded in the VLBI system. The nature of the correlation algorithm (similar operations applied on channel-by-channel basis) is very well suited for parallel computing architectures. Standard high-level programming languages and dedicated high-performance libraries allow to utilize software correlators effectively in different computing environments. In addition, software correlators can be also easily adapted to special tracking requirements and frequency setups (Duev et al., 2012; Haas et al., 2014).

Hardware correlators, used before the era of software correlators, were based on the XF algorithm, i.e., lag correlation on the raw data (X) and Fourier transform (F) to obtain cross-power spectra (Whitney et al., 2004). On the contrary, an FX-style correlator performs Fourier transform first, to obtain signal spectra ($s_i(\nu)$, $s_j(\nu)$), and then the digitized data streams are cross-multiplied to derive cross spectra ($S_{ij}(\nu)$). Based on the DiFX logic, the software correlation process can be divided into antenna-based and baseline-based operations. Most of the necessary information for correlation is contained in the experiment *.vex* file, which is supplemented with additional information on the data source (e.g. Mark 5 modules or VDIF files), EOP or offsets from GPS of the recorded time tags. In order to align all data to a common point (geocenter), first an a priori theoretical

geocentric VLBI delay for each station is computed, including also station clock offsets (and rates) w.r.t. the GPS time. All geocenter delays in the network have the same reference epoch as the time epoch is chosen to be the one when the wave front passes the geocenter. A number of samples from each telescope data stream is then selected for further processing. Prior to cross-multiplication, the data in time domain are converted into frequency-series data (channelized) through a complex fast Fourier transform (FFT) and the fringe rotation[10] and fractional-sample-error correction are applied to the data (Whitney, 2000; Deller et al., 2007). For each baseline, the channelized data are cross-multiplied on channel-by-channel basis to derive complex visibilities in the frequency domain (correlation amplitudes and interferometric phases). Correlation amplitudes $A_{ij}(\nu_m, t_n)$ and interferometric (fringe) phases $\phi_{ij}(\nu_m, t_n)$ are obtained for numerous frequency channels ν_m and times t_n, for each band/polarization. This includes also cross-polarization products in the case of dual-polarization data. Finally, the derived visibilities per spectral channel are accumulated (complex addition) for a given accumulation period, time-averaged and saved in a format convenient for geodetic post-processing (Whitney, 2000; Deller et al., 2007; Thompson et al., 2017). The level-0 data for a single geodetic observation consist therefore of a set of visibility spectra for each accumulation period (Thompson et al., 2017), representing small residuals w.r.t. the a priori model and further processed in order to produce a time delay for this observation.

3.6.4 Post-correlation Analysis

Although not perfect, the VLBI delay model and input information (e.g. source and station positions, EOP, station clocks) used at the correlation stage are usually sufficient enough to obtain a detectable signal, without the need for an adjustment of the a priori values. The reason is that the differences ($d\tau_{ij}(t)$) between the model and the reality are in this case within the search range of a correlator. The remaining interferometric phase errors ($d\phi_{ij} = 2\pi\,\nu\,d\tau_{ij}(t)$) will result in time- and frequency-dependent errors. For a single baseline, the first-order expansion of the error in the interferometric phase can be then expressed as a function of time and frequency (Cotton, 1995; Sovers et al., 1998)

$$\Delta\phi_{ij}(\nu_m, t_n) = \underbrace{\phi_{ij0}(\nu_0, t_0)}_{\substack{\text{phase offset}\\ \text{at } \nu_0 \text{ and } t_0}} + \underbrace{\frac{\partial\phi_{ij}}{\partial\nu}}_{\substack{\text{residual}\\ \text{delay}}} (\nu_m - \nu_0) + \underbrace{\frac{\partial\phi_{ij}}{\partial t}}_{\substack{\text{residual}\\ \text{delay rate}}} (t_n - t_0), \tag{3.18}$$

where $\Delta\phi_{ij}(\nu, t)$ is the residual fringe phase (in turns) and t_0 and ν_0 referring to the reference epoch and reference frequency, respectively. At the post-correlation analysis stage, commonly known as *fringe fitting*, corrections for the instrumental delays are applied and phase (ϕ_0), *residual group delay* (τ_{gd}), *residual phase-delay rate* ($\dot{\tau}_{pd}$) are fitted to the interferometric phases $\phi_{ij}(\nu_m, t_n)$ from the used

[10] The rotation of the Earth causes also frequency shift (*fringe rate*) along the line of sight to the source

frequency channels ν_m and times t_n (integration epochs). The resulting observables (in seconds) can be formulated as (Sovers et al., 1998; Thompson et al., 2017)

$$\tau_{gd} = \frac{\partial\phi}{\partial\omega} = \frac{1}{2\pi}\frac{\partial\phi}{\partial\nu}, \tag{3.19}$$

$$\dot{\tau}_{pd} = \frac{1}{2\pi\,\nu_0}\frac{\partial\phi}{\partial t}, \tag{3.20}$$

$$\tau_{pd} = \frac{\phi_0}{\omega_0} = \frac{1}{2\pi\,\nu_0}\,\phi_0, \tag{3.21}$$

where ω is the circular frequency and τ_{pd} refrerring to the *residual phase delay*. The τ_{gd}, τ_{pd} and $\dot{\tau}_{pd}$ quantities are expressed w.r.t. the correlator model. When added to the modeled delay, the *total* values of those parameters are obtained. Instrumental effects are addressed by applying delay and phase corrections to each frequency channel, based on the phase-cal signal or a strong calibrator source. The best estimates of correlation amplitudes, fringe phases, group delays and phase-delay rates are obtained by applying incremental changes to the values of group delays and phase-delay rates. A two-dimensional Fourier transform of the cross-correlation spectra is used to find the peaks of the delay/delay-rate resolution function in frequency (group delay) and time (delay rate) domains, i.e., maximize the coherent sum of all of the correlator output complex visibility points over frequency and time (Whitney et al., 1976; Whitney, 2000; Kondo and Takefuji, 2016). Fringe fitting is carried out in a specialized post-processing software such as dedicated routines (*FRING* and *MBDLY*) of the Astronomical Image Processing System (AIPS[11]) or *fourfit*, which is a part of the Haystack Observatory Post-processing System (HOPS)[12]. In the latter case, DiFX provides translation of the binary DiFX output to the HOPS-readable format (Mark4, Whitney et al., 2004), facilitating creation of databases (level-1 data) with quasar observations for the subsequent analysis.

For each baseline, the post-correlation analysis can be considered as a two-step process. In the initial stage, data for each frequency channel, frequency band and polarization are processed separately in order to obtain average phase at t_0, the residual fringe rate and rate of change (slope) of the phase within a frequency channel (τ_{gd}) referred also to as single-band delay (SBD). In the second stage, the individual channel-based estimates are combined in order to obtain one set of those parameters, with an enhanced precision of the group delay. This is realized through the bandwidth-synthesis technique (Rogers, 1970; Whitney, 2000; Shaffer, 2000; Takahashi et al., 2000; Kondo and Takefuji, 2016) where the bandwidth is virtually increased by combining all of the used channels, which are normally spread out over a much larger bandwidth using non-redundant spacing between channels. The group delay τ_g, refered to as the multi-band delay (MBD), is then found by estimating the linear phase change across multiple channels. The legacy systems utilize spanned bandwidths of 0.7 GHz at X-band[13], whereas VGOS-type observables, hereafter referred to as *broadband delays*, are derived based on a

[11] `http://www.aips.nrao.edu/aips_faq.html`

[12] `http://www.haystack.mit.edu/tech/vlbi/hops.html`

[13] S-band observations are used only for ionosphere calibration

spanned frequency range of several GHz (e.g. 7.7 GHz, Niell et al., 2018). The formal uncertainty (in seconds) of the S-band or X-band group delay (MBD) can be expressed as (Shaffer, 2000)

$$\sigma_{\tau_{gd}} = \frac{1}{2\pi\,\mathrm{SNR}\,\nu_{\mathrm{rms}}}, \tag{3.22}$$

where a factor of approximately 2.6 needs to be included in the case of a broadband observable (Niell et al., 2018) and with SNR as defined in Eq. 3.16. The ν_{rms} quantity refers to the root-mean-square spanned bandwidth, which corresponds to approximately 40 % of the total frequency span (Thompson et al., 2017) and is calculated using the channel center frequencies and their mean. In terms of a single-observation quality, the commonly used frequency-channel configuration leads to the precision of few tens of picoseconds for S/X systems and few picoseconds for broadband delays (Niell et al., 2018). In summary, fringe fitting provides baseline-based correlation amplitudes, residual phase delays, SBDs, MBDs and residual phase-delay rates, all expressed near at the middle of each scan. This results in X-band and S-band observables for the legacy system and a broadband delay for VGOS. An example of the delay-resolution function for multi-band delay and delay rate, derived for an X-band observation, is shown in Fig. 3.3.

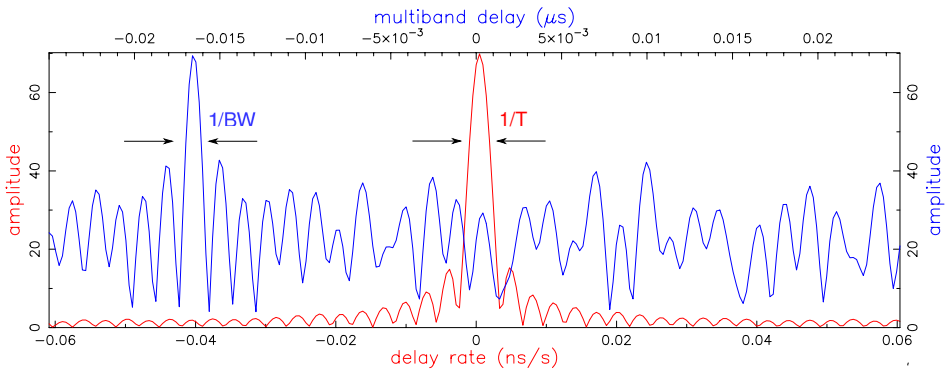

Fig. 3.3 The residual multi-band delay and residual phase-delay rate for an X-band observation. The multi-band delay (blue) obtained by synthesizing 8 channels with the bandwidth of 8 MHz. The width of the peak of the multi-band delay is inversely proportional to BW, which is the total bandwidth spanned by all channels. In the case of the delay rate (red), a similar relation occurs in connection to the scan length (T), also referred to as the integration time. The plot created with fourfit 3.11 rev 1142

Correctly aligned phases among frequency channels are necessary for obtaining MBDs, especially for VGOS, where the output from the four possible linear polarization combinations provides the broadband observables. Instrumental effects can affect each frequency channel differently resulting in different SBD per channel or a group of channels within a band, as mentioned in Sec. 3.6.2. Phases of phase-cal

tones, embedded in the observed signal, allow to use phase-cal-derived delays[14] and correct the data for those instrumental effects as any changes experienced by the IF signal affect similarly the accompanying phase-cal signal (Whitney et al., 1976; Cappallo, 2014; Cappallo, 2016). For VGOS, any remaining differences of delay and phase between the two polarizations, not addressed using the phase-cal approach, are also reduced at the post-correlation analysis stage (Niell et al., 2018). In the case of a corrupted phase-cal system or problems with using it, one can align phases manually (*manual phase-cal mode*) with the use of strong and reliable radio sources (Cotton, 1995; Shaffer, 2000). In this case however, one would loose track of the time-dependent instrumental delay changes at the observing sites. An alternative approach to the utilization of phase-cal systems could be direct RF sampling, applicable to both S/X and VGOS systems (Takefuji et al., 2012; Sekido et al., 2016; Kondo and Takefuji, 2016).

The most precise delay measurements possible can be achieved with the use of phase delays. The formal error of τ_{pd} is inversely proportional to SNR and ν_0 and can be expressed (in seconds) as (Takahashi et al., 2000)

$$\sigma_{\tau_{pd}} = \frac{1}{2\,\pi\,\nu_0\,\mathrm{SNR}}. \tag{3.23}$$

For the sake of completeness, the precision of the phase-delay rate (in seconds) can be formulated as

$$\sigma_{\dot{\tau}_{pd}} = \frac{\sqrt{12}}{2\pi\,\nu_0\,T_{int}\,\mathrm{SNR}}, \tag{3.24}$$

assuming that the samples are spaced uniformly in time (Takahashi et al., 2000). For frequency bands used in geodetic/astrometric VLBI, τ_{gd} is much less precise than τ_{pd} as $\nu_0 \gg \nu_{\mathrm{rms}}$. However, phase-delay measurements are ambiguous by the integer number of turns (cycles) with a small phase-delay ambiguity ($1/\nu_0$). The latter factor makes this observable problematic to use on global scales for frequencies commonly used in geodetic VLBI. It is hard to obtain an accurate a priori VLBI delay if the theoretical models are imprecise (telescope or source position errors, a lack of sufficient knowledge concerning EOP) and unmodelled phase errors exist (residual tropospheric and short-term ionospheric variations, instrumental errors). For baseline lengths on the order of a few thousand of kilometers, this implies a problem of solving for the phase-delay ambiguities, which need to be known prior to the geodetic analysis (Herring, 1992). In differential VLBI (Thompson et al., 2017) however, in addition to media errors, observations of pairs of nearby radio sources allow to address the problem of the ambiguous phase in a correct manner. The same can be achieved with radio telescopes located in close vicinity and observing the same radio source. The latter approach poses an attractive way for establishing local ties between legacy and VGOS antennas (Herring, 1992; Marknäs, 2019). Nevertheless, τ_{gd} is still the primary observable used in global geodetic VLBI observations. This may however change in the future

[14] multiple tones per channel are usually extracted (multi-tone phase-cal mode) and the correction is made for a delay within each channel as well as between the channels

with new ways for addressing the phase-delay ambiguity problem (Hobiger et al., 2009a) as well as with an improved a priori knowledge of geometric delays and a minimal contribution of all elements of the VLBI system (H-maser, antenna structure, various components of the signal chain) to the delay errors. In order to succeed, all those effects have to be controlled to much better than the phase-delay ambiguity.

Radio-Frequency Interference

Radio-frequency interference (RFI), understood as a disturbance of an observed signal by an external artificial radio source, can significantly and easily corrupt VLBI observations. For S/X systems, RFI was always of great concern as radio is widely used in modern technology and becomes even more problematic, especially for VGOS due to the frequency ranges it covers. If an external signal is picked up by an antenna via mainlobe, sidelobes or backlobes, high-power transmitters, such as ship radars or aircraft avoidance radars, can damage LNAs of the VLBI receiver. In terms of the quality of observations, RFI increases the SEFD of an antenna and degrades the baseline-based SNR in the affected channel. As the channel-related SNR is smaller, the phase error is larger leading to the reduced contribution of that channel in the determination of the group delay (fitting a slope across the channels). Moderate RFI levels (less than 50 % of the increase in the system noise in one channel) can cause noticeable group-delay biases, on the level of tens of picoseconds, besides the increased noise of the derived group delays (Shaffer, 2000). In the case of very strong RFI, it is sometimes also necessary to exclude the contaminated channels from the bandwidth synthesis in order to still obtain an usable observation, with the cost of its larger uncertainty. To minimize the susceptibility of VLBI to RFI, one could aim for an optimal frequency selection to avoid known sources of RFI or block out the unwanted signals by additional RF filters in the VLBI front-end. Another solution would be to derive regions of avoidance, which would be known right at the scheduling stage, in order to still maximize the sky coverage at the station, but prevent damaging LNAs by strong RFI sources present in the vicinity of a radio telescope (Niell et al., 2018).

Data Formats

The post-correlation processing provides VLBI observables along with the related information, both stored into databases (level-1 data) for the subsequent data analysis stage. The databases are made available through the IVS[15]. Previously, a few different database formats existed, which differed in terms of their flexibility, readability, data structure and the information content. An example can be the Mark 3 database (Mk3-DB, Gipson, 2012), a binary format used to store observables, correlation output and some auxiliary information for data analysis (meteorological data and geophysical models). The degree of modifications made to the database was indicated by its different version. The database containing only

[15] `ftp://cddis.gsfc.nasa.gov/pub/vlbi/ivsdata/`

the raw correlator output was marked as a version-1 database, whereas version-4 databases contained modified observations (after ionosphere correction, ambiguity resolution and outlier removal) and auxiliary information including meteorological data and cable-delay (relative to the beginning of each session) information. Based on version-4 of Mk3-DB, a subset of data necessary for a proper VLBI analysis was also exported to National Geodetic Survey (NGS) cards[16], one for each session. An NGS card was a single ASCII file with the human-readable content allowing for an easy-to-implement data interface.

The increasing requirements of VGOS, related to huge amounts of data, increasing number of stations, new observables as well as new types of session-related information, necessitated also the revision of data structures used in geodetic/astrometric VLBI. The VLBI Global Observing System Data Base (vgosDB, Gipson, 2014) became recently the new VLBI data format, officially replacing the MK3-DB/NGS for both S/X and VGOS systems. The new format provides a more compact data structure with an enhanced performance and possibility of including new data types into the session database. In vgosDB, one relies on the Network Common Data Form (NetCDF) format[17]. The latter is an open standard commonly used in the scientific community and designed for the fast data access. Similarly to Mk3-DB, different versions of the same database exist and the information content of a session in the vgosDB format includes correlation data, input from log-files and some necessary external information. The whole process concerning the database creation is carried out with a set of dedicated utilities (Bolotin et al., 2016). Data with the different information content are stored in individual NetCDF files (*.nc* files), separating in this way the data of different origin and use (meteorological data, group-delay observables, SNR values). The *.nc* files are also archived in separate directories, depending upon their scope (scan, observation, station). The list of files and directories in the database is present in the so-called *wrapper*, which is an ASCII file located in the main session directory and facilitating the data management within a session. In addition, any new operation on the database, resulting in the new database version, leads also to the new version of both the *.nc* files and the wrapper. The vgosDB data structure is illustrated in Fig. 3.4.

3.6.5 Data Analysis

The data analysis is the final stage of the processing chain and, in principle, similar schemes apply to both S/X-type and VGOS-type observations. The delay models discussed here are applicable in general to either group delays or phase-delay observations. The delay rates may be included in the analysis, but the benefit of using those observations is marginal (Takahashi et al., 2000). In the following subsections, the most important aspects of the parameter estimation process in geodetic VLBI are highlighted.

[16] `ftp://cddis.gsfc.nasa.gov/pub/reports/formats/ngs_card.format`
[17] `http://www.unidata.ucar.edu/software/netcdf/`

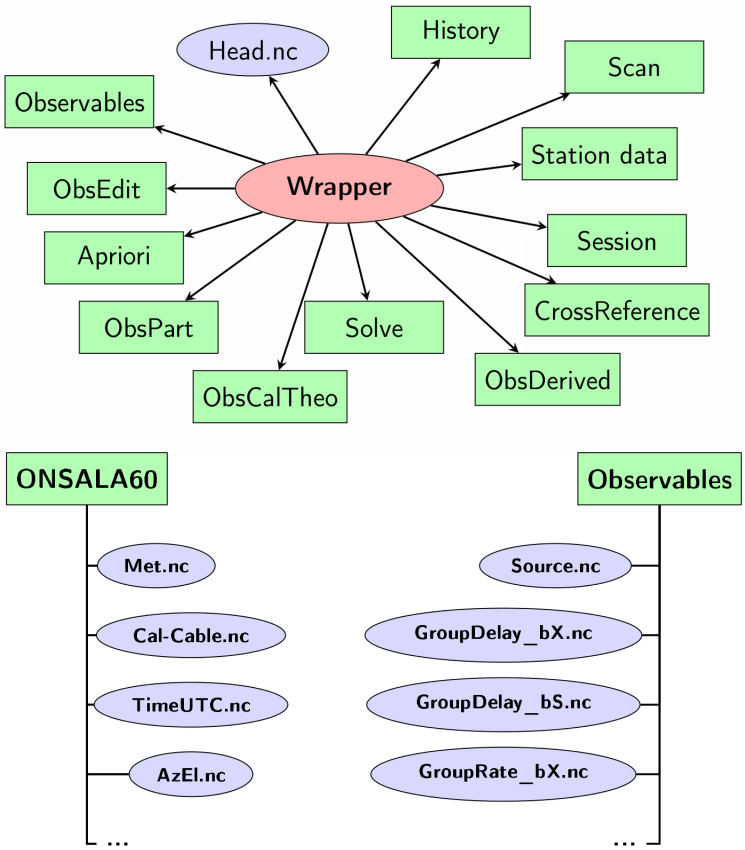

Fig. 3.4 Data organization in the vgosDB format. The *.nc* files (purple ellipses) are located in different session catalogues (green rectangles). The data access and management is facilitated with the wrapper (red ellipse), which is an ASCII file containing names of all session directories and files stored in the database. Fig. 3.2 from Klopotek (2017)

Ambiguities in the Bandwidth Synthesis

The bandwidth-synthesis technique is an efficient method for increasing the precision of group-delay observables without the necessity of recording continuous bandwidths of one GHz or more. However, the obtained observables contain an unknown number of integer ambiguities, which in delay corresponds to the inverse of the greatest common-frequency difference (Takahashi et al., 2000). Any unresolved delay ambiguities will propagate into the estimated geodetic parameters and, therefore, they need to be known prior to the VLBI analysis and parameter estimation. For the S/X and VGOS systems, the the group-delay ambiguity spacing τ_{amb} is

quite large and stringent a priori delay knowledge is not required, as opposed to phase-delay ambiguities. Typical geodetic VLBI frequency setups (IVS-R1, IVS-R4) produce usually τ_{amb} of 50 ns and 100 ns for X-band and S-band observations, respectively. In the case of VGOS, a typical VGOS frequency setup (Niell et al., 2018) should result in τ_{amb} of 31.25 ns (for the 32-MHz spacing). For sessions including multiple baselines, the ambiguity resolution can be carried out with different methods (Kareinen et al., 2016; Corbin et al., 2017), which rely mainly on the closure analysis of group delays and a rudimentary parametrization (clock polynomials and local tropospheres) applied during the ambiguity-detection process. In the case of experiments with single-baseline observations, such as INT sessions, τ_{amb} is less problematic as no closure conditions are needed in the process of obtaining ambiguity-free group delays (Hobiger et al., 2010). It is assumed that all ambiguities are detected properly if the post-fit residuals are much smaller than τ_{amb}. Once the ambiguities are resolved, the X- and S-band data are used to derive ionosphere-free observables (Eq. 3.12). In the case of VGOS observations, the TEC difference (dTEC) between stations forming a baseline is estimated simultaneously with the group delay and phase-delay rate, as a result, leading to an improved ionosphere calibration of broadband delays (Cappallo, 2014; Cappallo, 2016; Niell et al., 2018). Data stored in vgosDB version-4 (or higher) contain ambiguity- and ionospere-free observations. Such modified data are usually a starting point for the data analysis carried out with different VLBI analysis software packages, which are used to derive a wide range of geodetic parameters. Among other programs capable of processing VLBI data (Klopotek et al., 2016), a list of such packages includes (in no particular order) *Calc/Solve* (Ma et al., 1990), *OCCAM* (Titov et al., 2004), *νSolve* (Bolotin et al., 2014), *VieVS* (Böhm et al., 2018), *Where* (Kirkvik et al., 2017), *ivg::ASCOT* (Artz et al., 2016), *DOGS-RI* (Schmid et al., 2015) and *c5++* (Hobiger et al., 2010).

Parameter Estimation

In the data analysis, the least-squares (LSQ) approach addresses the problem of deriving values of parameters of a mathematical model based on a set of observations (or data), which are subject to errors. In general, the more observations that are available, the more accurately it will be possible to calculate the parameters in the model, leading to the topic of solving an over-determined linear/non-linear system of equations and the condition that minimizes the weighted sum of square residuals. The latter corresponds to the difference between the observed (O) and the sum of computed (C) and adjusted (ΔC) values. The C part is modelled with some uncertainty of the models used for that purpose. In the process of detecting ambiguities, it is important to keep the $(\text{O} - (\text{C} + \Delta\text{C}))$ differences smaller than the ambiguity spacing.

The functional Gauss-Markov model $\mathbf{f}(\mathbf{x})$ expresses the mathematical relationship between n independent observations stored in $\mathbf{y}$ and m target parameters

stored in $\mathbf{x}$ as

$$\mathbf{y} + \mathbf{v} = \mathbf{f}(\mathbf{x^0}) + \mathbf{A}\,\mathbf{\Delta x}, \tag{3.25}$$

$$\mathbf{v} \sim N\left(0, \sigma^2 \mathbf{W}^{-1}\right), \tag{3.26}$$

where $\mathbf{v}$ is the vector of residuals which is expected to be zero. In order to solve Eq. 3.25, precise models are used to linearize all parameters to a first approximation with the use of the first-order Taylor series around the a priori values $\mathbf{x^0}$

$$\mathbf{A} = \frac{\partial \mathbf{f}(\mathbf{x})}{\partial \mathbf{x}}\Big|_{\mathbf{x}=\mathbf{x^0}}. \tag{3.27}$$

The design matrix $\mathbf{A}$ consists of all possible partial derivatives of $\mathbf{f}(\mathbf{x})$ w.r.t. the estimated parameters $\mathbf{x}$ and evaluated at $\mathbf{x^0}$. For n observations and m estimated parameters, $\mathbf{A}_{n\times m}$ is given as

$$\mathbf{A}_{n\times m} = \begin{bmatrix} \frac{\partial \tau_1}{\partial x_1} & \cdots & \frac{\partial \tau_1}{\partial x_m} \\ \frac{\partial \tau_2}{\partial x_1} & \cdots & \frac{\partial \tau_2}{\partial x_m} \\ \vdots & \vdots & \vdots \\ \frac{\partial \tau_n}{\partial x_1} & \cdots & \frac{\partial \tau_n}{\partial x_m} \end{bmatrix}. \tag{3.28}$$

An adjustment (ΔC) to the calculated delays is made based on the set of chosen solve-for parameters. The estimation process uses the residual vector $\mathbf{l}$, which contains O − C and $\mathbf{\Delta x}$ denoting the estimated corrections to the solve-for parameters

$$\mathbf{l}_{n\times 1} = \begin{bmatrix} \tau_1 - {\tau^0}_1 \\ \tau_2 - {\tau^0}_2 \\ \vdots \\ \tau_n - {\tau^0}_n \end{bmatrix}, \tag{3.29}$$

$$\mathbf{\Delta x}_{m\times 1} = \mathbf{x} - \mathbf{x^0} = \begin{bmatrix} x_1 - x_1^0 \\ x_2 - x_2^0 \\ \vdots \\ x_m - x_m^0 \end{bmatrix}, \tag{3.30}$$

where $\tau_n - {\tau^0}_n$ is the difference between the observed and calculated delay for the n^{th} observation and $x_m - x_m^0$ denotes the difference between the true parameter value and the modeled equivalent for the m^{th} parameter. Typically, the (stochastic model) weight matrix ($\mathbf{W}$) is built under the assumption of no correlations between observations and that the observational noise equals the measurement noise. The diagonal matrix in this case consists of the formal errors of observations as present

in the database

$$\mathbf{W}_{n\times n} = {\sigma_0}^2\,{\mathbf{Q_{ll}}}^{-1} = {\sigma_0}^2 \begin{bmatrix} 1/\sigma_1^2 & & \\ & \ddots & \\ & & 1/\sigma_n^2 \end{bmatrix} \tag{3.31}$$

and assuming that the stochastic errors related to observations are normally distributed and are described by the known cofactor matrix $\mathbf{Q_{ll}}$ and the a priori variance of unit weight ${\sigma_0}^2$ (common-variance level). The uncertainty of a single observable in this case depends only upon the signal strength, sensitivity of the antennas, frequency sequence and the recording rate, as given in Eq. 3.22. The solve-for parameters (their correction w.r.t. the a priori) can be formulated as

$$\mathbf{\Delta x} = \left(\mathbf{A}^T\,\mathbf{W}\,\mathbf{A}\right)^{-1}\,\mathbf{A}^T\,\mathbf{W}\,\mathbf{l} = \mathbf{N}^{-1}\,\mathbf{b}, \tag{3.32}$$

$$\mathbf{v} = \mathbf{A}\,\hat{\mathbf{x}} - \mathbf{l}, \tag{3.33}$$

$$\mathbf{C_{xx}} = \hat{\sigma}_0^2\,\left(\mathbf{A}^T\,\mathbf{W}\,\mathbf{A}\right)^{-1}, \tag{3.34}$$

$$\hat{\sigma}_0^2 = \frac{\mathbf{v}^T\,\mathbf{W}\,\mathbf{v}}{u}, \tag{3.35}$$

with $\mathbf{N} = \left(\mathbf{A}^T\,\mathbf{W}\,\mathbf{A}\right)^{-1}$ as the NEQ matrix, $\mathbf{b} = \mathbf{A}^T\,\mathbf{W}\,\mathbf{l}$, $u = n - m$, $\mathbf{C_{xx}}$ referring to the variance-covariance matrix of the estimated parameters and $\hat{\sigma}_0^2$ is the a posteriori variance of unit weight. The errors of the estimated parameters are represented by the square root of the diagonal elements of $\mathbf{C_{xx}}$. The off-diagonal elements denote the correlations (covariances) between the estimated parameters. The correlation coefficient ($\rho_{a,b}$) between parameters a and b is then

$$\rho_{a,b} = \frac{\mathbf{C_{xx}}(a,b)}{\sqrt{\mathbf{C_{xx}}(a,a)\,\mathbf{C_{xx}}(b,b)}}, \tag{3.36}$$

where $\mathbf{C_{xx}}(a,b)$ is the covariance between parameters a and b, whereas $\mathbf{C_{xx}}(a,a)$ and $\mathbf{C_{xx}}(b,b)$ correspond to variances of a and b, respectively. The combination of space-geodetic techniques on the observation level is simply the procedure of generating technique-specific matrices, as defined above, stacking them and then addressing Eq. 3.32 with a reasonable weighting scheme (Hobiger and Otsubo, 2014).

The goodness-of-fit (χ^2) test indicates the correctness of the used model for the processed observations, in the presence of only Gaussian noise. A rather simple weighting scheme realized with $\mathbf{W}$ leads to uncertainties of the estimated parameters that are often too optimistic. This is usually verified with the use of external sources such as comparison of measurements from simultaneous or close-in-time VLBI sessions or based on products derived from other space-geodetic techniques. If the measurement error would be the only contributor to the error budget and if we could model the observations almost perfectly, χ^2 of the session would be close to unity. In more strict terms

$$\frac{\chi^2_{u,1-\alpha/2}}{u} < \hat{\sigma}_0^2 \leq \frac{\chi^2_{u,\alpha/2}}{u}, \tag{3.37}$$

where α is the significance level. In reality however, $\hat{\sigma}_0^2$ is much higher than unity, which indicates the presence of other error sources or remaining modeling errors increasing observation noise and, in some cases, introducing correlation between observations as in the case of station-dependent effects such as clock noise or atmospheric turbulence (Gipson, 2007). Typically, the observed measurement errors are reweighed (inflated) until $\hat{\sigma}_0^2 \approx 1$ in order to obtain more realistic uncertainties of the target parameters. There are many ways to alter the data weights such as adding (in quadrature) a constant session-dependent factor to all observations. This scheme of course can be also station-specific or realized on baseline-per-baseline basis. For each baseline, the simplest approach would be also to add an observation noise represented by the combined effect of two mapping functions (elevation-dependent down-weighting). The weight matrix can be also refined using more sophisticated strategies to improve the stochastic model of space-geodetic observations (Tesmer and Kutterer, 2004; Gipson et al., 2008; Halsig et al., 2016) or introduce variance re-weighting methods (Hobiger and Otsubo, 2017), both with the goal of the decreased (post-fit) baseline scatter, more realistic formal errors and a better agreement between VLBI-derived products and the corresponding estimates from other space-geodetic techniques.

An alternative choice to the LSQ method can be the utilization of the Kalman filter (KF, Kalman, 1960), which has already been known to space geodesy and the geodetic VLBI analysis (Herring et al., 1990; Nilsson et al., 2015; Karbon et al., 2017). At each observation epoch, the target parameters are estimated by an optimal combination of the available observations and a user-defined stochastic model, with the target parameters expressed as stochastic processes. In this case, only knowledge from the previous epoch is required for a parameter estimate at a given epoch. The benefit of using KF is mostly the reduced computational cost and estimation of instantaneous changes of the target parameters. While the accuracy of the KF algorithm improves as more observations are incorporated, a Kalman smoother (Bar-Shalom et al., 2001) can eliminate this issue. A rigorously chosen stochastic model can be also beneficial for an enhanced analysis of space-geodetic observations using KF (Nilsson et al., 2015; Soja et al., 2015).

The results of all individual experiments can be collected and analyzed together in a *global solution*, as mentioned in Sec. 2.3. This is usually a two-step procedure where first the epoch-wise parameters (clock and/or troposphere parameters) are eliminated from the session-wise NEQ systems (parameter pre-elimination) and then k equations are obtained

$$\mathbf{N_k}\,\mathbf{x_k} = \mathbf{b_k}, \tag{3.38}$$

$$\mathbf{A_k}^T\,\mathbf{W_k}\,\mathbf{A_k}\,\mathbf{x_k} = \mathbf{A_k}^T\,\mathbf{W_k}\,\mathbf{l_k}, \tag{3.39}$$

and with $\hat{\sigma}_{0k}^2$. In the subsequent step, the modified and properly arranged NEQ systems (must be of the same size) are combined (stacked) to derive one set of target parameters, such as station positions, EOP or radio source coordinates

(Seitz, 2015)

$$\mathbf{N_c} = \mathbf{N_1} + \cdots + \mathbf{N_k}, \tag{3.40}$$

$$\mathbf{b_c} = \mathbf{b_1} + \cdots + \mathbf{b_k}, \tag{3.41}$$

$$\mathbf{\Delta x_c} = \mathbf{N_c}^{-1}\,\mathbf{b_c}. \tag{3.42}$$

The combination on the NEQ level carried out in such fashion is also commonly utilized for an inter-technique combination of space-geodetic techniques (Thaller et al., 2007; Artz et al., 2012; Thaller et al., 2014; Sośnica et al., 2019), also applicable to the cases when different software packages are used to provide the NEQ systems for the combination procedure (Rothacher et al., 2011; Seitz et al., 2012).

Parameter Constraining

The data analysis with the LSQ method can be supplemented with additional, often artificial, conditions introduced to the solution at the observation level. These auxiliary conditions, hereafter referred to as *constraints*, generally tend to be beneficial whenever the utilized observations (geometry) is not very sensitive to a subset of the estimated parameters or to address high correlations between specific parameter types. Another example is the singularity of the NEQ system, which necessitates the utilization of additional information to obtain a system of linearized normal equations that is invertible (Kotsakis and Chatzinikos, 2017). The constraints are introduced to the estimation process as pseudo-observations. For z of such conditions, the observation equation in the linearized form is extended with

$$\mathbf{v_h} = \mathbf{H}_{z\times m}\,\mathbf{\Delta x}_{m\times 1} - \mathbf{h}_{z\times 1}, \tag{3.43}$$

with the vector of (reduced) pseudo-observations $\mathbf{h}$ and the Jacobian matrix $\mathbf{H}$ representing the functional relationship between pseudo-observations and the target parameters. The related weight matrix for such constraints can be defined in a fashion similar to the actual observations

$$\mathbf{W_h} = {\sigma_0}^2\,\mathbf{Q_{hh}}^{-1} = {\sigma_0}^2 \begin{bmatrix} 1/({\sigma_h}^2)_1 & & \\ & \ddots & \\ & & 1/({\sigma_h}^2)_z \end{bmatrix}_{z\times z}, \tag{3.44}$$

where cofactor matrix $\mathbf{Q_{hh}}^{-1}$ is diagonal as usually one considers no correlations between pseudo-observations. The solution with the constrained parameters can be obtained by combining the original observation geometry, as in Eq. 3.32, with the auxiliary conditions in Eq. 3.43 to obtain an extended NEQ system and corrections to the approximate values of the target parameters (Kotsakis, 2013)

$$\mathbf{\Delta x} = \left(\mathbf{N} + \mathbf{H}^T\mathbf{W}\mathbf{H}\right)^{-1}\,\mathbf{b} + \left(\mathbf{N} + \mathbf{H}^T\mathbf{W}\mathbf{H}\right)^{-1}\,\mathbf{h}, \tag{3.45}$$

with the degrees of freedom u increased by the number of the applied pseudo-observations. The employed constraints can be expressed in absolute terms and imposed upon the specific parameters, applied in a relative sense (relative constraints) or used as additional conditions to address the singularity of the NEQ system. Depending upon the values stated in $\mathbf{W_h}$, the applied constraints can be loose, moderate or tight. In the simplest case, an absolute constraint enforces the estimated parameter to be equal to its a apriori value with an uncertainty as defined in $\mathbf{W_h}$ for that pseudo-observation. This simple parameterization can be used to restrain any type of biases (clock biases, range biases) to any given value or magnitude. Another example could be station heights that are constrained to their a priori values, in the case of observations with a poor geometry. In this case, $\mathbf{v_h}$ is a zero vector and only the stochastic part is included in the estimation process. Lastly, the relative constraints refer to the case where differences between two consecutive parameters are subject to parameter constraining. Additional pseudo-observations are applied in this case in order to prevent the estimated parameters from large variations in time. This particular type of constraints is often used when estimating relative clock values or troposphere parameters (Artz et al., 2012). Such constraints are also useful in the solutions containing observation gaps, a situation that is not very uncommon in the case of VLBI observations.

Rank Defect and Datum Constraining

Geodetic observations prevent from a reliable definition of all components of the coordinate system (origin, orientation, and scale) with respect to which the station positions are estimated. In geodetic network adjustment, this leads to a rank-deficient system of NEQ. This problem is addressed by implying a set of auxiliary conditions, usually either by 1) constraining an individual set of station coordinates to known values or 2) by nullifying some or all of the Helmert transformation parameters between the sought solution and a set of known coordinates of carefully chosen reference (defining) stations. The latter actions are more commonly known as so-called minimal constraints (MC) and are realized in the form of no-net-translation (NNT), no-net-rotation (NNR) or no-net-scale (NNS) conditions. In the case of radio sources and their coordinates, this corresponds to NNR conditions realized with the use of a group of well-defined radio sources. In the case of global solutions (implying longer time spans), the set of NNT/NNR conditions is extended with their first time derivatives as one usually solves in that case for both station coordinates and station velocities (Petit and Luzum, 2010).

The aim of MC is to define components of the coordinate system without altering the internal geometry as defined by observations. The number of MC should always correspond to the rank defect of the original NEQ (Altamimi et al., 2002; Petit and Luzum, 2010). The principal difference between the two aforementioned schemes is that the first one enforces the estimated coordinates to be equal to their a priori values[18], whereas with the second one (MC) one expresses the estimated station

[18]to a given constraint, which can be tight or loose, alternatively by fixing coordinates of several stations to a priori values. If the datum constraints rely on real information of higher accuracy,

coordinates in the same TRF as the one represented by the a priori positions of reference stations. The configuration and quality of the chosen stations play a significant role in the MC conditions as position errors at some sites will be distributed within the whole network. A varying number of stations used for MC can affect also global geodetic parameters such as Earth rotation parameters (ERP), which refer to polar motion and the Earth rotation. The type of the rank defect (rotation, translation or scale) requires theoretical considerations, which take into account the nature of a particular space-geodetic technique or techniques. In the case of geodetic VLBI, the estimation of station positions while keeping the EOP fixed implies the rank defect of three and the utilization of the NNT condition as the technique itself is not directly sensitive to the frame origin, see Sec. 6.4.1.

Geodetic VLBI Analysis

Geodetic VLBI observations are utilized for the routine EOP estimation, TRF realization and also to derive parameters of physical models, described in previous sections and used to calculate the VLBI delays (Sovers et al., 1998). The delay residual, hereafter defined as the difference between the observed and modelled delay, can be used to derive numerous parameters of interest. This is feasible thanks to observations that are carried out at different times or pointing directions, also by using numerous baselines and multiple radio sources. The VLBI observation model can be formulated as a geometric delay τ_g, as defined in Eq. 3.5, and delay contributions of various nature

$$\begin{aligned} \tau_{21}(t) &= \overbrace{t_2 - t_1}^{\tau_g} + \overbrace{\tau_{\text{clk2}} - \tau_{\text{clk1}}}^{\Delta\tau_{\text{clk}}} + \overbrace{TSD_2\left(\varepsilon_2, \alpha_2\right) - TSD_1\left(\varepsilon_1, \alpha_1\right)}^{\Delta\tau_{\text{trop.}}} \\ &\quad + \Delta\tau_{\text{iono.}} + \Delta\tau_{\text{thermalDef.}} + \Delta\tau_{\text{axisOffset}} + ... + \varepsilon, \qquad (3.46) \\ TSD_i\left(\varepsilon_i, \alpha_i\right) &= m_h\left(\varepsilon_i\right) ZHD_i + m_w\left(\varepsilon_i\right)\ ZWD_i \\ &\quad + m_g\left(\varepsilon_i\right)\left[(G_N)_i \cos\left(\alpha_i\right) + (G_E)_i \sin\left(\alpha_i\right)\right],\ i = \{1, 2\}, \qquad (3.47) \end{aligned}$$

where $\Delta\tau_{\text{thermalDef.}}$ and $\Delta\tau_{\text{axisOffset}}$ are the delay contributions due to the thermal deformation and axis-offset effects at stations forming a baseline, respectively. In this case, $\Delta\tau_{\text{iono.}}$ is the residual ionosphere delay after ionosphere correction. Under the varying observing geometry, the model parameters usually affect the observed VLBI delays differently. This is reflected in partial derivatives of $\tau_{21}(t)$ w.r.t. the target parameters. For a subset of typically estimated parameters, the partial derivatives can be formulated as (Petit and Luzum, 2010)

$$\begin{aligned} \frac{\partial\tau_{21}(t)}{\partial\tau_{clk}^{poly}} &= \begin{bmatrix} 1 & t - t_0 & (t - t_0)^2 \end{bmatrix}, \qquad (3.48) \\ \frac{\partial\tau_{21}(t)}{\partial ZWD_i} &= a\, m_w(\varepsilon_i), a = \begin{cases} -1, & \text{if } i = 1 \\ 1, & \text{if } i = 2 \end{cases}, \qquad (3.49) \end{aligned}$$

this effect would then improve the solution while distorting the adjusted network

where t_0 is as an arbitrarily chosen reference epoch and τ_{clk}^{poly} referring to the quadratic clock polynomial expressed w.r.t. to the reference station in the network and calculated for both stations of a baseline. For poor spatio-temporal observing geometries, the partial derivatives may be similar (Nothnagel et al., 2002), which does not allow for obtaining reliable results. Hence, VLBI telescopes observe, throughout the course of an experiment, multiple radio sources, which are distributed almost uniformly on the local skies, and the minimum observation elevation angles tend to be as low as 5°. Likewise, radio sources used during an experiment cover as wide regions of the celestial sky as possible. However, this also depends upon the global distribution of the participating stations.

The quantity of estimated parameters and their type depend largely upon the used network and the analysis goals. There is no universal parameterization that could be applied to all sessions. At the final data analysis stage, a rudimentary parameterization includes however, at minimum, estimation of three site coordinates per station, ZWD per station and linear clock parameters, which account for the imperfect synchronization between the H-masers, expressed w.r.t. an arbitrarily chosen reference station in the network. For a reference station, the clock parameters are kept fixed. If the clock of the reference station varies from UTC, this effect will also introduce some errors (Takahashi et al., 2000; Hobiger et al., 2009b). Station-specific parameters are usually complemented with a number of global parameters, which are common to the entire network. This includes EOP/ERP or positions of the radio sources (two angular parameters per source). The distinction is also made between epoch-wise parameters (clocks, ZWD, GRD) and a set of estimates that is valid for the whole session (station coordinates, EOP[19]). Epoch-wise parameters are usually derived based on a piece-wise linear (PWL) function[20] with an hourly or sub-hourly resolution (Rothacher et al., 2011). INT sessions, which are devoted to $UT1$, consist usually of single-baseline observations. In this case, only several (5-6) parameters are estimated, i.e., relative clock parameters (clock polynomial or the PWL offset) at one site, ZWD offset for two stations forming the baseline and *UT1-UTC* (Kareinen et al., 2016). An analysis including global 24-hour VLBI sessions, see Tab. 3.1, allows for deriving a larger set of parameters. This includes station positions, ZWD, GRD, EOP/ERP or source positions. These parameters can be estimated in various ways such as by using PWL offsets or cubic splines (Rothacher et al., 2011; Artz et al., 2012). The estimation of all station positions of the network, while not solving for EOP/ERP, requires NNT conditions to be applied. In case the solve-for parameters include station positions and EOP/ERP, both NNT and NNR conditions are introduced in order to fully account for the datum deficiency (Mendes Cerveira et al., 2007). Likewise, NNR conditions can be applied using a large group of reliable radio sources, whenever all radio sources are estimated.

In geodetic VLBI, or concerning the analysis of space-geodetic observations

[19] can be also treated as epoch-wise parameters under the favorable instantaneous observing geometry present throughout the experiment, e.g., when investigating sub-daily EOP variations based on CONT-type networks (Karbon et al., 2017)

[20] expressed either as offsets and rates or only as offsets

in the microwave regime in general, station clocks and atmosphere parameters must be derived simultaneously, implying that low-elevation observations should be included in order to separate these parameters correctly and derive station positions in a reliable manner (Herring, 1986; Rothacher, 2002). The contribution of the troposphere to the position estimates can be further reduced with GRD estimated along with the ZWD (MacMillan, 1995; Chen and Herring, 1997). Accounting (with GRD) for the azimuthal variation of the tropospheric refraction tends to also have a positive impact on EOP (Landskron and Böhm, 2019) and contributes to the reduction of systematic errors concerning the scale parameter and declination angles of radio sources (MacMillan and Ma, 1997).

Baseline lengths can be used as performance quantifiers as they are insensitive to the unknown rotation errors arising from not estimating corrections to EOP (Herring, 1986). Due to the CIO-based convention, there is no high correlation between $UT1$ estimates and polar motion. This means that the $UT1$ estimates will absorb variations in $UT1$ and leave x_p and y_p unaffected. Both parameter types can be thus derived simultaneously with any (reasonable) time resolution, often accompanied also by the celestial pole offsets (nutation corrections) estimated once per session. Nutation corrections are, however, not fully separable from the influence of the sub-daily polar motion model and the simultaneous estimation of daily nutation offsets and sub-daily polar motion requires often special handling (Thaller et al., 2007; Panafidina et al., 2017). In addition, the applied models concerning the sub-daily polar motion and Earth rotation have a direct effect on x_p, y_p and $UT1$ (Artz et al., 2012), respectively. The so-called network effects (Collilieux et al., 2009), which all space-geodetic techniques suffer from, can lead to global parameters of a lower quality. In the case of inhomogeneously distributed and sparse networks, the derived ERP or EOP can be characterized by a low level of accuracy, sometimes even with a lack of sufficient separability of the EOP. Care has to be also taken when choosing the quantity and location of stations that are used in the NNT/NNR conditions. The distribution of stations used for those constraints has a direct impact on the estimated EOP/ERP. As already mentioned, large errors present at one site may also be propagated into the entire network, if a low-quality station is used in the MC conditions.

3.7 Data Analysis with the c5++ Analysis Software

The *c5++* analysis software (Hobiger et al., 2010) was developed in cooperation between the National Institute of Information and Communications Technology (NICT), Japan Aerospace Exploration Agency (JAXA), and Hitotsubashi University. The developer group currently includes also Chalmers University of Technology. The software consists of modules allowing to process geodetic VLBI, GNSS and SLR separately or in a multi-technique mode, where different geodetic data are combined on the observation level (Hobiger and Otsubo, 2014; Hobiger et al., 2014), also allowing for the inclusion of local ties. The GNSS, VLBI and SLR modules share the same library, which contains all geophysical models compliant with the latest IERS Conventions (Petit and Luzum, 2010). This is beneficial for the combined

data analysis as a single framework provides the highest consistency w.r.t. the a priori models and parameterization. The separation of the functionality of *c5++* into distinct and independent units allows theoretically for an unlimited extension of the software with different modules, e.g., LLR or DORIS. The software is written in C++ and utilizes reliable and open-source libraries such as netCDF, Eigen and boost. The *c5++* analysis software has been also equipped with interfaces to numerous space-geodetic formats and enables reading or writing files in the Solution INdependent EXchange (SINEX) format. The data analysis and satellite orbit determination is performed in an iterative LSQ fashion. Since usually the problems are non-linear, LSQ method is being carried out until the WRMS value between two consecutive runs results in a difference smaller than the predefined convergence threshold.

The software does not have a Graphical User Interface (GUI), but it is fully controllable with the use of external scripts. Therefore, *c5++* is suitable for an automated and parallel processing of space-geodetic data. In the present version of the program, parameter adjustment is carried out in an iterative least-squares fashion and with the possibility of employing the variance-component-estimation algorithm (Hobiger and Otsubo, 2017) for a relative weighting between different observation types. The main components of *c5++* and the new modules, developed in connection to the studies forming the basis of this dissertation, are shown in Fig. 3.5.

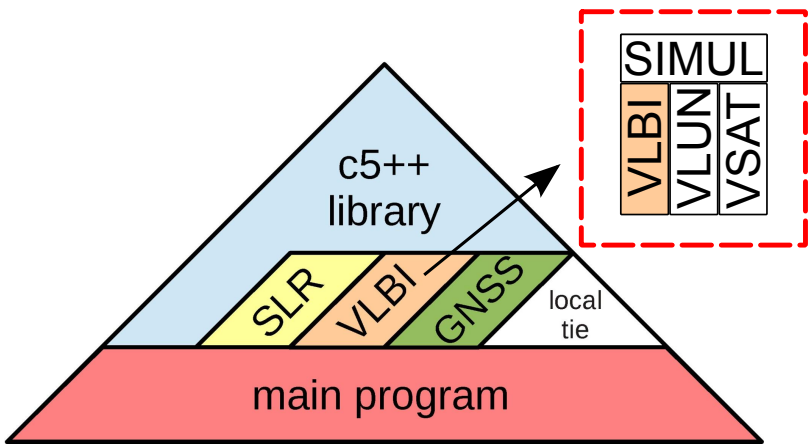

Fig. 3.5 The main components of c5++. Also shown are the modules (SIMUL, VLUN, VSAT) developed or updated (VLBI, c5++ library) in connection to the studies forming the basis of this thesis. The figure is a modified version of Fig. 1 from Hobiger and Otsubo (2014)

The VLBI module of *c5++* supports MK3-DB, vgosDB, ALIST, NGS cards and the raw correlator output from the K5 system. The VLBI-related and newly developed modules (apart from SIMUL) can work as separate entities and, similarly to other modules, provide a certain set of information to the main program, which

carries out the parameter adjustment. The new modules include

- VLUN - concerns lunar observations and provides related partial derivatives, reduced observations (O-C) and the stochastic information to the main program, see Sec. 5,
- VSAT - concerns observations of Earth satellites and provides related partial derivatives, reduced observations (O-C) and the stochastic information to the main program. In addition, the module employs an orbit integrator for precise orbit determination (POD),
- SIMUL - VLBI, VLUN and VSAT modules are coupled with the SIMUL module, which is capable of generating synthetic observables, see Sec. 3.8.

In *Paper I*, *Paper II* and *Paper III* lunar/satellite observations were either reduced with quasar-derived products or combined on the observation level with quasar data for an enhanced estimation of common and target parameters.

3.8 Geodetic VLBI Simulations

In the cases where one would like to validate new concepts or scheduling strategies and make reasonable design decisions, utilization of real data may be impractical due to the high cost of VLBI systems and related operations. The complex interactions in the VLBI analysis process prevent also from investigating, in an analytical fashion, the impact of new features on the quality of final products. Simulation studies are thus an effective tool for predicting the performance of the investigated ideas. An example for such tools can be Monte-Carlo-like simulations, already used in the studies covering geodetic VLBI (Petrachenko et al., 2009; Kareinen et al., 2017). In this approach, a large set of input data are simulated using parameters with a known stochastic behavior (probability distribution). All data sets created in such a way are then analyzed as if they were obtained from real experiments. This provides the basis for deriving statistical information on the parameters of interest, where one can investigate the bias and standard deviation of the obtained parameters. However, the Monte-Carlo simulations are only as realistic as the stochastic models used to produce the simulated input data.

The simulated VLBI delays (τ_{sim}) consist of the geometric part (τ_g) and three major error sources[21], i.e., fluctuations of water vapor (zenith wet delays ZWD_1 and ZWD_2), the instability of station clocks (clk_1, clk_2) and thermal noise (τ_{rnd}) referring to the overall performance of VLBI systems at stations forming a baseline. Such simulated observations can be expressed as

$$\tau_{sim} = \tau_g + (ZWD_2\, m_w(\varepsilon_2) + clk_2) - (ZWD_1\, m_w(\varepsilon_1) + clk_1) + \tau_{rnd}, \quad (3.50)$$

where ε_j refers to the source elevation angle at j^{th} station. Zenith wet delays can be simulated following the turbulence model, for which the algorithm is given, e.g.,

[21] Although not highlighted, source structure is also a major source for geodetic VLBI (Anderson and Xu, 2018)

by Nilsson et al. (2007) . The obtained zenith wet delays can be then mapped to slant directions using wet mapping functions m_w. VLBI station clocks *clk* are modeled as the sum of the random walk and integrated random walk processes (Herring et al., 1990), and τ_{rnd} can be modelled with the standard Gaussian white noise process.

The simulation module in *c5++* has been developed by the author of the following thesis and used in *Paper I* and *Paper III*. Extensive information concerning the implementation and the applied stochastic models are described in detail by Klopotek (2017) and given in *Paper I*.

Chapter 4

Artificial Radio Sources Observed with VLBI

An extension of radio-interferometric observations to artificial radio signals is possible and over the course of many years numerous dedicated experiments have already been performed for various studies, including missions to other planets or the Moon, and utilizing also different targets and observation/processing methods (King et al., 1976; Newhall et al., 1986; Sagdeyev et al., 1992; Kikuchi et al., 2009; Duev et al., 2012; Jones et al., 2015; Zhou et al., 2015). A remarkable example is the Huygens probe during its descent on Titan where (Earth-based) VLBI observations of that object resulted in new insights on the atmospheric properties of that Saturnian moon (Lebreton et al., 2005; Witasse et al., 2006). In addition to navigation purposes, observations of similar targets with VLBI can form a valuable input to the planetary orbit determination process with the advantage of measuring the position of the tracked objects in the celestial (radio) reference frame (Jones et al., 2020). An increasing interest in the topic of spacecraft tracking with VLBI have gained also ideas of prospective co-location Earth-orbiting satellites that, besides a dedicated VLBI transmitter, would be equipped with instruments used by other space-geodetic techniques, for the benefit of geodetic products and the reference frame parameters (Thaller et al., 2011; Thaller et al., 2014; Männel, 2016; Anderson et al., 2018). In terms of VLBI observations related to that topic however, only a handful of test experiments have been performed so far by either employing satellites that had a dedicated VLBI transmitter (Hellerschmied et al., 2018; Hellerschmied, 2018) or by observing signals of GNSS satellites directly (Plank et al., 2017).

Data acquired from tracking of such sources by radio telescopes can be processed in a similar fashion as in the case of natural radio sources observed in conventional VLBI. In order to succeed, the standard data processing chain, described in a comprehensive manner in Sec. 3.6, has to be refined at few of its stages, also taking into account characteristics of such signals and the dynamical aspects of the tracked spacecrafts. Artificial radio sources and their utilization in VLBI bring

thus several technical and theoretical challenges that need to be addressed correctly. The following section introduces the concept of VLBI observations of artificial radio sources of any kind and provides the underpinnings of methods for processing of related data, leading to observables that can be used at the data analysis stage.

4.1 VLBI Delay Model for Objects in the Solar System

The VLBI delay model described in Sec. 3.1 can be applied only to observations of natural radio sources, treated as objects at a infinite distance. In other words, for extragalactic radio sources, one uses a plane-wave approximation, which ignores the effect of source distances w.r.t. the Earth. In the case of spacecrafts in our solar system, the incoming radio waves (curved wave fronts) can not be treated as planary, see Fig. 3.1, and so-called near-field effects have to be accounted for in the calculation of the VLBI delay for such objects. It is assumed that an object is located in the near-field if the distance R between the source and an array of telescopes is small compared to D^2/λ.

The formulation of the VLBI delay model for artificial radio sources in the near-field can be conducted in different ways (Moyer, 2000; Klioner, 2003; Sekido and Fukushima, 2006; Duev et al., 2012). The model can be represented just like the standard model (for natural radio sources), but using a pseudo-source vector in order to account for the effect of the curved wave front. Alternatively, the time difference of the signal reception between two stations forming a baseline can be also expressed as a difference between two light-travel times LT_1 and LT_2 from a radio source to the first and second VLBI station. This reflects the situation of two ray paths from one radio source to two Earth observers. Using the reception time T_1 at the first station, one can determine, in an iterative fashion, the transmission time T_0 of an object

$$T_1 - T_0 = \frac{|\vec{\mathbf{R}}_{01}|}{c} + RLT_{01}, \tag{4.1}$$

where $|\vec{\mathbf{R}}_{01}|$ is the distance between the BCRS position of the first station at the reception time T_1 and the BCRS position of the tracked object at its transmission time T_0. The associated relativistic terms are included in RLT_{01}. Next, the derived transmission epoch (T_0) is used to solve for the reception time T_2 at the second station, similarly as in the case of the T_1-T_0 difference (Moyer, 2000; Duev et al., 2012). Similarly to the conventional model used for quasar observations, the relativistic terms (RLT_{01}, RLT_{02}) should consider all planets of our solar system (including the Earth) as well as the Sun and the Moon. For RLT_{01}, this can be formulated as (Moyer, 2000; Duev et al., 2012)

$$\begin{aligned} RLT_{01} = \frac{(1+\gamma)\cdot GM_S}{c^3} \cdot \ln \frac{|\vec{\mathbf{R}}_0^S| + |\vec{\mathbf{R}}_1^S| + |\vec{\mathbf{R}}_{01}^S| + \dfrac{(1+\gamma)\cdot GM_S}{c^2}}{|\vec{\mathbf{R}}_0^S| + |\vec{\mathbf{R}}_1^S| - |\vec{\mathbf{R}}_{01}^S| + \dfrac{(1+\gamma)\cdot GM_S}{c^2}} \\ + \sum_{B=1}^{10} \frac{(1+\gamma)\cdot GM_B}{c^3} \cdot \ln \frac{|\vec{\mathbf{R}}_0^B| + |\vec{\mathbf{R}}_1^B| + |\vec{\mathbf{R}}_{01}^B|}{|\vec{\mathbf{R}}_0^B| + |\vec{\mathbf{R}}_1^B| - |\vec{\mathbf{R}}_{01}^B|}, \end{aligned} \tag{4.2}$$

$$\vec{\mathbf{R}}_i^{\alpha} = \vec{\mathbf{R}}_i(T_i) - \vec{\mathbf{R}}_{\alpha}(T_i), i = 0, 1; \alpha = \{S, B\}, \tag{4.3}$$

$$\vec{\mathbf{R}}_{01}^{\alpha} = \vec{\mathbf{R}}_1^{\alpha}(T_1) - \vec{\mathbf{R}}_0^{\alpha}(T_0), \alpha = \{S, B\}, \tag{4.4}$$

with S and B referring to the Sun and a celestial body, respectively. The second relativistic term can be calculated in a simillar fashion. RLT_{01} and RLT_{02} should include the moment of the closest approach of the photon to the gravitating body J or the position of the gravitating body at the retarded moment of time (Klioner, 2003).

The derived delay (T_2-T_1) is expressed in the barycentric dynamical time (TDB) as the spacecraft motion and positions of reference points of VLBI telescopes are computed in the BCRS (Sekido and Fukushima, 2006). As the observed signals are time tagged in the proper time of the station clocks, the observed VLBI delays are measured in terrestrial time (TT), the theoretical time scale for clocks at sea level (Petit and Luzum, 2010). Therefore, the obtained near-field VLBI delay needs to be reformulated (Lorentz transformation) in order to express the computed geometric delay in the time scale of the observing stations (Duev et al., 2012)

$$t_{v2} - t_{v1} = \left(\frac{T_2 - T_1}{1 - L_C} \cdot \left[1 - \frac{1}{c^2} \left(\frac{|\vec{\mathbf{V}}_{\oplus}|^2}{2} + U_E \right) \right] - \frac{\vec{\mathbf{V}}_{\oplus} \cdot \vec{\mathbf{b}}}{c^2} \right) \cdot \left(1 + \frac{\vec{\mathbf{V}}_{\oplus} \cdot \dot{\vec{\mathbf{r}}}_{2,gc}}{c^2} \right)^{-1}, \tag{4.5}$$

with $L_C = 1.48082686741 \cdot 10^{-8}$ and $U_E = \sum_{E \neq j} \frac{GM_J}{r_{Ej}}$ as the Newtonian potential at the geocenter computed for all solar system bodies excluding the Earth. $\vec{\mathbf{V}}_{\oplus}$ and $\dot{\vec{\mathbf{r}}}_{2,gc}$ are the barycentric velocity vector of the Earth and the GCRS velocity vector of the second telescope, respectively. Once t_{v2}-t_{v1} is obtained and acounted for the atmospheric propagation delay at the reference station, as in Eq. 3.5, it can be used as the theoretical VLBI delay and applied in correlation and at the data analysis stage.

4.2 Technical Aspects

Typical natural radio sources for geodesy goals are characterized by observed flux densities on the order of $10^{-26}\,\mathrm{Wm^{-2}Hz^{-1}}$, which corresponds to 1 Jy. Assuming a VLBI-like transmitter on a GNSS satellite, this criterion would be met for signals transmitted with the power well below one watt over a bandwidth of one MHz[22]. Shorter integration times and more precise observations could be obtained from observations of stronger signals. However, the signal strength can not be increased arbitrarily in this case as very strong signals might be problematic, if not potentially damage the VLBI front-ends. Relatively strong signals (compared to quasars) could also introduce the problem of varying attenuation levels at the observing sites (McCallum et al., 2017), also problematic at the data analysis stage (Plank et al., 2017). Low-power artificial radio signals could be beneficial in this case, allowing

[22]Standard microwave link budget calculations (Seybold, 2005) for the 3 dBi transmitter gain and a distance of 20 000 km

also to employ phase-cal tones at VLBI stations equipped with such a calibration system.

Although possible, legacy VLBI antennas are not fully suitable for following Earth satellites on the sky as a step-wise source tracking is still used at most of the VLBI sites (Hellerschmied, 2018). At sub-observation times, step-wise tracking can also lead to unwanted effects both in the amplitude and the estimated phase (McCallum et al., 2017). In the VGOS era, the tracking-related problems could be reduced due to the utilization of the continuous tracking and noticeably higher antenna slew rates (Fukuzaki et al., 2015), sufficient in this case for satellite orbits of any (reasonable) height.

GNSS L-band signals are usually not observable with most of the VLBI receiving systems for geodesy as they are primarily utilized for X-band and S-band observations. In order to observe such signals, either the telescopes have to be equipped with suitable L-band receivers (Plank et al., 2017) or some technical modifications of the antennas need to be made. In terms of quasar observations at L-band, that could potentially augment satellite observations, utilization of such data would be rather problematic due to a more complex intrinsic structure of radio sources, compared to the same radio sources observed at higher frequencies (frequency-dependent structure index, Fey and Charlot, 1997). Ionosphere delays are also an additional factor that can degrade the quality of single-frequency quasar observations at L band as their contribution to the error budget is substantial in relation to the same effects present in X-band or K-band observations. This issue could be addressed with externally derived ionosphere delays, e.g., using GNSS data (Männel and Rothacher, 2016). However, non-negligible delay contributions can still be present in the residuals (Sekido et al., 2003). In the VGOS era, the situation is not going to change significantly in terms of observations of L-band signals. As mentioned in Sec. 3.6.2, frequencies below 2 GHz are not considered in VGOS and filtered out by means of feeds, filters or the back-end software. Therefore, future transmitters for VLBI could operate on VGOS-compliant frequencies, i.e., located between 3 and 12 GHz. Observations encompassing two frequency bands, and with proper separation between them, should be also guaranteed in order to derive ionosphere-free observables.

Spacecraft navigation in the solar system consists of methods utilizing distance (ranges w.r.t. a ground station) and Doppler (range-rate) measurements. This allows to obtain highly precise observations in the line-of-sight direction. Another approach, commonly known as differential one-way ranging (Delta-DOR or ΔDOR), is used in order to derive angular positions of spacecrafts relative to the nearby natural radio sources[23]. This leads to an additional and high-quality source of information for the direction perpendicular to the line of sight (Curkendall and Border, 2013). In other words, ΔDOR-derived spacecraft positions are expressed in the quasar frame. DOR signals consist of very narrow tones separated from the carrier frequency by several or tens of MHz. The received signals are usually not strong, in relation to quasars (Curkendall and Border, 2013). DOR refers

[23]as opposed to Doppler and range measurements that position a spacecraft, e.g., in the frame of a planet

to the difference between the arrival times of the same spacecraft signal at both receiving stations and *differential* indicates the use of quasar signals. In this way, the accuracy of stand-alone spacecraft measurements is improved by differencing out common model errors between spacecrafts and nearby radio sources. For X-band observations, the error in the measure of the delay (differenced range) is typically on the order of 0.1-0.5 ns (Iess et al., 2014; Zheng et al., 2014), which translates to about 0.03-0.15 m. If incorporated into typical geodetic schedules efficiently, this poses an attractive way of using such approach with VLBI antennas (Fiori, 2019). This concept has already been initiated by including an X-band DOR transmitter on board of an Earth-orbiting satellite (Tang et al., 2016) or used during lunar exploration missions utilizing S-band or X-band observations (Zheng et al., 2014). An example of a DOR signal for X-band observations is illustrated in Fig. 4.1.

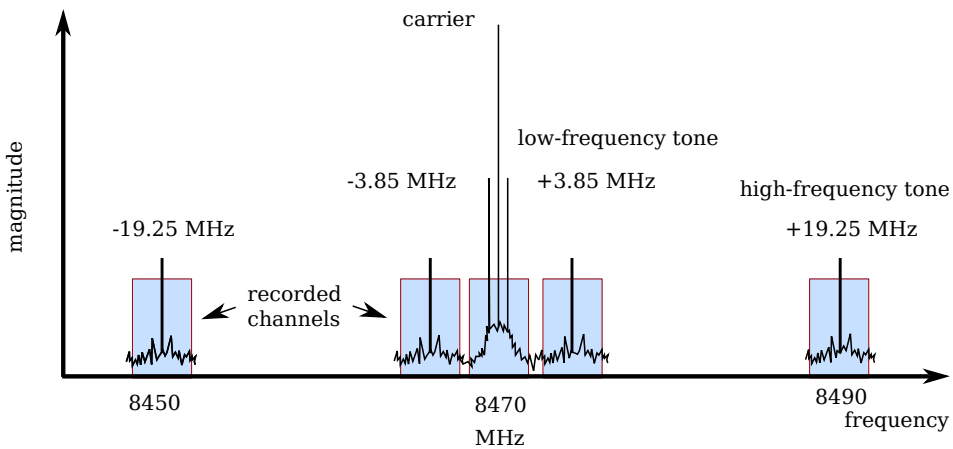

Fig. 4.1 The spectrum of an X-band DOR signal and the coincident recorded channels. The following frequency allocation used during the lunar missions (Zheng et al., 2014), see Sec. 5. In the case of ΔDOR, the differential range is extracted by means of a software phase-locked loop (Fiori, 2019) and the same frequency setup is used to record quasar signals and DOR tones (Curkendall and Border, 2013)

A prospective VLBI-like transmitter on a satellite could also transmit random signals with equal intensity over wide frequency bands. Such quasar-like signals could be then easily processed using standard tools of VLBI. Multiple several-MHz-wide channels that span few tens of MHz would be favorable in this case. In addition, such a concept would not require any signal modulation as the signal itself gives the correlation peak, resulting in relative delays on each baseline.

4.3 Data Processing

The scheduling procedure concerning artificial radio sources, not described in detail here, requires utilization of standard scheduling solutions applied to quasars (frequency setup, sky coverage, scan duration, observing modes) and solving satellite-specific issues (tracking, orbit data) in order to derive schedules meeting various scientific goals (Jones et al., 2010; Plank et al., 2017; Haas et al., 2017; Hellerschmied et al., 2018). Extensive information on scheduling of satellite observations for geodetic purposes can be found, e.g., in Hellerschmied (2018) . The data acquisition process for both quasar and spacecraft observations is in principle the same[24] as the goal in VLBI is the correlation peak that provides the relative delay on each baseline (Tornatore et al., 2014; Haas et al., 2017). However, first alterations need to be carried out at the correlation stage, where the conventional VLBI delay model needs to be replaced with the near-field VLBI model. In addition to its dedicated routines that can generate the appropriate correlator input model, the DiFX structure allows also to introduce a proper model by updating the files containing that information. This is illustrated in Fig. 4.2, where the *c5++* analysis software can be used for that purpose (Klopotek et al., 2017). If required, the correlation setup can include the zoom-band option of DiFX (alternatively, *fourfit*'s passband option at the post-correlation stage), responsible for the sub-channel frequency selection. This however depends upon the structure of the signals that are correlated (Plank et al., 2017; Hellerschmied et al., 2018; Klopotek et al., 2019). At the post-correlation analysis stage, a single software can be used to process quasar and spacecraft/observations (Jones et al., 2015; Plank et al., 2017; Hellerschmied et al., 2018), but it may also include dedicated post-processing schemes applied to spacecraft data, based on which different types of observables can be derived (Duev et al., 2012; Fiori, 2019).

With some technical and theoretical challenges stated in Sec. 4.2, that need to be addressed prior to the data analysis, observations of artificial radio sources allow to derive group-delay (τ_{gd}) and phase-delay (τ_{pd}) observables, as defined in Sec. 3.6.4. DOR tones have already been used to derive τ_{gd} and apply this observable in the geodetic VLBI analysis in the form of either X-band-only data (Klopotek et al., 2019) or both S-band and X-band observations (Hellerschmied et al., 2018). The procedure for obtaining and processing DOR-derived τ_{gd} is also given in *Paper II*. The theoretical precision of the group delay in this case is inversely proportional to the frequency span between two outer tones, resulting in the sub-nanosecond precision for X-band observations (Zheng et al., 2014; Klopotek et al., 2019). In the case of observations of GNSS signals at L band, only SBD can be derived, leading to the observation precision on a similar level (Plank et al., 2017). One has to keep in mind that this is only the measurement precision, which does not include systematic effects such as electronic biases or errors connected to the Earth atmosphere. In the case of ionosphere-free and DOR-derived τ_{gd}, a sophisticated data analysis allows to reduce the remaining errors and can further

[24]For experiments including observations of spacecrafts, station-specific *.vex* files need to be created. On the contrary, conventional VLBI operates only with a single *.vex* file per experiment

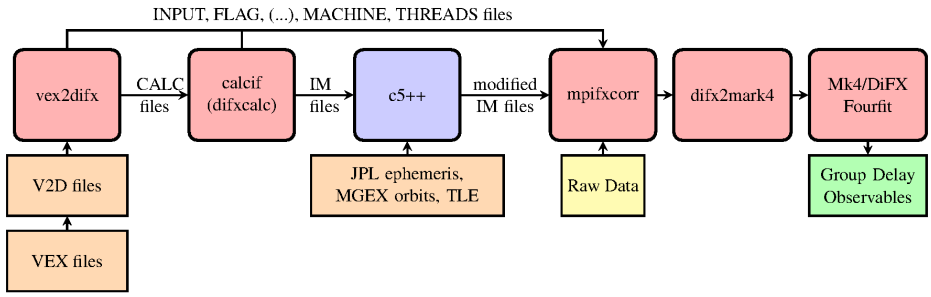

Fig. 4.2 Processing baseband data with DiFX using external a priori VLBI delay models. For artificial radio sources at a finite space, an appropriate model needs to be calculated and supplied to the processing pipeline. In this case, the conventional VLBI delay model is replaced with the near-field equivalent by updating the files containing the delay coefficients, which are then used for correlation. The flowchart from Klopotek et al. (2017)

improve the results (Hellerschmied et al., 2018).

The utilization of phase-delay observables is possible in the case of differential methods (ΔVLBI), where the position of a target is derived w.r.t. the nearby (calibrator) radio sources (Jones et al., 2015; Jones et al., 2020) or when only a relative difference between the observed objects is of interest (King et al., 1976; Zhou et al., 2015). The benefit of using ΔVLBI (or same-beam interferometry) is primarily an access to highly precise relative angular positions of spacecrafts via differential phase delays and, similarly to ΔDOR, a minimal contribution of errors connected to the Earth atmosphere (Kikuchi et al., 2009).

Chapter 5

VLBI Observations of Lunar Radio Sources

On September 13, 1959, the first man-made object reached the surface of the Moon becoming also the first artificial object on an extraterrestrial body and initiating in this way an era of space exploration. This historical event was a part of the Soviet Union's Luna 2 mission, in which the first hard (unpowered) Moon landing was performed. Few years later, its successor (Luna 9) was the first vehicle that achieved a controlled soft landing and took close-up pictures of the lunar surface. As a response to the Sovet Union's space-exploration project, the Apollo program (U.S.) went even further and between 1968 and 1972 it included manned missions to the Moon. On July 21, 1969, Neil Armstrong became the first man to walk on the Moon.

The continuous progress in space sciences has led to numerous missions with the aim to study the Moon and gain knowledge on lunar dynamics and the Earth-Moon system. The VLBI technique has also been used in this area. First observations of artificial radio sources on the Moon were carried out in the 1970's using Apollo Lunar Surface Experiment Packages (ALSEP), which were placed on the lunar surface during the Apollo program. Combined with range observations to lunar retroreflectors, ΔVLBI measurements at S band allowed to determine the relative position between the ALSEP transmitters with an uncertainty of about 10 m in the transverse components and 30 m along the Earth-Moon direction (King et al., 1976; Davies and Colvin, 2000). The differential approach used in this case provided highly precise relative angular coordinates, based on phase measurements, while canceling out the common media contributions. During the SELENE (SELenological and ENgineering Explorer) mission, the VLBI technique was used for the spacecraft orbit determination by employing same-beam interferometry to derive precise differential phase delays (Kikuchi et al., 2009). In late 2013, a Chinese lander and rover were deployed on the surface of the Moon (north-west) to realize scientific tasks of the Chang'e 3 (CE-3) mission such as examination of the geological structure of the Moon or observations of celestial objects in the visible/near-infrared spectrum (Li

et al., 2015). The mission included X-band DOR tones for positioning and an X-band communication channel (Haas et al., 2017) in order to send the acquired information back to the Earth. Since the successful landing of the CE-3 probes, various efforts have been made to determine their relative and absolute positions based upon the signals that those objects transmitted towards the Earth. The relative position of the rover w.r.t. the lander was derived with a meter-level accuracy (Zhou et al., 2015). Unfortunately, the same level of accuracy has not been achieved in terms of the absolute positioning of the CE-3 lander on the Moon, i.e., in the Moon-fixed reference frame. In the following subsection, a concise description of VLBI observations of the CE-3 lander in the geodetic mode are given. In other words, the utilization of group delays, which are combined with quasar observations.

5.1 Geodetic VLBI Data Analysis

Observations of CE-3 signals with geodetic VLBI were carried out first in April 2014 with the use of a single baseline (Klopotek et al., 2017). This was just a test undertaking, but subsequently, twelve OCEL (Observing the Chang'e Lander with VLBI) sessions were approved by the IVS Observing Program Committee and subsequent global-scale observations were carried out between 2014 and 2016 (Haas et al., 2017). The employed schedules consisted of both lunar and quasar observations, arranged into two types of thirty-minute observing blocks and scheduled in an alternating sequence (quasar-lunar-quasar). The creation of the 24-hour OCEL schedules was carried out in a semi-automatic fashion using SKED (Gipson, 2010).

The processing of lunar baseband data can be carried out using standard tools of geodetic VLBI, with the exceptions mentioned in Sec. 4.3. The processing scheme applied to OCEL data is depicted in Fig. 5.1 and described in more detail by Klopotek et al. (2019) . The post-correlation analysis provides two databases as quasar and lunar observations are correlated separately. At the data analysis stage, both observation types can be combined on the observation level. In this case, quasar observations are used to derive the troposphere and clock models at each station. As a consequence, VLBI telescopes have to spend a substantial amount of time pointing at many different directions on the sky, to estimate nuisance parameters, rather than observing a single lunar target very frequently. However, such an approach allows to reduce lunar observations with epoch-wise ZWD and clock values, both hard to derive using exclusively lunar observations.

The primary aspect to investigate is the ability of VLBI to determine the position of the lander in the selenocentric reference frame. Due to its nature, VLBI is characterized by a poor measurement sensitivity in the direction parallel to the line of sight. Coupled with a specific Earth-Moon geometry (the Moon faces the Earth always with the same side), this poses a problem in estimation (decoupling) of all three position components of lunar objects, as shown in *Paper I*. In order to prevent this, the position of the lander can be parameterized in the Moon-fixed (Mean-Earth) reference frame (Archinal et al., 2011) as lunar latitude, longitude and height w.r.t. a reference surface, with the height component constrained to a

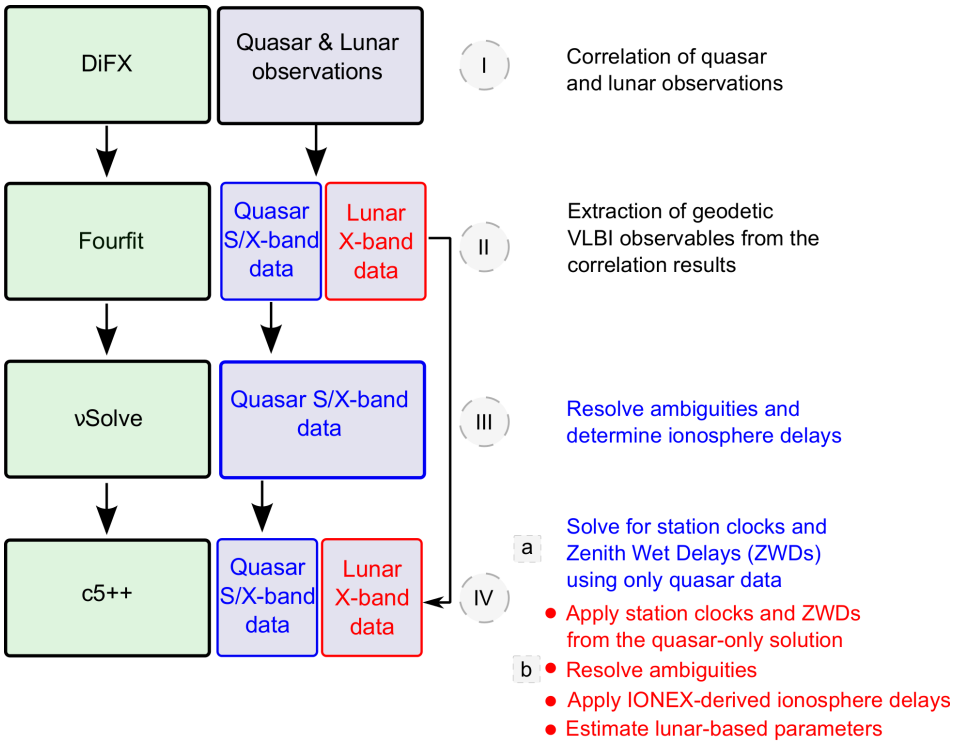

Fig. 5.1 The processing of quasar and lunar observations (group delays) based on OCEL sessions. Fig. 2 from *Paper II*

well-known a priori value, see *Paper I*.

The parameter estimation includes here only X-band observations and thus a special care has to be taken as ionosphere contribution needs to be addressed in this case. In the presence of no lunar dual-frequency data, ionospheric delays can be obtained using global ionospheric maps (GIM, Schaer et al., 1996) and utilized in the data analysis. In addition, any residual ionosphere effects can be addressed by the (constrained) estimation of station-based VTEC biases, estimated along with the lander position. The list of solve-for parameters needs to also include one clock offset (per station), expressed relative to the reference station of the network and estimated using only lunar data. Such an additional clock parameter absorbs the difference in instrumental delays between S band and X band, usually absorbed by the clock model in the parameter estimation with the use of dual-frequency data (Sekido et al., 2003; Hobiger et al., 2006). Besides residual ionosphere contributions, observations of the CE-3 lander with geodetic VLBI are subject to residual troposphere and clock errors. These error sources also limit the accuracy of the lunar-based parameters, as shown in *Paper I*. However, other

systematic effects[25] can also be present in the data and thus further degrade the accuracy of the solve-for parameters.

5.2 Selenodesy

The manned Moon missions have left behind plenty of scientific equipment, including corner-cube retroreflectors, which are used nowadays in LLR for lunar research (Müller et al., 2007). This space-geodetic technique relies on the round-trip flight time of a laser pulse fired from an Earth observatory and bouncing off of a retroreflector on the Moon. LLR is sensitive to the line-of-sight direction with the measurement accuracy of about 2 cm and the coordinates of the lunar retroreflectors known to a meter level (Williams et al., 2006). The related research includes a wide range of scientific investigations and the lunar ephemeris is produced solely based upon this type of observations. In LLR, strong laser systems and large telescopes are needed to perform such sophisticated observations. As a consequence, only a small set of laser stations is currently capable of performing LLR observations, with two of them gathering most of the data (Müller et al., 2007). In the case of the LLR targets, the current configuration of five retroreflectors, located near the equator and at mid-northern latitudes, would benefit from any expansion towards the lunar limb as a larger geographic extent of such targets improves the sensitivity of LLR to lunar-based parameters (Williams et al., 2006; Müller et al., 2007).

The combination of LLR (or range and range-rate measurements in general) with interferometric observations could be pursued in order to fully exploit the strengths of those methods and overcome the technique-specific weaknesses. The interferometric techniques are sensitive to the lunar rotation. Once one gains an access to improved VLBI observables as well as related technical and theoretical challenges are addressed, VLBI, ΔVLBI or ΔDOR have, in addition to their known applications, also the potential to complement LLR, e.g., in determination of coordinates of artificial optical-radio targets that realize a selenocentric reference system. As a consequence, this may lead to better knowledge on the lunar rotation as well as decreased correlations between the estimated coordinates and related lunar-based parameters (Hofmann et al., 2018). VLBI observations of artificial radio sources on the Moon could be incorporated into regular IVS schedules with almost no additional organizational effort, allowing to observe lunar targets on a daily basis and with a global network of radio telescopes.

[25] such as those connected to our current knowledge on the lunar ephemeris

Chapter 6

Geodetic Observations of Earth Satellites

Interferometric observations of Earth satellites is not a new concept and it was already used for observations of Sputnik 1 in the late 1950's (King-Hele, 2008). Nowadays, only a few dedicated experiments have been performed so far with the purpose of tracking satellites at low Earth orbit (LEO) or medium Earth orbit (MEO) in the geodetic VLBI mode (Haas et al., 2014; Plank et al., 2017; Hellerschmied et al., 2018; Hellerschmied, 2018). Although they provided first insights concerning the theoretical and technical aspects of that observing concept, those observations were neither performed with global networks nor have fully exploited this subject. Apart from observations, several interesting aspects have been discussed over the past years (Dickey, 2010) and various simulation studies have been performed (Plank et al., 2014; Plank et al., 2016; Anderson et al., 2018) in order to investigate the usefulness of such observations for the geodetic community, co-location in space (Männel, 2016) and for the benefit of GGOS. The following chapter highlights the main aspects associated with the data analysis, parameter estimation and orbit determination with regard to observations of Earth-orbiting satellites by space-geodetic techniques. In terms of geodetic VLBI, the concept of satellite observations is presented in the aspect of their combination with quasar observations.

6.1 Satellite Reference Frames and Orbital Elements

Orbit modelling requires definition of three additional frames, which facilitate description of satellite-related effects and the estimation of related parameters. This includes (Teunissen and Montenbruck, 2017; Montenbruck et al., 2015a)

1) a satellite-fixed frame attached to the satellite body where the +z axis coincides with the antenna boresight direction, the +y-axis is parallel to the rotation axis of solar panels and the x-axis completes the right-handed coordinate frame,

2) an orbit-fixed frame with radial (R), along-track (S) and cross-track (W) directions, aligned with the unit vectors (Colombo, 1989; Prange et al., 2020)

$$\hat{\mathbf{e}}_R = \frac{\vec{\mathbf{r}}}{||\vec{\mathbf{r}}||}, \tag{6.1}$$

$$\hat{\mathbf{e}}_S = \frac{\dot{\vec{\mathbf{r}}}}{||\dot{\vec{\mathbf{r}}}||}, \tag{6.2}$$

$$\hat{\mathbf{e}}_W = \hat{\mathbf{e}}_R \times \hat{\mathbf{e}}_S, \tag{6.3}$$

which are defined by the instantaneous GCRS position $\vec{\mathbf{r}}$ and velocity $\dot{\vec{\mathbf{r}}}$ vectors of the satellite,

3) a Sun-oriented frame with principal axes in the direction of the Sun (D), along the solar panels of satellites (Y) and the B direction completing the right-handed coordinate frame, and with the unit vectors (Meindl et al., 2013; Arnold et al., 2015)

$$\hat{\mathbf{e}}_D = \frac{\vec{\mathbf{r}}_\odot - \vec{\mathbf{r}}}{||\vec{\mathbf{r}}_\odot - \vec{\mathbf{r}}||}, \tag{6.4}$$

$$\hat{\mathbf{e}}_Y = -\hat{\mathbf{e}}_R \times \hat{\mathbf{e}}_D, \tag{6.5}$$

$$\hat{\mathbf{e}}_B = \hat{\mathbf{e}}_D \times \hat{\mathbf{e}}_Y. \tag{6.6}$$

In the case of the satellite-fixed frame for GNSS satellites, the orientation of axes varies across constellations and is also connected (for some constellations) to the yaw-steering (YS) and orbit-normal (ON) attitude modes (Teunissen and Montenbruck, 2017; Prange et al., 2020), employed in dependence of the elevation of the Sun above the orbital plane. The adopted convention (Montenbruck et al., 2015a) defines however the +x axis in a way that is permanently sunlit and the corresponding +y axis is defined via +x and +z, as defined above. The three aforementioned frames are illustrated in Fig. 6.1.

The satellite state vector (position and velocity) at a particular epoch (t) can be expressed with the use of a set of orbital parameters (Keplerian elements)

- $a(t)$ semi-major axis,
- $e(t)$ eccentricity,
- $i(t)$ orbit inclination w.r.t. the equatorial plane,
- $\Omega(t)$ right ascension of the ascending node,
- $\omega(t)$ argument of perigee,
- $\upsilon_0(t)$ true anomaly.

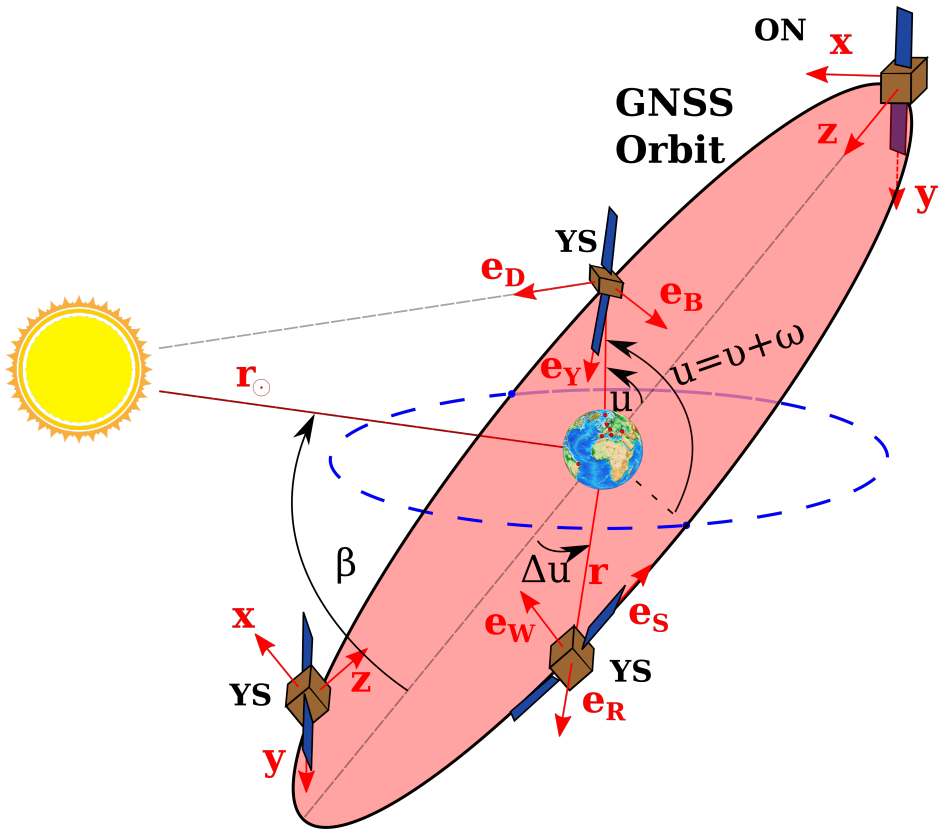

Fig. 6.1 Satellite-fixed (XYZ), orbit-fixed (RSW) and Sun-oriented (DYB) reference frames. The elevation of the Sun above the orbital plane is referred to as β. Argument of latitude of the satellite is depicted with u, whereas υ and ω refer to true anomaly and argument of perigee, respectively. YS and ON refer to the yaw-steering and orbit-normal modes (Montenbruck et al., 2015a), respectively

6.2 Satellite Orbit Modelling

The orbital motion of an artificial Earth satellite can be described to a large extent by Newton's law of universal gravitation. In highly precise models however, small unmodeled forces may be accounted for using the concept of empirical accelerations or other orbit parameters (pseudo-stochastic pulses, Beutler et al., 2006). This results in the satellite acceleration vector $\ddot{\vec{\mathbf{r}}}$ (Montenbruck and Gill, 2000)

$$\ddot{\vec{\mathbf{r}}} = -\frac{GM}{r^3}\vec{\mathbf{r}} + \vec{\mathbf{a}}_p(t, \vec{\mathbf{r}}, \dot{\vec{\mathbf{r}}}, d_1, \cdots, d_m, s_1, \cdots, s_n), \tag{6.7}$$

with the perturbing acceleration $\vec{\mathbf{a}}_p$ expressing the overall impact of all considered perturbations. The $d_1, \cdots, d_m$ and $s_1, \cdots, s_n$ terms refer to (dynamic) empirical and other orbit parameters, respectively. Most of such effects occur at a frequency of one cycle per orbital revolution. The empirical acceleration a_i in the direction i can be parameterized using the unit vector $\hat{\mathbf{e}}_i$ in the direction i, a constant (a_0) acceleration and once-per-revolution (OPR) accelerations in the form of sine (a_S) and cosine (a_C) terms

$$a_i = (a_{0i} + a_{Ci} \cos u + a_{Si} \sin u)\, e_i. \tag{6.8}$$

The satellite state vector (geocentric position and velocity vectors) fully defines a set of initial conditions for an equation of motion of artificial satellites. Even the most detailed models are, however, limited by uncertainties in knowledge concerning the time-varying orientation (orbit maneuvers, attitude control), material properties, surface temperatures of satellites and, in general, the force fields acting upon them (Colombo, 1989; Springer et al., 1999). Among the latter forces, these include non-gravitational effects such as the atmospheric drag (for satellites with altitudes below 2000 km), antenna-thurst effects (Steigenberger et al., 2018), Earth radiation pressure or solar radiation pressure (SRP). The latter effect is known to be the most dominant non-gravitational force impacting Earth-orbiting satellites at GNSS-like altitudes (Rodriguez-Solano et al., 2012a). Earth radiation tends to have a small impact on GNSS due to the large distances between satellites and the Earth (Rodriguez-Solano et al., 2012b). The handling of the SRP-induced effects for GNSS satellites is thus crucial, but it is not a trivial task. SRP modelling for Galileo satellites is challenging due to their lower masses and a noticeably elongated bus shape (Montenbruck et al., 2015b), compared to GPS satellites. In addition, a better understanding of the attitude control during shadow transits is also of great importance for an enhanced determination of GNSS orbits. In the case of LAGEOS (LAser GEOdynamics Satellite) satellites (LAGEOS-1 and LAGEOS-2), the Earth radiation pressure and SRP are still non-negligible, but tend to be less problematic due to the lower orbital heights of those satellites, their spherical shape and smaller ratios of the cross-sectional area to the mass (Meindl et al., 2013).

The estimation of empirical accelerations, in the form of additional parameters, absorbs to a large extent deficiencies in the modelling of non-gravitational and gravitational forces perturbing satellite orbits (Sośnica et al., 2014; Montenbruck et al., 2017), but these parameter types are often substantially correlated with some of the geodetic parameters. For perturbations due to general relativity, empirical accelerations can be expressed in the RSW frame as

$$R(u) = R_0 + R_C \cos u + R_S \sin u, \tag{6.9}$$

$$S(u) = S_0 + S_C \cos u + S_S \sin u, \tag{6.10}$$

$$W(u) = W_0 + W_C \cos u + W_S \sin u, \tag{6.11}$$

$$\tag{6.12}$$

where u is the argument of latitude of the satellite. Such an approach is often used in SLR, where usually one set of S_0, $S_{C,S}$, $W_{C,S}$ is estimated over a multiple-day

arc (Sośnica et al., 2019). Box-wing satellites, such as GNSS satellites, require empirical accelerations to be expressed in the Sun-oriented reference frame. The latter is more suitable for handling the SRP-induced perturbations. Commonly, the solar radiation acceleration is estimated along with the orbit determination process using an n-parameter Empirical CODE Orbit Model (ECOM) such as ECOM1 or ECOM2 (Beutler et al., 1994; Arnold et al., 2015). Within the ECOM1 model for instance, empirical accelerations are parameterized with the use of three constant accelerations in DYB directions (D_0, Y_0, B_0) and six OPR accelerations ($D_{C,S}$, $Y_{C,S}$, $B_{C,S}$). This results in a total number of nine parameters expressed as a function of satellite latitude

$$D(u) = D_0 + D_C \cos u + D_S \sin u, \tag{6.13}$$

$$Y(u) = Y_0 + Y_C \cos u + Y_S \sin u, \tag{6.14}$$

$$B(u) = B_0 + B_C \cos u + B_S \sin u, \tag{6.15}$$

where all nine SRP parameters are scaled to one Astonomical Unit (AU) with the related scaling factor $(1\,\mathrm{AU/d})^2$ utilizing satellite-Sun distance (d). Usually only five (D_0, Y_0, B_0, $B_{C,S}$) of the nine parameters of the model are estimated in the orbit determination process[26] and by constraining some of them in order to handle correlations between those parameters. A good performance of the model can be also achieved without the a priori SRP models. In addition, constrained velocity changes (pseudo-stochastic pulses) can be introduced in order to handle the remaining modeling deficiencies (Beutler et al., 2006). The same SRP model can include parameterization of the OPR accelerations in terms of Δu or μ. Similar models can also include additional terms to properly handle SRP-induced effects (higher-order SRP terms) for different satellite constellations and generations (Springer et al., 1999; Montenbruck et al., 2017). Although it tends to provide good results, the limitations of the stand-alone ECOM model have been identified, especially for cuboid-shaped satellite bodies or the ON attitude (Montenbruck et al., 2017; Prange et al., 2020). In addition, the ECOM parameters do not take into account the physical processes causing those accelerations and a large number of such parameters tends to weaken the solution. An adjustable box-wing model is an alternative approach for handling the SRP-induced effects (Rodriguez-Solano et al., 2012a; Montenbruck et al., 2015b). It is constructed using approximate dimensions of satellites and assumed optical properties of satellite surfaces. It represents an empirical model with the physical interpretation of the estimated parameters with regard to the optical properties (absorption, diffusion and reflection coefficients) of the illuminated surfaces of a GNSS satellite. It is assumed that a GNSS satellite consists of a satellite box and solar-panel arrays with defined geometrical dimensions. In this case, optical properties of the illuminated surfaces are estimated during the orbit determination process. Such an approach helps to decrease the negative impact of the modelling deficiencies, related to the solar radiation pressure, on geodetic parameters such as ERP or station positions (Rodriguez-Solano et al., 2014).

[26] correlations of OPR terms in D and Y directions with the orientation of the orbital plane

6.3 Precise Orbit Determination

Earth science missions require accurate orbit and frame parameters when solving for global parameters of geophysical interests. Deficiencies in the orbit modelling or inaccurate frame parameters can thus bias the solutions and may lead to the misinterpretation of results (Bertiger et al., 1994; Couhert et al., 2018). Deriving precise orbits is also of great importance for a highly stable and accurate ITRF, a fundamental basis for geosciences, as satellite orbit errors map into many geodetic parameters such as geocenter motion, station positions or ERP.

Precise orbit determination (POD) does not have a standard solution length to be applied during the data analysis. Its selection depends upon many factors such as satellite orbital height or the type and quantity of parameters that one would like to estimate. In the dynamic or reduced-dynamic approach (Jäggi et al., 2009), solutions with longer observation periods (5-day solutions, 7-day solutions) would result in an increased number of satellite observations, satellite revolutions and an improved observation geometry. This is in general beneficial for diminishing correlations between parameters of different nature (Haines et al., 2015). However, an extension of solution periods can degrade the orbit parameters due to the insufficient modelling of some external forces, which may change throughout the considered periods. Purely or nearly kinematic solutions, on the contrary, tend to use only few or no non-gravitational force models and a large number of empirical parameters to address the occuring model deficiencies in an efficient manner (Montenbruck et al., 2008; Peter et al., 2017).

6.3.1 Impact on Geodetic Parameters

The center of mass (CM) of the Earth refers to the whole Earth including the interior of the Earth, surface ground water, oceans, and atmosphere. Conventionally, one also refers to the center of figure of the outer surface (CF) as satellite dynamics is sensitive to CM, but the term geocenter (offset) refers to the observable vector offset of CF relative to CM. Geocenter motion reflects thus temporal variations triggered by the time-varying global-mass redistribution and is not expected to be zero (Watkins and Eanes, 1997; Kang et al., 2006; Cheng et al., 2013). The seasonal motion is a major unmodeled effect and thus critical for the improvement of the ITRF origin and interpretation of geodetic observations.

Satellite geodesy allows for determination of the geocenter motion and different methods can be used for its retrieval (Lavallée and Blewitt, 2002; Dong et al., 2003; Wu et al., 2012) including geocenter components estimated simultaneously with other dynamical parameters (Cheng et al., 2013; Sośnica et al., 2019). Due to the limited coverage of the Earth by geodetic stations, the CF concept is rather theoretical and geocenter motion is derived based on the center-of-network (CN) frame. Therefore, the CN-derived geocenter motion is technique-specific as it depends to large degree upon the network configuration, and relative motions between CF and CN may occur (Tregoning and van Dam, 2005). Satellite data with longer time spans (months, years) allows to investigate diurnal or inter-seasonal

geocenter motion, which can be estimated with different temporal resolution and parameterized with the use of periodic functions, compliant with a seasonal nature of that parameter (Moore and Wang, 2003; Dong et al., 2003; Petit and Luzum, 2010). In terms of the ITRF origin, which is defined at the mean CM at secular time scales, SLR measurements to geodetic satellites at low altitudes are exclusively used for deriving that frame parameter (Sośnica et al., 2014), mainly due to the orbit characteristics of those satellites and the low impact of non-gravitational perturbing forces. Different orbit inclinations of those satellites (LAGEOS-1 and LAGEOS-2) facilitate also the retrieval of station coordinates by reducing the aliasing by orbital errors. The SLR network is rather sparse and not all tracking stations are available all the time. Together with high weather dependency, this results in a time-varying observing network introducing systematic effects into the geocenter time series (Collilieux et al., 2009). On the contrary, the GNSS-derived geocenter motion (at GNSS altitudes) is rather problematic due to the amount of additional solve-for parameters, GNSS orbit characteristics, satellite shapes, and applied orbit parameterization (Meindl et al., 2013; Thaller et al., 2014). This affects negatively geocenter estimates and tend to introduce offsets or spurious signals visible as peaks in the draconitic periods[27] (Meindl et al., 2013; Rodriguez-Solano et al., 2014). Compared to LAGEOS-1 and LAGEOS-2, higher orbits and less revolutions reduce the sensitivity of GNSS constellations to the geocenter motion, further degrading the retrieval of that parameter. The validation of SLR-derived geocenter products could be in principle carried out with DORIS as its observing network does not vary and stations themselves are homogeneously distributed on the globe. Similarly to GNSS however, the quality of the derived geocenter estimates is still insufficient, and the degraded quality, compared to the SLR-derived products, can be also attributed to the challenges in modelling of the non-gravitational forces affecting the utilized satellites (Couhert et al., 2018). A low quality of geocenter estimates maps directly into errors in station positions. In addition, errors in the satellite orbits bias also station coordinates, mostly in the vertical direction (Rothacher, 2002).

6.4 Geodetic VLBI Observations of Earth Satellites

The concept of VLBI observations of geodetic satellites in the geodetic mode has several potential applications. Primarily, co-location of space-geodetic techniques via satellite targets could facilitate the connection between the ITRS and GCRS. While constraining satellite orbits to respective products derived from other techniques, VLBI station positions could be determined using satellite observations and thus provide means for co-location at core sites. In addition, deriving positions of satellites with respect to quasars could realize the concept of co-location in space. In this case, the performance of technique-specific satellite orbits are evaluated. Among other parameters, VLBI-only POD can also include simultaneous determination of positions of VLBI telescopes.

[27] the time between two consecutive passages of the object through its ascending node

VLBI is a purely geometrical technique. While it has the unique capability of simultaneous determination of a full set of EOP, information that relates to the gravity field or geocenter motion can be only accessed directly by satellite geodesy (GNSS, SLR and DORIS). For VLBI telescopes observing satellites orbiting the Earth's center of mass, this geometric relation can be expressed in terms of the position vector of the geocenter offset $\vec{\mathbf{x}}_G$ w.r.t. the ITRF origin and ITRF position vectors $\vec{\mathbf{x}}_1$, $\vec{\mathbf{x}}_2$ of stations forming a particular baseline. For an Earth satellite with the ITRF position vector $\vec{\mathbf{x}}_{sat}$, the partial derivatives of the near-field VLBI delay (τ) w.r.t. the geocenter coordinates in the Earth-fixed reference frame can be written with a sufficient degree of approximation as (Fukushima, 1994; Sekido and Fukushima, 2006; Meindl et al., 2013)

$$\frac{\partial \tau}{\partial \vec{\mathbf{x}}_G} = \frac{\hat{\mathbf{k}}_{02} - \hat{\mathbf{k}}_{01}}{c}, \tag{6.16}$$

$$\hat{\mathbf{k}}_{01} = \frac{\vec{\mathbf{x}}_{sat} - (\vec{\mathbf{x}}_1 - \vec{\mathbf{x}}_G)}{||\vec{\mathbf{x}}_{sat} - (\vec{\mathbf{x}}_1 - \vec{\mathbf{x}}_G)||}, \tag{6.17}$$

$$\hat{\mathbf{k}}_{02} = \frac{\vec{\mathbf{x}}_{sat} - (\vec{\mathbf{x}}_2 - \vec{\mathbf{x}}_G)}{||\vec{\mathbf{x}}_{sat} - (\vec{\mathbf{x}}_2 - \vec{\mathbf{x}}_G)||}. \tag{6.18}$$

For vectors expressed in the GCRS, Eq. 6.16 can also be used to obtain partial derivatives of τ w.r.t. the position of a satellite. Additionally, either a similar approach or numerical differentiation can be applied to derive Earth rotation parameters with the use of satellite observations. In this case however, one needs to also investigate the sensitivity of such observation types to these solve-for parameters. In essence, the utilization of natural radio sources and dedicated co-location satellites within the same experiments could provide the basis for deriving CRF, TRF, EOP and satellite orbits in a consistent manner. Although such a concept is theoretically possible, the aforementioned parameters can suffer, similarly to GNSS or DORIS, from the orbit modelling issues, network effects or additional solve-for parameters that are often highly correlated with the target parameters. The feasibility of geodetic VLBI for POD of Earth-orbiting satellites and the impact of the orbit determination process on the station-based and global geodetic parameters are investigated in *Paper III* based on a set of Monte-Carlo simulations performed using the *c5++* analysis software.

The co-location of VLBI with other techniques on board of dedicated satellites and the related multi-technique data analysis would assure the homogeneity of global geodetic parameters, allowing also to investigate physically-ambiguous systematic biases that are still present in the single-technique solutions (Böder et al., 2001; Couhert et al., 2018; Luceri et al., 2019; Nothnagel et al., 2019). The reduction of the negative effects of biases is important for various geodetic products and reference frame parameters (Riddell et al., 2017). In the case of GNSS, receiver antenna phase-center patterns, multipath and environment effects (antenna radome changes, monument design) can result in height changes of reference stations. Coupled with satellite antenna phase-center patterns, this subsequently leads to scale errors (common height bias) in the global GNSS solutions (Böder et al., 2001;

Rothacher, 2002). In VLBI however, the observation issues related to receiver (station) antenna phase-center patterns and multipath do not exist. If successful, VLBI-only POD could find its application also in orbit validation. Apart from its significant role in the determination of the TRF, Earth's gravity field and ERP, SLR is also used in the validation of microwave-based GNSS orbits for satellites equipped with corner-cube retroreflectors (Otsubo et al., 2001; Hackel et al., 2015). However, laser observations to GNSS satellites are highly weather dependent, performed during good weather conditions, which may be problematic for obtaining a proper number of observations for the validation purposes (Montenbruck et al., 2015b). Nevertheless, SLR is an important tool for the orbit validation due to fact that laser measurements are free from ionosphere and (significant) troposphere effects as well as not affected by other signal characteristics such as phase ambiguities, satellite clock offsets or phase-center variations.

6.4.1 Rank Defect in Satellite-Quasar Schedules

Proper handling of the datum defect is important in order to correctly represent relations between the observed quantities and not introduce any spurious signals into the time series of parameters of various kinds, see Sec. 3.6.5. Proper (minimum) datum constraints for satellite-quasar schedules have to be identified on a case-by-case basis by performing a rank-defect analysis in order to avoid an over-constrained solution (Kotsakis and Chatzinikos, 2017). An example of the rank defects for the combined satellite-quasar schedules in relation to the quantity (and type) of the estimated parameters is given in Tab. 6.1.

The inclusion of satellite observations into geodetic schedules would allow to reduce the rank defect by three (network origin). In practice however, both the characteristics of satellite orbits and orbit modelling play a significant role in the number of additional constraints that need to be applied. SLR observations to geodetic satellites allow, for instance, to observe the natural origin of satellite orbits, whereas GNSS observations define the TRF origin only in a weak manner due to an overall impact of technique-specific errors and model uncertainties (see Sec. 6.3.1). The combination of satellite and quasar observations requires NNT and NNR conditions imposed on a set of stations in case the analysis would include the simultaneous estimation of ERP, station positions, geocenter offsets and satellite orbits as the rank defect in this case equals six. If the unknown parameters additionally include celestial pole offsets and positions of radio sources, the rank defect is increased to nine. In this case, additional constrains or the source-related NNR condition are required. In the case of satellite-only schedules, a simultaneous estimation of all parameters and the POD process can lead to the scale issue, i.e., a bias affecting all sites in the network. This can again be attributed to the height determination and modelling issues present in the solution, not handled properly when using only satellite observations.

Tab. 6.1 The rank defect in quasar-only, satellite-only and satellite-quasar schedules. The analysis performed based on schedules utilized in *Paper III* considering satellites at GNSS-like and LAGEOS-like altitudes

Network Type	Estimated Parameters				Rank Defect	
	Station Coordinates	ERP	Geocenter	Orbits	GNSS	LAGEOS
Quasars	●	○	-	-	3	
	●	●	-	-	6	
Satellites	●	○	○	○	0	0
	●	○	○	●	1	1
	●	○	●	●	4	4
	●	●	○	●	4	4
	●	●	○	○	3	3
	●	●	●	○	6	6
	●	●	●	●	7	7
Quasars & Satellites	●	○	○	○	0	0
	●	○	○	●	0	0
	●	○	●	●	3	3
	●	●	○	●	3	3
	●	●	○	○	3	3
	●	●	●	○	6	6
	●	●	●	●	6	6

6.4.2 Sensitivity to Geodetic Parameters

The overall sensitivity of global quasar-satellite schedules to geodetic parameters of various kinds should be considered as a combined effect of the network geometry, satellite orbit types, orbit modelling accuracy, residual troposphere and station clock effects, and finally precision of satellite observations. The combination of satellite and quasar observations seems to be a reasonable solution when estimating global geodetic parameters such as ERP or positions of VLBI telescopes, especially for poor satellite geometries. For a low number of satellite passes and non-varying satellite tracks over local skies of the participating stations, the separation between maximum and minimum elevation angles and their azimuthal range is small. This would lead to difficulties in the separation of clock estimates, troposphere parameters and station heights. Apart from other missmodelling effects impacting determination of station positions (non-tidal loading effects, instrumental calibration), the quality of the height estimates is highly dependent upon the applied clock and troposphere models (Herring, 1986; Rothacher, 2002; Männel, 2016). An inclusion of quasar observations can therefore improve the sky coverage and subsequently lead to the enhanced quality of the estimated station coordinates. On the contrary to satellite geodesy, conventional geodetic VLBI benefits also from the absence of satellite orbits and orbit errors. A multi-satellite schedule could in principle allow to sample the sky more uniformly and thus resolve station-based parameters in a correct

manner. However, even a sophisticated satellite-only scheduling approach, utilizing homogeneous networks and determining station positions with centimeter-level accuracy (Plank et al., 2014; Plank et al., 2016; Männel, 2016), can be outperformed by a quasar-only solution with a considerable VLBI network and shorter experiment duration. Moreover, the combination of satellite and quasar scans within the same observing network has also the benefit of identifying prospective timing and technique-specific effects (Himwich et al., 2017; Hellerschmied et al., 2018; Klopotek et al., 2019). Due to mutual visibility constraints, related to the orbital characteristics of satellites and the differential nature of VLBI, it is also unclear whether satellite-only global schedules would be suitable for the simultaneous POD and ERP estimation as the quality of the latter is also related to the separation between the VLBI stations forming a baseline (Nothnagel and Schnell, 2008; Plank et al., 2016). In view of the aforementioned parameters of interest, the optimal schedules are of high importance in order to correctly balance the quantity of quasar observations w.r.t. satellite observations[28], utilize a proper network geometry and quantity/distribution of satellites for a reliable estimation of global geodetic parameters of various kinds, and thus fully exploit the concept of satellite observations by means of VLBI.

[28] also taking into account the distribution of observations over orbital arcs

Chapter 7

Summary & Outlook

Very long baseline interferometry is a mature and fascinating technique, whose applications in astronomy, geodesy and planetary sciences are unique and indisputable. The space-time reference frame realized with the use of VLBI assures the foundation for local and global-scale measurements of various kinds in order to advance our knowledge concerning the Earth system and phenomena that cause it to alter. VLBI for geodesy and astrometry evolves towards more frequent global geodetic schedules with a better spatio-temporal coverage and realized with an increased number of well-distributed stations and radio sources. The next-generation VLBI system, VGOS, has already reached an operationally stable and a global network of several stations. It continuously expands into a truly global infrastructure, with the aim of delivering geodetic parameters and reference frame parameters with an unprecedented quality as well as stimulating new observing concepts for GGOS. Taking the full advantage of high-rate VGOS observations will require improvements in many areas of VLBI, starting with the scheduling process through the continuous monitoring and updating of the radio-source catalogue, data transfer, correlation, post-correlation analysis and modelling of subtle phenomena and effects of the local and global extent. With the anticipated real-time or near real-time observations, automation of this system of complex components remains also a major challenge. Maintaining and improving the geodetic infrastructure is the prerequisite for the long-term sustainability of the ITRF and ICRF. The incorporation of VGOS antennas into the existing reference frame, still defined by the legacy system, is crucial in order to benefit from the long history of legacy observations and enable the continuity of ICRF and ITRF. In addition to classical local-tie measurements, such a task could be also realized with the local interferometry at core sites consisting of multiple radio telescopes or by employing global sessions including radio telescopes of both legacy and VGOS systems, the so-called mixed-mode observations. The transition from the legacy system is thus an important task as frame parameters are a result of the coherent and simultaneous response of all observations and stations materializing the reference system.

The developments made in the VGOS area can be also considered as a fundamental step towards the participation of VLBI in the co-location in space thanks to the broadband characteristics, an increased observation density, improved tracking capabilities and an enhanced measurement precision reaching a single millimeter. In essence, observations of artificial radio sources within the framework of geodetic VLBI would allow for a consistent determination of ICRF, ITRF, Earth orientation parameters, geocenter motion, satellite orbits, lunar targets (absolute/relative positioning) and planetary ephemerides (relative positioning). With VLBI gaining an access to a new set of parameters, this offers also new possibilities for parameter enhancements and cross-validation of geodetic products derived from different space-geodetic observations. However, care has to be taken whenever new observing concepts are considered. Geodetic VLBI augmented with observations of artificial radio sources brings an opportunity of accessing a number of new parameters. However, there are some major challenges related to the observing strategy and the technical feasibility of this concept, both needed to be addressed in a reliable manner. In case future lunar or satellite observations are incorporated into routine geodetic schedules, they should not have any negative impact on the station-based or global geodetic parameters, both being the fundamental and long-term product of space-geodetic techniques. This implies the utilization of optimized schedules that combine all observation types efficiently and that can routinely provide target parameters with the accuracy required for a particular scientific project to thrive. In order to extend the field of space-geodetic research with new applications, a truly multi-disciplinary approach in this area is necessary as it involves specialized system configurations, dedicated instruments and revised data processing routines. The information content of this thesis may be considered as a further step towards observations of artificial radio sources in the framework of geodetic VLBI, with the long-term goal of introducing VLBI into satellite geodesy, for the benefit of the technique itself, consistency among space-geodetic techniques and products that they provide.

Needless to say, geodesy continues to add a huge impact on our lives, from ancient Egypt through the measurements of the Moon and hundreds of satellites orbiting the Earth today. And all because of somebody, who a long time ago looked down into a well...

Chapter 8

Summary of the Appended Papers

Paper I

Geodetic VLBI with an artificial radio source on the Moon: a simulation study

The combination on the observation level of VLBI observations of quasar and lunar targets in the geodetic mode is investigated using Monte-Carlo simulations performed with the *c5++* analysis software. The basis of this simulation study form geodetic schedules reflecting the performance of both the current and the next-generation VLBI systems. The concept itself is investigated by incorporating observations of an artificial radio source on the Moon into the chosen geodetic schedules. Throughout a set of extensive simulations it is investigated how the quality and quantity of lunar observations affect the estimated position of the lunar lander as well as the derived geodetic parameters (station positions, x_p, y_p, $UT1$-UTC). In addition, the impact of major error sources on the determined position of the lunar lander is also described and the limiting factors of the proposed approach are discussed.

I was responsible for implementing the near-field VLBI models and the simulation module (SIMUL) in the c5++ analysis software. I also extended its interface with the new module (VLUN) in order to analyze the simulated lunar observations. Concerning the article, I performed all the simulations, created the figures and wrote the manuscript. The article was prepared in collaboration with my co-authors, who contributed to the study design and helped to improve the manuscript immensely.

Paper II

Position determination of the Chang'e 3 lander with geodetic VLBI

The article concerns VLBI observations of the Chang'e 3 (CE-3) lander in the geodetic mode and describes the results from the analysis of 24-hour sessions dedicated to observations of this lunar target with the use of a global network of VLBI telescopes. The article highlights the processing strategy for deriving quasar and lunar observations as well as the parameterization applied at the data analysis stage. The precision of the obtained lunar observations is also discussed along with the quality of the estimated lunar-based parameters, i.e., coordinates of the CE-3 lander in the Moon-fixed reference frame. The derived position of the lander is also compared with results from other studies and a good agreement is found.

I have implemented all the necessary changes to the interface of c5++ in order to process and analyze the data. My contribution to the following article consisted of the data analysis and the estimation of lunar-based parameters, writing the manuscript and creating the figures. The manuscript was prepared in cooperation with my co-authors, who contributed with valuable feedback.

Paper III

Geodetic VLBI for precise orbit determination of Earth satellites: A simulation study

The manuscript describes a study on the feasibility of the VLBI-only orbit determination of Earth-orbiting satellites and the impact of VLBI observations of satellites on various geodetic products. The proposed concept is investigated with the use of extensive Monte-Carlo simulations, which are carried out with the *c5++* analysis software. The basis of the study form 3-day CONT17 (continuous VLBI campaign 2017) and VGOS schedules, which contain both quasar and satellite observations. The latter are created based on the orbital information of LAGEOS and a set of Galileo satellites located on different orbital planes. Quasar and satellite observations are combined on the observation level and used to derive common parameters as well as satellite orbits and geocenter offsets. The impact of satellite observations and the orbit determination process on geodetic parameters (station positions, x_p, y_p, $UT1$-UTC, geocenter offsets) is investigated with the use of multiple schedules and different assumptions concerning the precision of satellite observations.

I have implemented the new module (VSAT) of c5++ related to VLBI observations of satellites as well as extended its interface with the possibility of carrying out the precise orbit determination of Earth satellites. Concerning the article, I performed all the simulations, created the figures, and wrote the manuscript. My co-authors contributed to the development of the module and provided valuable feedback concerning the study design and the manuscript content.

Bibliography

Agnew, D. C. (2007). Earth Tides. *Treatise on Geophysics: Geodesy*. Edited by T. A. Herring. New York: Elsevier, 163–195.

Altamimi, Z., C. Boucher, and P. Willis (2005). Terrestrial reference frame requirements within GGOS perspective. *Journal of Geodynamics*, 40(4). The Global Geodetic Observing System, 363–374. ISSN: 0264-3707. DOI: 10.1016/j.jog.2005.06.002.

Altamimi, Z., X. Collilieux, and L. Métivier (2013). ITRF Combination: Theoretical and Practical Considerations and Lessons from ITRF2008. *Reference Frames for Applications in Geosciences*. Edited by Z. Altamimi and X. Collilieux. Berlin, Heidelberg: Springer Berlin Heidelberg, 7–12.

Altamimi, Z., C. Boucher, and P. Sillard (2002). New trends for the realization of the international terrestrial reference system. *Advances in Space Research*, 30(2), 175–184. ISSN: 0273-1177. DOI: 10.1016/S0273-1177(02)00282-X.

Altamimi, Z., P. Rebischung, L. Métivier, and X. Collilieux (2016). ITRF2014: A new release of the International Terrestrial Reference Frame modeling nonlinear station motions. *Journal of Geophysical Research: Solid Earth*. ISSN: 2169-9356. DOI: 10.1002/2016JB013098.

Anderson, J. M., G. Beyerle, S. Glaser, L. Liu, B. Männel, T. Nilsson, R. Heinkelmann, and H. Schuh (2018). Simulations of VLBI observations of a geodetic satellite providing co-location in space. *Journal of Geodesy*, 92 (9), 1023–1046. DOI: 10.1007/s00190-018-1115-5.

Anderson, J. M. and M. H. Xu (2018). Source Structure and Measurement Noise Are as Important as All Other Residual Sources in Geodetic VLBI Combined. *Journal of Geophysical Research: Solid Earth*, 123(11), 10, 162–10, 190. DOI: 10.1029/2018JB015550.

Archinal, B. A., M. F. A'Hearn, E. Bowell, A. Conrad, G. J. Consolmagno, R. Courtin, T. Fukushima, D. Hestroffer, J. L. Hilton, G. A. Krasinsky, G. Neumann, J. Oberst, P. K. Seidelmann, P. Stooke, D. Tholen, P. Thomas, and I. Williams (2011). Report of the IAU Working Group on Cartographic Coordinates and Rotational Elements: 2009. *Celestial Mechanics and Dynamical*

Astronomy, 109(2), 101–135. ISSN: 1572-9478. DOI: 10.1007/s10569-010-9320-4.

Arnold, D., M. Meindl, G. Beutler, R. Dach, S. Schaer, S. Lutz, L. Prange, K. Sośnica, L. Mervart, and A. Jäggi (2015). CODE's new solar radiation pressure model for GNSS orbit determination. *Journal of Geodesy*, 89(8), 775–791. ISSN: 1432-1394. DOI: 10.1007/s00190-015-0814-4.

Artz, T., S. Halsig, A. Iddink, and A. Nothnagel (2016). ivg::ASCOT: Development of a New VLBI Software Package. *IVS 2016 General Meeting Proceedings*. (Johannesburg, South Africa). Edited by D. Behrend, K. D. Baver, and K. L. Armstrong. International VLBI Service for Geodesy and Astrometry, 217–221.

Artz, T., L. Bernhard, A. Nothnagel, P. Steigenberger, and S. Tesmer (2012). Methodology for the combination of sub-daily Earth rotation from GPS and VLBI observations. *Journal of Geodesy*, 86(3), 221–239. ISSN: 1432-1394. DOI: 10.1007/s00190-011-0512-9.

Baars, J. W. M. (2007). The Paraboloidal Reflector Antenna in Radio Astronomy and Communication: Theory and Practice. Volume 348. Astrophysics and Space Science Library. Springer, New York, NY. ISBN: 978-0-387-69734-5.

Bar-Shalom, Y., X.-R. Li, and T. Kirubarajan (2001). Estimation with Applications to Tracking and Navigation: Theory Algorithms and Software. Wave summit course. John Wiley & Sons, Inc. ISBN: 0-471-22127-9.

Bare, C., B. G. Clark, K. I. Kellermann, M. H. Cohen, and D. L. Jauncey (1967). Interferometer Experiment with Independent Local Oscillators. *Science*, 157(3785), 189–191. ISSN: 0036-8075. DOI: 10.1126/science.157.3785.189.

Beckley, B. D., F. G. Lemoine, S. B. Luthcke, R. D. Ray, and N. P. Zelensky (2007). A reassessment of global and regional mean sea level trends from TOPEX and Jason-1 altimetry based on revised reference frame and orbits. *Geophysical Research Letters*, 34(14). DOI: 10.1029/2007GL030002.

Bertiger, W. I., Y. E. Bar-Sever, E. J. Christensen, E. S. Davis, J. R. Guinn, B. J. Haines, R. W. Ibanez-Meier, J. R. Jee, S. M. Lichten, W. G. Melbourne, R. J. Muellerschoen, T. N. Munson, Y. Vigue, S. C. Wu, T. P. Yunck, B. E. Schutz, P. A. M. Abusali, H. J. Rim, M. M. Watkins, and P. Willis (1994). GPS precise tracking of TOPEX/POSEIDON: Results and implications. *Journal of Geophysical Research: Oceans*, 99(C12), 24449–24464. DOI: 10.1029/94JC01171.

Beutler, G., E. Brockmann, W. Gurtner, U. Hugentobler, L. Mervart, M. Rothacher, and A. Verdun (1994). Extended orbit modeling techniques at the CODE processing center of the international GPS service for geodynamics (IGS): theory and initial results. *Manuscr. Geod.* 19(6), 367–386.

Beutler, G., A. Jäggi, U. Hugentobler, and L. Mervart (2006). Efficient satellite orbit modelling using pseudo-stochastic parameters. *Journal of Geodesy*, 80(7), 353–372. ISSN: 1432-1394. DOI: 10.1007/s00190-006-0072-6.

Bevis, M., D. Alsdorf, E. Kendrick, L. P. Fortes, B. Forsberg, R. Smalley Jr., and J. Becker (2005). Seasonal fluctuations in the mass of the Amazon River system and Earth's elastic response. *Geophysical Research Letters*, 32(16). DOI: 10.1029/2005GL023491.

Blewitt, G., Z. Altamimi, J. Davis, R. Gross, C.-Y. Kuo, F. G. Lemoine, A. W. Moore, R. E. Neilan, H.-P. Plag, M. Rothacher, C. K. Shum, M. G. Sideris, T. Schöne, P. Tregoning, and S. Zerbini (2010). Geodetic Observations and Global Reference Frame Contributions to Understanding Sea-Level Rise and Variability. *Understanding Sea-Level Rise and Variability*. John Wiley & Sons, Ltd. Chapter 9, pages 256–284. DOI: 10.1002/9781444323276.ch9.

Boccardi, B., T. P. Krichbaum, U. Bach, M. Bremer, and J. A. Zensus (2016). First 3mm-VLBI imaging of the two-sided jet in Cygnus A. *Astronomy & Astrophysics*, 588, L9. ISSN: 1432-0746. DOI: 10.1051/0004-6361/201628412.

Böder, V., F. Menge, G. Seeber, G. Wübbena, and M. Schmitz (2001). How to Deal With Station Dependent Errors - New Developments of the Absolute Field Calibration of PCV and Phase-Multipath With a Precise Robot. *Proceedings of the 14th International Technical Meeting of the Satellite Division of The Institute of Navigation (ION GPS 2001)*. Salt Lake City, Utah, 2166–2176.

Böhm, J., S. Böhm, J. Boisits, A. Girdiuk, J. Gruber, A. Hellerschmied, H. Krásná, D. Landskron, M. Madzak, D. Mayer, J. McCallum, L. McCallum, M. Schartner, and K. Teke (2018). Vienna VLBI and Satellite Software (VieVS) for Geodesy and Astrometry. *Publications of the Astronomical Society of the Pacific*, 130(986), 044503. DOI: 10.1088/1538-3873/aaa22b.

Bolotin, S., K. Baver, J. M. Gipson, D. Gordon, and D. MacMillan (2016). Transition to the vgosDb format. *IVS 2016 General Meeting Proceedings*. (Johannesburg, South Africa). Edited by D. Behrend, K. D. Baver, and K. L. Armstrong. International VLBI Service for Geodesy and Astrometry, 222–224.

Bolotin, S., K. Baver, O. Bolotina, J. M. Gipson, K. Gordon, K. Le Bail, and D. MacMillan (2019). The Source Structure Effect in Broadband Observations. *Proceedings of the 24th European VLBI Group for Geodesy and Astrometry Working Meeting*. Edited by R. Haas, S. Garcia-Espada, and J. A. López Fernández. Las Palmas de Gran Canaria, Spain: Centro Nacional de Información Geográfica (CNIG), 224–228. ISBN: 978-84-416-5634-5. DOI: 10.7419/162.08.2019.

Bolotin, S., K. Baver, J. M. Gipson, D. Gordon, and D. MacMillan (2014). The VLBI Data Analysis Software νSolve: Development Progress and Plans for the Future. *IVS 2014 General Meeting Proceedings*. (Beijing, China). Edited by

D. Behrend, K. D. Baver, and K. L. Armstrong. Science Press, 253–257. ISBN: 978-7-03-042974-2.

Broten, N. W., T. H. Legg, J. L. Locke, C. W. McLeish, R. S. Richards, R. M. Chisholm, H. P. Gush, J. L. Yen, and J. A. Galt (1967). Long Base Line Interferometry: A New Technique. *Science*, 156(3782), 1592–1593. DOI: 10.1126/science.156.3782.1592.

Capitaine, N., B. Guinot, and D. D. McCarthy (2000). Definition of the Celestial Ephemeris Origin and of UT1 in the International Celestial Reference Frame. *Astronomy & Astrophysics*, 335, 398–405.

Capitaine, N., P. T. Wallace, and J. Chapront (2003). Expressions for IAU 2000 precession quantities. *Astronomy & Astrophysics*, 412, 567–586. DOI: 10.1051/0004-6361:20031539.

Cappallo, R. (2014). Correlating and Fringe-fitting Broadband VGOS Data. *IVS 2014 General Meeting Proceedings*. (Beijing,China). Edited by D. Behrend, K. D. Baver, and K. L. Armstrong. International VLBI Service for Geodesy and Astrometry, 91–96.

Cappallo, R. (2016). Delay and Phase Calibration in VGOS Post-Processing. *IVS 2016 General Meeting Proceedings*. (Johannesburg, South Africa). Edited by D. Behrend, K. D. Baver, and K. L. Armstrong. International VLBI Service for Geodesy and Astrometry, 61–64.

Carter, W. E., D. S. Robertson, and J. R. MacKay (1985). Geodetic radio interferometric surveying: Applications and results. *Journal of Geophysical Research: Solid Earth*, 90(B6), 4577–4587. DOI: 10.1029/JB090iB06p04577.

Chao, B. F., D. N. Dong, H. S. Liu, and T. A. Herring (1991). Libration in the Earth's rotation. *Geophysical Research Letters*, 18(11), 2007–2010. ISSN: 1944-8007. DOI: 10.1029/91GL02491.

Chen, G. and T. A. Herring (1997). Effects of atmospheric azimuthal asymmetry on the analysis of space geodetic data. *Journal of Geophysical Research: Solid Earth*, 102(B9), 20489–20502. DOI: 10.1029/97JB01739.

Cheng, M. K., J. C. Ries, and B. D. Tapley (2013). Geocenter Variations from Analysis of SLR Data. *Reference Frames for Applications in Geosciences*. Edited by Z. Altamimi and X. Collilieux. Berlin, Heidelberg: Springer Berlin Heidelberg, 19–25. ISBN: 978-3-642-32998-2.

Cohen, M. H. (1972). Accurate Positions for Radio Sources. *Astrophysical Letters*, 12, 81–85.

Collilieux, X., Z. Altamimi, D. Coulot, J. Ray, and P. Sillard (2007). Comparison of very long baseline interferometry, GPS, and satellite laser ranging height residuals from ITRF2005 using spectral and correlation methods. *Journal of Geophysical Research: Solid Earth*, 112(B12). DOI: 10.1029/2007JB004933.

Collilieux, X., Z. Altamimi, J. Ray, T. van Dam, and X. Wu (2009). Effect of the satellite laser ranging network distribution on geocenter motion estimation. *Journal of Geophysical Research: Solid Earth*, 114(B4). DOI: 10.1029/2008JB005727.

Colombo, O. L. (1989). The dynamics of global positioning system orbits and the determination of precise ephemerides. *Journal of Geophysical Research: Solid Earth*, 94(B7), 9167–9182. DOI: 10.1029/JB094iB07p09167.

Corbin, A., S. Halsig, A. Iddink, F. Jaron, and A. Nothnagel (2017). Automated Ambiguity Resolution With Clustering and Analysisof Intensive Sessions Within ivg::ASCOT. *Proceedings of the 23rd European VLBI Group for Geodesy and Astrometry Working Meeting*. Edited by R. Haas and G. Elgered. Gothenburg, Sweden: Chalmers University of Technology, 238–242. ISBN: 978-91-88041-09-8.

Cotton, W. D. (1995). Fringe fitting. *Very Long Baseline Interferometry and the VLBA*. (Hobart, Australia). Edited by J. A. Zensus, P. J. Diamond, and P. J. Napier. Volume 82. ASP Conference Series, 189–208.

Couhert, A., F. Mercier, J. Moyard, and R. Biancale (2018). Systematic Error Mitigation in DORIS-Derived Geocenter Motion. *Journal of Geophysical Research: Solid Earth*, 123(11), 10, 142–10, 161. DOI: 10.1029/2018JB015453.

Curkendall, D. W. and J. S. Border (2013). Delta-DOR: The One-Nanoradian Navigation Measurement System of the Deep Space Network – History, Architecture, and Componentry. The Interplanetary Network Progress Report, 42–193, 46.

Davies, M. E. and T. R. Colvin (2000). Lunar coordinates in the regions of the Apollo landers. *Journal of Geophysical Research: Planets*, 105(E8), 20277–20280. DOI: 10.1029/1999JE001165.

Davis, J. L., T. A. Herring, I. I. Shapiro, A. E. E. Rogers, and G. Elgered (1985). Geodesy by radio interferometry: Effects of atmospheric modeling errors on estimates of baseline length. *Radio Science*, 20(6), 1593–1607. ISSN: 1944-799X. DOI: 10.1029/RS020i006p01593.

Deller, A. T., W. F. Brisken, C. J. Phillips, J. Morgan, W. Alef, R. Cappallo, E. Middelberg, J. Romney, H. Rottmann, S. J. Tingay, and R. Wayth (2011). DiFX-2: A More Flexible, Efficient, Robust, and Powerful Software Correlator. *Publications of the Astronomical Society of the Pacific*, 123(901), 275.

Deller, A. T., S. Tingay, M. Bailes, and C. West (2007). DiFX: A Software Correlator for Very Long Baseline Interferometry Using Multi-processor Computing Environments. *Publications of the Astronomical Society of the Pacific*, 119(853), 318–336. DOI: 10.1086/513572.

Desai, S. D. and A. E. Sibois (2016). Evaluating predicted diurnal and semidiurnal tidal variations in polar motion with GPS-based observations. *Journal of Geophysical Research: Solid Earth*, 121(7), 5237–5256. DOI: 10.1002/2016JB013125.

Desai, S. D. (2002). Observing the pole tide with satellite altimetry. *Journal of Geophysical Research: Oceans*, 107(C11), 7-1–7-13. ISSN: 2156-2202. DOI: 10.1029/2001JC001224.

Dickey, J. M. (2010). How and Why to Do VLBI on GPS. *IVS 2010 General Meeting Proceedings*. (Hobart, Australia). Edited by D. Behrend and K. D. Baver. International VLBI Service for Geodesy and Astrometry, 65–69.

Dong, D., T. Yunck, and M. Heflin (2003). Origin of the International Terrestrial Reference Frame. *Journal of Geophysical Research: Solid Earth*, 108(B4). DOI: 10.1029/2002JB002035.

Duev, D. A., M. G. Calvés, S. V. Pogrebenko, L. I. Gurvits, G. Cimo, and T. B. Bahamon (2012). Spacecraft VLBI and Doppler tracking: algorithms and implementation. *Astronomy & Astrophysics*, 541, A43. DOI: 10.1051/0004-6361/201218885.

Eriksson, D. and D. S. MacMillan (2014). Continental hydrology loading observed by VLBI measurements. *Journal of Geodesy*, 88(7), 675–690. ISSN: 1432-1394. DOI: 10.1007/s00190-014-0713-0.

Fey, A. L. and P. Charlot (1997). VLBA Observations of Radio Reference Frame Sources. II. Astrometric Suitability Based on Observed Structure. *The Astrophysical Journal Supplement Series*, 111(1), 95–142. DOI: 10.1086/313017.

Fey, A. L., D. Gordon, and C. S. Jacobs, editors (2009). The Second Realization of the International Celestial Reference Frame by Very Long Baseline Interferometry, Presented on behalf of the IERS / IVS Working Group. IERS Technical Note 35. Frankfurt am Main: Verlag des Bundesamts für Kartographie und Geodäsie.

Fiori, F. (2019). Delta-DOR Observations Using VLBI Antennas. *Aerotecnica Missili & Spazio*, 98(3), 175–185. ISSN: 2524-6968. DOI: 10.1007/s42496-019-00023-4.

Fomalont, E. (1995). Astrometry. *Very Long Baseline Interferometry and the VLBA*. (Hobart, Australia). Edited by J. A. Zensus, P. J. Diamond, and P. J. Napier. Volume 82. ASP Conference Series, 363–394.

Fomalont, E., K. Johnston, A. L. Fey, D. Boboltz, T. Oyama, and M. Honma (2011). The Position/Structure Stability of Four ICRF2 Sources. *The Astronomical Journal*, 141(3), 91. DOI: 10.1088/0004-6256/141/3/91.

Fritsche, M., K. Sośnica, C. J. Rodríguez-Solano, P. Steigenberger, K. Wang, R. Dietrich, R. Dach, U. Hugentobler, and M. Rothacher (2014). Homogeneous reprocessing of GPS, GLONASS and SLR observations. *Journal of Geodesy*, 88(7), 625–642. ISSN: 1432-1394. DOI: 10.1007/s00190-014-0710-3.

Fukushima, T. (1994). Lunar VLBI observation model. *Astronomy & Astrophysics*, 291, 320–323.

Fukuzaki, Y., K. Wada, R. Kawabata, M. Ishimoto, and T. Wakasugi (2015). First Geodetic Result of Ishioka VGOS Station. *Proceedings of the 22nd European VLBI Group for Geodesy and Astrometry Working Meeting*. Edited by R. Haas and F. Colomer, 67–70. ISBN: 978-989-20-6191-7.

Gaia Collaboration (2016). The Gaia mission. *A&A*, 595, A1. DOI: 10.1051/0004-6361/201629272.

Gaia Collaboration (2018a). Gaia Data Release 2 - Summary of the contents and survey properties. *A&A*, 616, A1. DOI: 10.1051/0004-6361/201833051.

Gaia Collaboration (2018b). Gaia Data Release 2 - The celestial reference frame (Gaia-CRF2). *A&A*, 616, A14. DOI: 10.1051/0004-6361/201832916.

Gipson, J. M. (1996). Very long baseline interferometry determination of neglected tidal terms in high-frequency Earth orientation variation. *Journal of Geophysical Research: Solid Earth*, 101(B12), 28051–28064. DOI: 10.1029/96JB02292.

Gipson, J. M. (2010). An Introduction to Sked. *IVS 2010 General Meeting Proceedings*. (Hobart, Australia). Edited by D. Behrend and K. D. Baver. International VLBI Service for Geodesy and Astrometry, 77–84.

Gipson, J. M. (2012). IVS Working Group 4: VLBI Data Structures. *IVS 2012 General Meeting Proceedings*. (Madrid, Spain). Edited by D. Behrend and K. D. Baver. International VLBI Service for Geodesy and Astrometry, 212–221.

Gipson, J. M. (2014). IVS Working Group IV and the New Open Format Database. *IVS 2014 General Meeting Proceedings*. (Beijing, China). Edited by D. Behrend, K. D. Baver, and K. L. Armstrong. Science Press, 248–252. ISBN: 978-7-03-042974-2.

Gipson, J. M. (2007). Incorporating Correlated Station Dependent Noise Improves VLBI Estimates. *Proceedings of the 18th Working Meeting on European VLBI for Geodesy and Astrometry*. (Vienna, Austria). Edited by J. Böhm, A. Pany, and H. Schuh. Geowissenschaftliche Mitteilungen, Schriftenreihe der Studienrichtung Vermessung und Geoinformation, Technische Universität Wien, 129–134.

Gipson, J. M. and K. Baver (2016). Improvement of the IVS-INT01 sessions by source selection: development and evaluation of the maximal source strategy. *Journal of Geodesy*, 90(3), 287–303. ISSN: 1432-1394. DOI: 10.1007/s00190-015-0873-6.

Gipson, J. M., D. MacMillan, and L. Petrov (2008). Improved Estimation in VLBI through Better Modelling and Analysis. *IVS 2008 General Meeting Proceedings*. (St. Petersburg, Russia). Edited by A. Finkelstein and D. Behrend. International VLBI Service for Geodesy and Astrometry, 157–162. ISBN: 978-5-02-025332-2.

Gwinn, C. R., T. M. Eubanks, T. Pyne, M. Birkinshaw, and D. N. Matsakis (1997). Quasar Proper Motions and Low-Frequency Gravitational Waves. *The Astrophysical Journal*, 485(1), 87–91. DOI: 10.1086/304424.

Haas, R., S. Casey, J. Conway, G. Elgered, R. Hammargren, L. Helldner, K.-Å. Johansson, U. Kylenfall, M. Lerner, L. Pettersson, and Wennerbäck (2019). Status of the Onsala Twin Telescopes – Two Years After the Inauguration. *Proceedings of the 24th European VLBI Group for Geodesy and Astrometry Working Meeting*. Edited by R. Haas, S. Garcia-Espada, and J. A. López Fernández. Las Palmas de Gran Canaria, Spain: Centro Nacional de Información Geográfica (CNIG), 5–9. ISBN: 978-84-416-5634-5. DOI: 10.7419/162.08.2019.

Haas, R., S. Halsig, S. Han, A. Iddink, F. Jaron, L. La Porta, J. Lovell, A. Neidhardt, A. Nothnagel, C. Plötz, G. Tang, and Z. Zhang (2017). Observing the Chang'E-3 Lander with VLBI (OCEL): Technical Setups and First Results. *Proceedings of the First International Workshop on VLBI Observations of Near-field Targets,October 5 - 6, 2016*. Edited by A. Nothnagel and F. Jaron. Volume 54. *Schriftenreihe des Inst. f. Geodäsie u. Geoinformation*, Vol. 54, ISSN 1864-1113, Bonn, 41–64.

Haas, R., A. Neidhardt, J. Kodet, C. Plötz, U. Schreiber, G. Kronschnabl, S. Pogrebenko, D. Duev, S. Casey, I. Marti-Vidal, and L. Plank (2014). The Wettzell-Onsala G130128 experiment – VLBI-observations of a GLONASS satellite. *IVS 2014 General Meeting Proceedings*. (Beijing, China). International VLBI Service for Geodesy and Astrometry, 451–455.

Hackel, S., P. Steigenberger, U. Hugentobler, M. Uhlemann, and O. Montenbruck (2015). Galileo orbit determination using combined GNSS and SLR observations. *GPS Solutions*, 19(1), 15–25. ISSN: 1521-1886. DOI: 10.1007/s10291-013-0361-5.

Haines, B. J., Y. E. Bar-Sever, W. I. Bertiger, S. D. Desai, N. Harvey, A. E. Sibois, and J. P. Weiss (2015). Realizing a terrestrial reference frame using the Global Positioning System. *Journal of Geophysical Research: Solid Earth*, 120(8), 5911–5939. DOI: 10.1002/2015JB012225.

Halsig, S., A. Bertarini, R. Haas, A. Iddink, J. Kodet, G. Kronschnabl, A. Neidhardt, A. Nothnagel, C. Plötz, and T. Schüler (2019). Atmospheric refraction and system stability investigations in short-baseline VLBI observations. *Journal of Geodesy*, 93(4), 593–614. ISSN: 1432-1394. DOI: 10.1007/s00190-018-1184-5.

Halsig, S., T. Artz, A. Iddink, and A. Nothnagel (2016). Using an atmospheric turbulence model for the stochastic model of geodetic VLBI data analysis. *Earth, Planets and Space*, 68(1). B03407, 1–14. DOI: 10.1186/s40623-016-0482-5.

Hawarey, M., T. Hobiger, and H. Schuh (2005). Effects of the 2nd order ionospheric terms on VLBI measurements. *Geophysical Research Letters*, 32(11). ISSN: 1944-8007. DOI: 10.1029/2005GL022729.

Hellerschmied, A. (2018). Satellite Observations with VLBI. Geowissenschaftliche Mitteilungen 102. Vienna, Austria: Schriftenreihe der Studienrichtung Vermessung und Geoinformation, Technische Universität Wien. URL: http://repositum.tuwien.ac.at/urn:nbn:at:at-ubtuw:1-118370.

Hellerschmied, A., L. McCallum, J. McCallum, J. Sun, J. Böhm, and J. Cao (2018). Observing APOD with the AuScope VLBI Array. *Sensors*, 18(1587). DOI: 10.3390/s18051587.

Herring, T. A. (1986). Precision of vertical position estimates from Very Long Baseline Interferometry. *Journal of Geophysical Research: Solid Earth*, 91(B9), 9177–9182. DOI: 10.1029/JB091iB09p09177.

Herring, T. A. (1992). Submillimeter Horizontal Position Determination Using Very Long Baseline Interferometry. *Journal of Geophysical Research: Solid Earth*, 97(B2), 1981–1990. ISSN: 2156-2202. DOI: 10.1029/91JB02649.

Herring, T. A., J. L. Davis, and I. I. Shapiro (1990). Geodesy by radio interferometry: The application of Kalman Filtering to the analysis of very long baseline interferometry data. *Journal of Geophysical Research: Solid Earth*, 95(B8), 12561–12581. ISSN: 2156-2202. DOI: 10.1029/JB095iB08p12561.

Herring, T. A., I. I. Shapiro, T. A. Clark, C. Ma, J. W. Ryan, B. R. Schupler, C. A. Knight, G. Lundqvist, D. B. Shaffer, N. R. Vandenberg, B. E. Corey, H. F. Hinteregger, A. E. E. Rogers, J. C. Webber, A. Whitney, G. Elgered, B. O. Ronnang, and J. L. Davis (1986). Geodesy by radio interferometry: Evidence for contemporary plate motion. *Journal of Geophysical Research: Solid Earth*, 91(B8), 8341–8347. DOI: 10.1029/JB091iB08p08341.

Himwich, E. (2000). Introduction to the Field System for Non-Users. *IVS 2000 General Meeting Proceedings*. (Kötzting, Germany). Edited by N. R. Vandenberg and K. D. Baver. NASA/CP-2000-209893. International VLBI Service for Geodesy and Astrometry, 86–90.

Himwich, E., A. Bertarini, B. Corey, K. D. Baver, D. Gordon, and L. La Porta (2017). Impact of Station Clocks on UT1–TAI Estimates. *Proceedings of the 23rd European VLBI Group for Geodesy and Astrometry Working Meeting*. Edited by R. Haas and G. Elgered. Gothenburg: Chalmers University of Technology, 172–176. ISBN: 978-91-88041-09-8.

Hobiger, T., C. Rieck, R. Haas, and Y. Koyama (2015). Combining GPS and VLBI for inter-continental frequency transfer. *Metrologia*, 52(2), 251–261. DOI: 10.1088/0026-1394/52/2/251.

Hobiger, T., M. Sekido, Y. Koyama, and T. Kondo (2009a). Integer phase ambiguity estimation in next-generation geodetic Very Long Baseline Interferometry. *Advances in Space Research*, 43(1), 187–192. ISSN: 0273-1177. DOI: 10.1016/j.asr.2008.06.004.

Hobiger, T., R. Ichikawa, Y. Koyama, and T. Kondo (2008). Fast and accurate ray-tracing algorithms for real-time space geodetic applications using numerical weather models. *Journal of Geophysical Research: Atmospheres*, 113(D20). ISSN: 2156-2202. DOI: 10.1029/2008JD010503.

Hobiger, T., T. Kondo, and H. Schuh (2006). Very Long Baseline Interferometry as a tool to probe the ionosphere. *Radio Science*, 41(1). ISSN: 1944-799X. DOI: 10.1029/2005RS003297.

Hobiger, T., Y. Koyama, J. Böhm, T. Kondo, and R. Ichikawa (2009b). The effect of neglecting VLBI reference station clock offsets on UT1 estimates. *Advances in Space Research*, 43(6), 910–916. ISSN: 0273-1177. DOI: 10.1016/j.asr.2008.11.005.

Hobiger, T. and T. Otsubo (2014). Combination of GPS and VLBI on the observation level during CONT11—common parameters, ties and inter-technique biases. *Journal of Geodesy*, 88(11), 1017–1028. ISSN: 1432-1394. DOI: 10.1007/s00190-014-0740-x.

Hobiger, T. and T. Otsubo (2017). Combination of Space Geodetic Techniques on the Observation Level with c5++: Common Nuisance Parameters and Data Weighting. *REFAG 2014*. Edited by T. van Dam. Cham: Springer International Publishing, 31–37.

Hobiger, T., T. Otsubo, and M. Sekido (2014). Observation level combination of SLR and VLBI with c5++: A case study for TIGO. *Advances in Space Research*, 53(1), 119–129. ISSN: 0273-1177.

Hobiger, T., T. Otsubo, M. Sekido, T. Gotoh, T. Kubooka, and H. Takiguchi (2010). Fully automated VLBI analysis with c5++ for ultra rapid determination of UT1. *Earth Planets Space*, 62(12), 933–937. DOI: 10.5047/eps.2010.11.008.

Hofmann, F., L. Biskupek, and J. Müller (2018). Contributions to reference systems from Lunar Laser Ranging using the IfE analysis model. *Journal of Geodesy*, 92(9), 975–987. DOI: 10.1007/s00190-018-1109-3.

Hofmeister, A. and J. Böhm (2017). Application of ray-traced tropospheric slant delays to geodetic VLBI analysis. *Journal of Geodesy*, 1–20.

Iess, L., M. Di Benedetto, N. James, M. Mercolino, L. Simone, and P. Tortora (2014). Astra: Interdisciplinary study on enhancement of the end-to-end accuracy for spacecraft tracking techniques. *Acta Astronautica*, 94(2), 699–707. ISSN: 0094-5765. DOI: 10.1016/j.actaastro.2013.06.011.

Jäggi, A., R. Dach, O. Montenbruck, U. Hugentobler, H. Bock, and G. Beutler (2009). Phase center modeling for LEO GPS receiver antennas and its impact on precise orbit determination. *Journal of Geodesy*, 83(12), 1145. ISSN: 1432-1394. DOI: 10.1007/s00190-009-0333-2.

Jones, D. L., W. M. Folkner, R. A. Jacobson, C. S. Jacobs, V. Dhawan, J. Romney, and E. Fomalont (2015). Astrometry of Cassini With the VLBA to Improve the Saturn Ephemeris. *The Astronomical Journal*, 149, 28. DOI: 10.1088/0004-6256/149/1/28.

Jones, D. L., W. M. Folkner, R. A. Jacobson, C. S. Jacobs, J. Romney, and V. Dhawan (2020). Very Long Baseline Array Astrometry of Cassini: The Final

Epochs and an Improved Orbit of Saturn. *The Astronomical Journal*, 159(2), 72. DOI: 10.3847/1538-3881/ab5f5d.

Jones, D. L., E. Fomalont, V. Dhawan, J. Romney, W. M. Folkner, G. Lanyi, J. Border, and R. A. Jacobson (2010). Very Long Baseline Array Astrometric Observations of the *Cassini* Spacecraft at Saturn. *The Astronomical Journal*, 141(2), 29. DOI: 10.1088/0004-6256/141/2/29.

Kalman, R. E. (1960). A New Approach to Linear Filtering and Prediction Problems. *Journal of Basic Engineering*, 82(1), 35–45. ISSN: 0021-9223. DOI: 10.1115/1.3662552.

Kang, Z., B. Tapley, S. Bettadpur, J. Ries, P. Nagel, and R. Pastor (2006). Precise orbit determination for the GRACE mission using only GPS data. *Journal of Geodesy*, 80(6), 322–331. ISSN: 1432-1394. DOI: 10.1007/s00190-006-0073-5.

Karbon, M., B. Soja, T. Nilsson, Z. Deng, R. Heinkelmann, and H. Schuh (2017). Earth orientation parameters from VLBI determined with a Kalman filter. *Geodesy and Geodynamics*, 8(6), 396–407. ISSN: 1674-9847. DOI: 10.1016/j.geog.2017.05.006.

Karbon, M., S. Belda, and T. Nilsson (2019). Impact of the terrestrial reference frame on the determination of the celestial reference frame. *Geodesy and Geodynamics*, 10(1), 58–71. ISSN: 1674-9847. DOI: 10.1016/j.geog.2018.11.001.

Kareinen, N., T. Hobiger, and R. Haas (2015). Automated analysis of Kokee–Wettzell Intensive VLBI sessions—algorithms, results, and recommendations. *Earth, Planets and Space*, 67(1), 181. DOI: 10.1186/s40623-015-0340-x.

Kareinen, N., T. Hobiger, and R. Haas (2016). Automated ambiguity estimation for VLBI Intensive sessions using L1-norm. *Journal of Geodynamics*, 102, 39–46. ISSN: 0264-3707. DOI: 10.1016/j.jog.2016.07.003.

Kareinen, N., G. Klopotek, T. Hobiger, and R. Haas (2017). Identifying optimal tag-along station locations for improving VLBI Intensive sessions. *Earth, Planets and Space*, 69(16), 1–9. DOI: 10.1186/s40623-017-0601-y.

Kedar, S., G. A. Hajj, B. D. Wilson, and M. B. Heflin (2003). The effect of the second order GPS ionospheric correction on receiver positions. *Geophysical Research Letters*, 30(16). DOI: 10.1029/2003GL017639.

Keimpema, A., M. M. Kettenis, S. V. Pogrebenko, R. M. Campbell, G. Cimó, D. A. Duev, B. Eldering, N. Kruithof, H. J. van Langevelde, D. Marchal, G. Molera Calvés, H. Ozdemir, Z. Paragi, Y. Pidopryhora, A. Szomoru, and J. Yang (2015). The SFXC software correlator for very long baseline interferometry: algorithms and implementation. *Experimental Astronomy*, 39(2), 259–279. ISSN: 1572-9508. DOI: 10.1007/s10686-015-9446-1.

Kikuchi, F., Q. Liu, H. Hanada, N. Kawano, K. Matsumoto, T. Iwata, S. J. Goossens, K. Asari, Y. Ishihara, S. Tsuruta, T. Ishikawa, H. Noda, N. Namiki, N. Petrova, Y. Harada, J. Ping, and S. Sasaki (2009). Picosecond accuracy VLBI of the

two subsatellites of SELENE (KAGUYA) using multifrequency and same beam methods. *Radio Science*, 44(2). ISSN: 1944-799X. DOI: 10.1029/2008RS003997.

King-Hele, D. (2008). A Tapestry of Orbits. Cambrige Univeristy Press. ISBN: 9780521017329.

King, R. W., C. C. Counselman, and I. I. Shapiro (1976). Lunar dynamics and selenodesy: Results from analysis of VLBI and laser data. *Journal of Geophysical Research*, 81(35), 6251–6256. ISSN: 2156-2202. DOI: 10.1029/JB081i035p06251.

Kirkvik, A.-S., G. A. Hjelle, M. Dähnn, I. Fausk, and E. Mysen (2017). Where - A New Software for Geodetic Analysis. *Proceedings of the 23rd European VLBI Group for Geodesy and Astrometry Working Meeting*. Edited by R. Haas and G. Elgered. Gothenburg, Sweden: Chalmers University of Technology, 248–252. ISBN: 978-91-88041-09-8.

Klioner, S. A. (2003). A Practical Relativistic Model for Microarcsecond Astrometry in Space. *The Astronomical Journal*, 125(3), 1580. DOI: 10.1086/367593.

Klopotek, G. (2017). Simulation studies of new observing concepts for geodetic Very Long Baseline Interferometry. Licentiate Thesis of the Department of Space, Earth and Environment, Chalmers University of Technology. Gothenburg.

Klopotek, G., T. Artz, A. Bellanger, G. Bourda, M. Gerstl, D. Gordon, R. Haas, S. Halsig, G. A. Hjelle, T. Hobiger, U. Hugentobler, A. Iddink, A.-S. Kirkvik, S. Lambert, L. Plank, R. Schmid, F. Shu, O. Titov, F. Tong, and G. Wang (2016). Results from the VLBI Analysis Software Comparison Campaign 2015. *IVS 2016 General Meeting Proceedings*. (Johannesburg, South Africa). Edited by D. Behrend, K. D. Baver, and K. L. Armstrong. International VLBI Service for Geodesy and Astrometry, 203–207.

Klopotek, G., T. Hobiger, and R. Haas (2017). Implementation of VLBI Near-Field Delay Models in the c5++ Analysis Software. *Proceedings of the First International Workshop on VLBI Observations of Near-field Targets,October 5 - 6, 2016*. Edited by A. Nothnagel and F. Jaron. Volume 54. *Schriftenreihe des Inst. f. Geodäsie u. Geoinformation*, Vol. 54, ISSN 1864-1113, Bonn, 29–33.

Klopotek, G., T. Hobiger, and R. Haas (2018). Geodetic VLBI with an artificial radio source on the Moon: a simulation study. *Journal of Geodesy*, 92 (5), 457–469. DOI: 10.1007/s00190-017-1072-4.

Klopotek, G., T. Hobiger, R. Haas, F. Jaron, L. La Porta, A. Nothnagel, Z. Zhang, S. Han, A. Neidhardt, and C. Plötz (2019). Position determination of the Chang'e 3 lander with geodetic VLBI. *Earth, Planets and Space*, 71(23). ISSN: 1880-5981. DOI: 10.1186/s40623-019-1001-2.

Klopotek, G., T. Hobiger, R. Haas, and T. Otsubo (2020). Geodetic VLBI for precise orbit determination of Earth satellites: A simulation study. *Journal of Geodesy*. under rewiev.

Kondo, T. and K. Takefuji (2016). An algorithm of wideband bandwidth synthesis for geodetic VLBI. *Radio Science*, 51(10), 1686–1702. DOI: 10.1002/2016RS006070.

Kotsakis, C. (2013). Generalized inner constraints for geodetic network densification problems. *Journal of Geodesy*, 87(7), 661–673. ISSN: 1432-1394. DOI: 10.1007/s00190-013-0637-0.

Kotsakis, C. and M. Chatzinikos (2017). Rank defect analysis and the realization of proper singularity in normal equations of geodetic networks. *Journal of Geodesy*, 91(6), 627–652. ISSN: 1432-1394. DOI: 10.1007/s00190-016-0989-3.

Koyama, Y. (2013). Developments of K3, K4, and K5 VLBI Systems and Considerations for the new K6 VLBI System. *Technology Development Center News. National Institute of Information and Communications Technology* (33), 39–43.

Krásná, H., Z. Malkin, and J. Böhm (2015). Non-linear VLBI station motions and their impact on the celestial reference frame and Earth orientation parameters. *Journal of Geodesy*, 89(10), 1019–1033. ISSN: 1432-1394. DOI: 10.1007/s00190-015-0830-4.

Krügel, M., D. Thaller, V. Tesmer, M. Rothacher, D. Angermann, and R. Schmid (2007). Tropospheric parameters: combination studies based on homogeneous VLBI and GPS data. *Journal of Geodesy*, 81(6), 515–527. ISSN: 1432-1394. DOI: 10.1007/s00190-006-0127-8.

Lagler, K., M. Schindelegger, J. Böhm, H. Krásná, and T. Nilsson (2013). GPT2: Empirical slant delay model for radio space geodetic techniques. *Geophysical Research Letters*, 40(6), 1069–1073. ISSN: 1944-8007. DOI: 10.1002/grl.50288.

Landskron, D. and J. Böhm (2018). VMF3/GPT3: refined discrete and empirical troposphere mapping functions. *Journal of Geodesy*, 92(4), 349–360. ISSN: 1432-1394. DOI: 10.1007/s00190-017-1066-2.

Landskron, D. and J. Böhm (2019). Improving dUT1 from VLBI intensive sessions with GRAD gradients and ray-traced delays. *Advances in Space Research*, 63(11), 3429–3435. ISSN: 0273-1177. DOI: 10.1016/j.asr.2019.03.041.

Lavallée, D. and G. Blewitt (2002). Degree-1 Earth deformation from very long baseline interferometry measurements. *Geophysical Research Letters*, 29(20), 28-1-28-4. DOI: 10.1029/2002GL015883.

Lebreton, J.-P., O. Witasse, C. Sollazzo, T. Blancquaert, P. Couzin, A.-M. Schipper, J. B. Jones, D. L. Matson, L. I. Gurvits, D. H. Atkinson, B. Kazeminejad, and M. Perez-Ayucar (2005). An overview of the descent and landing of the Huygens probe on Titan. *Nature*, 438 (7069), 758–764. DOI: 10.1038/nature04347.

Leek, J., T. Artz, and A. Nothnagel (2015). Optimized scheduling of VLBI UT1 intensive sessions for twin telescopes employing impact factor analysis. *Journal of Geodesy*, 89, 911–924. DOI: 10.1007/s00190-015-0823-3.

Li, C., J. Liu, X. Ren, W. Zuo, X. Tan, W. Wen, H. Li, L. Mu, Y. Su, H. Zhang, J. Yan, and Z. Ouyang (2015). The Chang'e 3 Mission Overview. *Space Science Reviews*, 190(1), 85–101. ISSN: 1572-9672. DOI: 10.1007/s11214-014-0134-7.

Lösler, M., R. Haas, C. Eschelbach, and A. Greiwe (2019). Gravitational deformation of ring-focus antennas for VGOS: first investigations at the Onsala twin telescopes project. *Journal of Geodesy*, 93(10), 2069–2087. ISSN: 1432-1394. DOI: 10.1007/s00190-019-01302-5.

Luceri, V., M. Pirri, J. Rodríguez, G. Appleby, E. C. Pavlis, and H. Müller (2019). Systematic errors in SLR data and their impact on the ILRS products. *Journal of Geodesy*, 93(11), 2357–2366. ISSN: 1432-1394. DOI: 10.1007/s00190-019-01319-w.

Ma, C., E. F. Arias, T. M. Eubanks, A. L. Fey, A.-M. Gontier, C. S. Jacobs, O. J. Sovers, B. A. Archinal, and P. Charlot (1998). The International Celestial Reference Frame as Realized by Very Long Baseline Interferometry. *The Astronomical Journal*, 116(1), 516.

Ma, C., J. M. Sauber, L. J. Bell, T. A. Clark, D. Gordon, W. E. Himwich, and R. J. W. (1990). Measurement of horizontal motions in Alaska using very long baseline interferometry. *Journal of Geophysical Research: Solid Earth*, 95(B13), 21991–22011. ISSN: 2156-2202. DOI: 10.1029/JB095iB13p21991.

MacMillan, D. S., A. Fey, J. M. Gipson, D. Gordon, C. S. Jacobs, H. Krásná, S. B. Lambert, Z. Malkin, O. Titov, G. Wang, and M. H. Xu (2019). Galactocentric acceleration in VLBI analysis - Findings of IVS WG8. *Astronomy & Astrophysics*, 630, A93. DOI: 10.1051/0004-6361/201935379.

MacMillan, D. S. and C. Ma (1997). Atmospheric gradients and the VLBI terrestrial and celestial reference frames. *Geophysical Research Letters*, 24(4), 453–456. DOI: 10.1029/97GL00143.

MacMillan, D. S. (1995). Atmospheric gradients from very long baseline interferometry observations. *Geophysical Research Letters*, 22(9), 1041–1044. ISSN: 1944-8007. DOI: 10.1029/95GL00887.

Malkin, Z. (2013). Impact of seasonal station motions on VLBI UT1 intensives results. *Journal of Geodesy*, 87(6), 505–514. ISSN: 1432-1394. DOI: 10.1007/s00190-013-0624-5.

Malkin, Z., C. S. Jacobs, E. F. Arias, D. Boboltz, J. Böhm, S. Bolotin, G. Bourda, P. Charlot, A. De Witt, A. L. Fey, R. Gaume, R. Heinkelmann, S. Lambert, C. Ma, A. Nothnagel, D. Seitz, D. Gordon, E. Skurikhina, J. Souchay, and O. Titov (2015). The ICRF-3: Status, plans, and progress on the next generation International Celestial Reference Frame. *Proceedings of the Journées 2014 'Systèmes de référence Spatio-temporels' (JSR2014)*. Edited by Z. Malkin and N. Capitaine, 3–8.

Männel, B. (2016). Co-location of Geodetic Observation Techniques in Space. Doctoral Thesis, ETH NO. 23796. Zürich. DOI: 10.3929/ethz-a-010811791.

Männel, B. and M. Rothacher (2016). Ionospheric corrections for single-frequency tracking of GNSS satellites by VLBI based on co-located GNSS. *Journal of Geodesy*, 90(2), 189–203. ISSN: 1432-1394. DOI: 10.1007/s00190-015-0865-6.

Marknäs, V. (2019). Connecting the Onsala Telescope Cluster Using Local Interferometry. Master's thesis. Chalmers University of Technology.

Mathews, P. M., T. A. Herring, and B. A. Buffett (2002). Modeling of nutation and precession: New nutation series for nonrigid Earth and insights into the Earth's interior. *Journal of Geophysical Research: Solid Earth*, 107(B4), ETG 3-1–ETG 3-26. ISSN: 2156-2202. DOI: 10.1029/2001JB000390.

McCallum, J., L. Plank, A. Hellerschmied, J. Böhm, and J. Lovell (2017). Technical Challenges in VLBI Observations of GNSS Sources. *Proceedings of the First International Workshop on VLBI Observations of Near-field Targets,October 5 - 6, 2016*. Edited by A. Nothnagel and F. Jaron. Volume 54. *Schriftenreihe des Inst. f. Geodäsie u. Geoinformation*, Vol. 54, ISSN 1864-1113, Bonn, 7–10.

Meindl, M., G. Beutler, D. Thaller, R. Dach, and A. Jäggi (2013). Geocenter coordinates estimated from GNSS data as viewed by perturbation theory. *Advances in Space Research*, 51(7), 1047–1064. ISSN: 0273-1177. DOI: 10.1016/j.asr.2012.10.026.

Mendes Cerveira, P. J., J. Böhm, E. Tanir, J. Wresnik, H. Schuh, and V. Tesmer (2007). Datum Deficiency in VLBI Analysis: Case Study of Session 021020XA. *Proceedings of the 18th Working Meeting on European VLBI for Geodesy and Astrometry*. (Vienna, Austria). Edited by J. Böhm, A. Pany, and H. Schuh. Geowissenschaftliche Mitteilungen, Schriftenreihe der Studienrichtung Vermessung und Geoinformation, Technische Universität Wien, 209–215.

Montenbruck, O., Y. Andres, H. Bock, T. van Helleputte, J. van den Ijssel, M. Loiselet, C. Marquardt, P. Silvestrin, P. Visser, and Y. Yoon (2008). Tracking and orbit determination performance of the GRAS instrument on MetOp-A. *GPS Solutions*, 12, 289–299. DOI: 10.1007/s10291-008-0091-2.

Montenbruck, O., R. Schmid, F. Mercier, P. Steigenberger, C. Noll, R. Fatkulin, S. Kogure, and A. Ganeshan (2015a). GNSS satellite geometry and attitude models. *Advances in Space Research*, 56(6), 1015–1029. ISSN: 0273-1177. DOI: 10.1016/j.asr.2015.06.019.

Montenbruck, O. and E. Gill, editors (2000). Satellite Orbits – Models, Methods and Applications. Springer-Verlag Berlin Heidelberg. ISBN: 978-3-642-58351-3. DOI: 10.1007/978-3-642-58351-3.

Montenbruck, O., P. Steigenberger, and U. Hugentobler (2015b). Enhanced solar radiation pressure modeling for Galileo satellites. *Journal of Geodesy*, 89(3), 283–297. ISSN: 1432-1394. DOI: 10.1007/s00190-014-0774-0.

Montenbruck, O., P. Steigenberger, L. Prange, Z. Deng, Q. Zhao, F. Perosanz, I. Romero, C. Noll, A. Stürze, G. Weber, R. Schmid, K. MacLeod, and S. Schaer (2017). The Multi-GNSS Experiment (MGEX) of the International GNSS Service (IGS) – Achievements, prospects and challenges. *Advances in Space Research*, 59(7), 1671–1697. ISSN: 0273-1177.

Moore, P. and J. Wang (2003). Geocentre variation from laser tracking of LAGEOS12 and loading data. *Advances in Space Research*, 31(8), 1927–1933. ISSN: 0273-1177. DOI: 10.1016/S0273-1177(03)00170-4.

Moyer, T. D. (2000). Formulation for Observed and Computed Values of Deep Space Network Data Types for Navigation. JPL Deep-Space Communications and Navigation Series. JPL Monbograph2 (JPL Publication 00-7).

Müller, J., J. G. Williams, S. G. Turyshev, and P. J. Shelus (2007). Potential Capabilities of Lunar Laser Ranging for Geodesy and Relativity. *Dynamic Planet: Monitoring and Understanding a Dynamic Planet with Geodetic and Oceanographic Tools IAG Symposium Cairns, Australia 22–26 August, 2005*. Edited by P. Tregoning and C. Rizos. Berlin, Heidelberg: Springer Berlin Heidelberg, pages 903–909. ISBN: 978-3-540-49350-1. DOI: 10.1007/978-3-540-49350-1_126.

Newhall, X. X., R. A. Preston, and F. B. Esposito (1986). Relating the JPL VLBI Reference Frame and the Planetary Ephemerides. *Astrometric Techniques*. Edited by H. K. Eichhorn and R. J. Leacock. Dordrecht: Springer Netherlands, 789–794. ISBN: 978-94-009-4676-7.

Niell, A., M. Bark, C. Beaudin, W. Brisken, H. Ben Frej, S. Doeleman, S. Durand, M. Guerra, A. Hinton, M. Luce, R. McWhirter, K. Morris, G. Peck, M. Revnell, A. Rogers, J. Romney, C. Ruszczyk, M. Taveniku, R. Walker, and A. Whitney (2010). RDBE Development and Progress. *IVS 2010 General Meeting Proceedings*. (Hobart, Australia). Edited by D. Behrend and K. D. Baver. International VLBI Service for Geodesy and Astrometry, 396–399.

Niell, A. (1996). Global mapping functions for the atmosphere delay at radio wavelengths. *Journal of Geophysical Research: Solid Earth*, 101(B2), 3227–3246. ISSN: 2156-2202. DOI: 10.1029/95JB03048.

Niell, A., J. Barrett, A. Burns, R. Cappallo, B. Corey, M. Derome, C. Eckert, P. Elosegui, R. McWhirter, M. Poirier, G. Rajagopalan, A. E. E. Rogers, C. Ruszczyk, J. SooHoo, M. Titus, A. R. Whitney, D. Behrend, S. Bolotin, J. M. Gipson, D. Gordon, E. Himwich, and B. Petrachenko (2018). Demonstration of a Broadband Very Long Baseline Interferometer System: A New Instrument for High-Precision Space Geodesy. *Radio Science*, 53(10), 1269–1291. DOI: 10.1029/2018RS006617.

Niell, A., A. R. Whitney, B. Petrachenko, W. Schlüter, N. Vandenberg, H. Hase, Y. Koyama, C. Ma, H. Schuh, and G. Tuccari (2006). VLBI2010: Current and Future Requirements for Geodetic VLBI Systems. *International VLBI Service*

for Geodesy and Astrometry 2005 Annual Report. Edited by D. Behrend and K. Baver. NASA/TP-2006-214136. IVS Coordinating Center.

Nilsson, T., R. Haas, and G. Elgered (2007). Simulations of Atmospheric Path Delays Using Turbulence Models. *Proceedings of the 18th Working Meeting on European VLBI for Geodesy and Astrometry*. (Vienna, Austria). Edited by J. Böhm, A. Pany, and H. Schuh. Geowissenschaftliche Mitteilungen, Schriftenreihe der Studienrichtung Vermessung und Geoinformation, Technische Universität Wien, 175–180.

Nilsson, T., B. Soja, M. Karbon, R. Heinkelmann, and H. Schuh (2015). Application of Kalman filtering in VLBI data analysis. *Earth, Planets and Space*, 67(1), 136. ISSN: 1880-5981. DOI: 10.1186/s40623-015-0307-y.

Nosov, E., D. Ivanov, and A. Ipatov (2018). Extending of 'Quasar' VLBI-network: VGOS-compatible radio telescopein Svetloe. *IVS 2018 General Meeting Proceedings*. (Longyearbyen, Norway). Edited by K. L. Armstrong, K. D. Baver, and D. Behrend. NASA/CP–2019-219039. International VLBI Service for Geodesy and Astrometry, 12–16.

Nothnagel, A. (2019). The correlation process in Very Long Baseline Interferometry. *GEM - International Journal of Geomathematics*, 10(18). DOI: 10.1007/s13137-019-0130-x.

Nothnagel, A., C. Holst, and R. Haas (2019). A VLBI delay model for gravitational deformations of the Onsala 20 m radio telescope and the impact on its global coordinates. *Journal of Geodesy*. ISSN: 1432-1394. DOI: 10.1007/s00190-019-01299-x.

Nothnagel, A. (2009). Conventions on thermal expansion modelling of radio telescopes for geodetic and astrometric VLBI. *Journal of Geodesy*, 83(8), 787–792. ISSN: 1432-1394. DOI: 10.1007/s00190-008-0284-z.

Nothnagel, A., T. Artz, D. Behrend, and Z. Malkin (2016). International VLBI Service for Geodesy and Astrometry - Delivering high-quality products and embarking on observations of the next generation. *Journal of Geodesy*.

Nothnagel, A. and D. Schnell (2008). The impact of errors in polar motion and nutation on UT1 determinations from VLBI Intensive observations. *Journal of Geodesy*, 82(12), 863–869. ISSN: 1432-1394. DOI: 10.1007/s00190-008-0212-2.

Nothnagel, A., M. Vennebusch, and J. Campbell (2002). On Correlations Between Parameters in Geodetic VLBI Data Analysis. *IVS 2002 General Meeting Proceedings*. (Tsukuba, Japan). Edited by N. Vandenberg and K. D. Baver. International VLBI Service for Geodesy and Astrometry, 260–264.

Otsubo, T., G. M. Appleby, and P. Gibbs (2001). Glonass Laser Ranging Accuracy With Satellite Signature Effect. *Surveys in Geophysics*, 22(5), 509–516. ISSN: 1573-0956. DOI: 10.1023/A:1015676419548.

Panafidina, N., U. Hugentobler, M. Seitz, and H. Krásná (2017). Influence of subdaily polar motion model on nutation offsets estimated by very long baseline interferometry. *Journal of Geodesy*, 91(12), 1503–1512. ISSN: 1432-1394. DOI: 10.1007/s00190-017-1039-5.

Pavlov, D. (2020). Role of lunar laser ranging in realization of terrestrial, lunar, and ephemeris reference frames. *Journal of Geodesy*, 94(5). DOI: 10.1007/s00190-019-01333-y.

Peter, H., A. Jäggi, J. Fernández, D. Escobar, F. Ayuga, D. Arnold, M. Wermuth, S. Hackel, M. Otten, W. Simons, P. Visser, U. Hugentobler, and P. Féménias (2017). Sentinel-1A – First precise orbit determination results. *Advances in Space Research*, 60(5), 879–892. ISSN: 0273-1177. DOI: 10.1016/j.asr.2017.05.034.

Petit, G. and B. Luzum, editors (2010). IERS Conventions (2010). IERS Technical Note 36. Frankfurt am Main: Verlag des Bundesamts für Kartographie und Geodäsie, 179. ISBN: 3-89888-989-62.

Petrachenko, B., A. Niell, D. Behrend, B. Corey, J. Böhm, P. Charlot, A. Collioud, J. M. Gipson, R. Haas, T. Hobiger, Y. Koyama, D. MacMillan, Z. Malkin, T. Nilsson, A. Pany, G. Tuccari, A. R. Whitney, and J. Wresnik (2009). Design aspects of the VLBI2010 system. *Progress report of the IVS VLBI2010 committee*.

Piner, B. G., M. Mahmud, A. L. Fey, and K. Gospodinova (2007). Relativistic Jets in the Radio Reference Frame Image Database. I. Apparent Speeds from the First 5 Years of Data. *The Astronomical Journal*, 133(5), 2357–2388. DOI: 10.1086/514812.

Plag, H. P. and M. Pearlman, editors (2009). Global Geodetic Observing System: Meeting the Requirements of a Global Society on a Changing Planet in 2020. Springer-Verlag Berlin Heidelberg, 332. DOI: 10.1007/978-3-642-02687-4.

Plank, L., J. Böhm, and H. Schuh (2014). Precise station positions from VLBI observations to satellites: a simulation study. *Journal of Geodesy*, 88(7), 659–673. ISSN: 1432-1394. DOI: 10.1007/s00190-014-0712-1.

Plank, L., J. Böhm, and H. Schuh (2016). Simulated VLBI Satellite Tracking of the GNSS Constellation: Observing Strategies. *IAG 150 Years*. Edited by C. Rizos and P. Willis. Cham: Springer International Publishing, 85–90. ISBN: 978-3-319-30895-1.

Plank, L., A. Hellerschmied, J. McCallum, J. Böhm, and J. Lovell (2017). VLBI observations of GNSS-satellites: from scheduling to analysis. *Journal of Geodesy*, 91(7), 867–880. ISSN: 1432-1394. DOI: 10.1007/s00190-016-0992-8.

Prange, L., G. Beutler, R. Dach, D. Arnold, S. Schaer, and A. Jäggi (2020). An empirical solar radiation pressure model for satellites moving in the orbit-normal mode. *Advances in Space Research*, 65(1), 235–250. ISSN: 0273-1177. DOI: 10.1016/j.asr.2019.07.031.

Ray, J. and Z. Altamimi (2005). Evaluation of co-location ties relating the VLBI and GPS reference frames. *Journal of Geodesy*, 79(4), 189–195. ISSN: 1432-1394. DOI: 10.1007/s00190-005-0456-z.

Ray, R. D. and R. M. Ponte (2003). Barometric tides from ECMWF operational analyses. *Annales Geophysica*, 21, 1897–1910. DOI: 10.5194/angeo-21-1897-2003.

Riddell, A. R., M. A. King, C. S. Watson, Y. Sun, R. E. M. Riva, and R. Rietbroek (2017). Uncertainty in geocenter estimates in the context of ITRF2014. *Journal of Geophysical Research: Solid Earth*, 122(5), 4020–4032. DOI: 10.1002/2016JB013698.

Robertson, D. S. and W. E. Carter (1984). Relativistic deflection of radio signals in the solar gravitational field measured with VLBI. *Nature*, 310 (5978), 572–574. DOI: 10.1038/310572a0.

Rodriguez-Solano, C. J., U. Hugentobler, P. Steigenberger, M. Bloßfeld, and M. Fritsche (2014). Reducing the draconitic errors in GNSS geodetic products. *Journal of Geodesy*, 88(6), 559–574. ISSN: 1432-1394. DOI: 10.1007/s00190-014-0704-1.

Rodriguez-Solano, C. J., U. Hugentobler, and P. Steigenberger (2012a). Adjustable box-wing model for solar radiation pressure impacting GPS satellites. *Advances in Space Research*, 49(7), 1113–1128. ISSN: 0273-1177. DOI: doi.org/10.1016/j.asr.2012.01.016.

Rodriguez-Solano, C. J., U. Hugentobler, P. Steigenberger, and S. Lutz (2012b). Impact of Earth radiation pressure on GPS position estimates. *Journal of Geodesy*, 86(5), 309–317. ISSN: 1432-1394. DOI: 10.1007/s00190-011-0517-4.

Rogers, A. E. E. (1970). Very Long Baseline Interferometry with Large Effective Bandwidth for Phase-Delay Measurements. *Radio Science*, 5(10), 1239–1247. ISSN: 1944-799X. DOI: 10.1029/RS005i010p01239.

Rogers, A. E. E., R. J. Cappallo, H. F. Hinteregger, J. I. Levine, E. F. Nesman, J. C. Webber, A. R. Whitney, T. A. Clark, C. Ma, J. Ryan, B. E. Corey, C. C. Counselman, T. A. Herring, I. I. Shapiro, C. A. Knight, D. B. Shaffer, N. R. Vandenberg, R. Lacasse, R. Mauzy, B. Rayhrer, B. R. Schupler, and J. C. Pigg (1983). Very-Long-Baseline Radio Interferometry: The Mark III System for Geodesy, Astrometry, and Aperture Synthesis. *Science*, 219(4580), 51–54. ISSN: 0036-8075. DOI: 10.1126/science.219.4580.51.

Rothacher, M. (2002). Estimation of Station Heights with GPS. *Vertical Reference Systems*. Edited by H. Drewes, A. H. Dodson, L. P. S. Fortes, L. Sánchez, and P. Sandoval. Berlin, Heidelberg: Springer Berlin Heidelberg, 81–90. ISBN: 978-3-662-04683-8.

Rothacher, M., D. Angermann, T. Artz, W. Bosch, H. Drewes, M. Gerstl, R. Kelm, D. König, R. König, B. Meisel, H. Müller, A. Nothnagel, N. Panafidina,

B. Richter, S. Rudenko, W. Schwegmann, M. Seitz, P. Steigenberger, S. Tesmer, V. Tesmer, and D. Thaller (2011). GGOS-D: homogeneous reprocessing and rigorous combination of space geodetic observations. *Journal of Geodesy*, 85(10), 679–705. ISSN: 1432-1394. DOI: 10.1007/s00190-011-0475-x.

Sagdeyev, R. Z., V. v. Kerzhanovitch, L. R. Kogan, V. I. Kostenko, V. M. Linkin, L. I. Matveyenko, R. R. Nazirov, S. V. Pogrebenko, I. A. Struckov, R. A. Preston, J. Purcel, C. E. Hildebrand, V. A. Grishmanovskiy, A. N. Kozlov, E. P. Molotov, J. E. Blamont, L. Boloh, G. Laurans, P. Kaufmann, J. Galt, F. Biraud, A. Boischot, A. Ortega-Molina, C. Rosolen, G. Petit, P. Mezger, S. R., B. O. Rönnäng, R. E. Spencer, G. Nicolson, A. E. E. Rogers, M. H. Cohen, R. M. Martirosyan, L. G. Moiseyev, and J. S. Jatskiv (1992). Differential VLBI Measurements of the Venus Atmosphere Dynamics by Balloons - VEGA Project. *A&A*, 254, 387–392.

Salminen, T. (2015). Flexible and transparent buffering of radio astronomy measurements: VLBI-streamer and Flexbuff. Master's thesis. Aalto University.

Sarti, P., C. Abbondanza, L. Petrov, and M. Negusini (2011). Height bias and scale effect induced by antenna gravitational deformations in geodetic VLBI data analysis. *Journal of Geodesy*, 85(1), 1–8. ISSN: 1432-1394. DOI: 10.1007/s00190-010-0410-6.

Schaer, S., G. Beutler, M. Rothacher, and T. A. Springer (1996). Daily global ionosphere maps based on GPS carrier phase data routinely produced by the CODE. *Proceedings of the IGS Analysis Center Workshop*. (Silver Spring, Maryland, United States of America). Edited by R. E. Neilan, P. A. Van Scoy, and J. F. Zumberge. International GNSS Service.

Schartner, M. and J. Böhm (2019). VieSched++: A New VLBI Scheduling Software for Geodesy and Astrometry. *Publications of the Astronomical Society of the Pacific*, 131(1002), 084501.

Scherneck, H.-G. (2016). Loading Effects. *Encyclopedia of Geodesy*. Edited by E. Grafarend. Cham: Springer International Publishing, 1–12. ISBN: 978-3-319-02370-0. DOI: 10.1007/978-3-319-02370-0_52-1.

Schmid, R., M. Gerstl, M. Seitz, and D. Angermann (2015). DGFI Analysis Center Annual Report 2014. *International VLBI Service for Geodesy and Astrometry 2014 Annual Report*. Edited by K. D. Baver, D. Behrend, and K. L. Armstrong. NASA/TP–2015–217532. International VLBI Service for Geodesy and Astrometry, 210–212.

Schwab, F. R. and W. D. Cotton (1983). Global fringe search techniques for VLBI. *The Astronomical Journal*, 88(5), 688.

Seitz, M. (2015). Comparison of Different Combination Strategies Applied for the Computation of Terrestrial Reference Frames and Geodetic Parameter Series. *The 1st International Workshop on the Quality of Geodetic Observation and Monitoring Systems (QuGOMS'11)*. Edited by H. Kutterer, F. Seitz, H. Alkhatib,

and M. Schmidt. Cham: Springer International Publishing, 57–64. ISBN: 978-3-319-10828-5.

Seitz, M., D. Angermann, M. Bloßfeld, H. Drewes, and M. Gerstl (2012). The 2008 DGFI realization of the ITRS: DTRF2008. *Journal of Geodesy*, 86(12), 1097–1123. ISSN: 1432-1394. DOI: 10.1007/s00190-012-0567-2.

Sekido, M., K. Takefuji, H. Ujihara, T. Kondo, M. Tsutsumi, Y. Miyauchi, E. Kawai, H. Takiguchi, S. Hasegawa, R. Ichikawa, Y. Koyama, Y. Hanado, K. Watabe, T. Suzuyama, J. Komuro, K. Terada, K. Namba, R. Takahashi, Y. Okamoto, T. Aoki, and T. Ikeda (2016). An Overview of the Japanese GALA-V Wideband VLBI System. *IVS 2016 General Meeting Proceedings*. (Johannesburg, South Africa). Edited by D. Behrend, K. D. Baver, and K. L. Armstrong. International VLBI Service for Geodesy and Astrometry, 1–9.

Sekido, M. and T. Fukushima (2006). A VLBI Delay Model for Radio Sources at a Finite Distance. *Journal of Geodesy*, 80(3), 137–149. DOI: 10.1007/s00190-006-0035-y.

Sekido, M., T. Kondo, E. Kawai, and M. Imae (2003). Evaluation of GPS-based ionospheric TEC map by comparing with VLBI data. *Radio Science*, 38(4). ISSN: 1944-799X. DOI: 10.1029/2000RS002620.

Seybold, J. S. (2005). Introduction to RF Propagation. John Wiley & Sons, Inc. ISBN: 9780471743699. DOI: 10.1002/0471743690.

Shaffer, D. B. (2000). RFI: Effects on Bandwidth Synthesis. *IVS 2000 General Meeting Proceedings*. (Kötzting, Germany). Edited by N. R. Vandenberg and K. D. Baver. NASA/CP-2000-209893. International VLBI Service for Geodesy and Astrometry, 402–406.

Soja, B., T. Nilsson, M. Karbon, F. Zus, G. Dick, Z. Deng, J. Wickert, R. Heinkelmann, and H. Schuh (2015). Tropospheric delay determination by Kalman filtering VLBI data. *Earth, Planets and Space*, 67(144). DOI: 10.1186/s40623-015-0293-0.

Sośnica, K., G. Bury, R. Zajdel, D. Strugarek, M. Drożdżewski, and K. Kaźmierski (2019). Estimating global geodetic parameters using SLR observations to Galileo, GLONASS, BeiDou, GPS, and QZSS. *Earth, Planets and Space*, 71(1), 20. ISSN: 1880-5981. DOI: 10.1186/s40623-019-1000-3.

Sośnica, K., A. Jäggi, D. Thaller, G. Beutler, and R. Dach (2014). Contribution of Starlette, Stella, and AJISAI to the SLR-derived global reference frame. *Journal of Geodesy*, 88(8), 789–804. ISSN: 1432-1394. DOI: 10.1007/s00190-014-0722-z.

Sovers, O. J., P. Charlot, A. Fey, and D. Gordon (2002). Structure Corrections in Modeling VLBI Delays for RDV Data. *IVS 2002 General Meeting Proceedings*. (Tsukuba, Japan). Edited by N. Vandenberg and K. D. Baver. International VLBI Service for Geodesy and Astrometry, 243–247.

Sovers, O. J., J. L. Fanselow, and C. S. Jacobs (1998). Astrometry and geodesy with radio interferometry: experiments, models, results. *Reviews of Modern Physics*, 70(4), 1393–1454. DOI: 10.1103/RevModPhys.70.1393.

Springer, T. A., G. Beutler, and M. Rothacher (1999). A New Solar Radiation Pressure Model for GPS Satellites. *GPS Solutions*, 2(3), 50–62. ISSN: 1080-5370. DOI: 10.1007/PL00012757.

Steigenberger, P., S. Thoelert, and O. Montenbruck (2018). GNSS satellite transmit power and its impact on orbit determination. *Journal of Geodesy*, 92(6), 609–624. ISSN: 1432-1394. DOI: 10.1007/s00190-017-1082-2.

Takahashi, F., T. Kondo, Y. Takahashi, and Y. Koyama (2000). Very Long Baseline Interferometer. Wave summit course. Ohmsha, Ltd.

Takefuji, K., T. Kondo, M. Sekido, T. Kumazawa, K. Harada, T. Nakayama, S. Kurihara, K. Kokado, R. Kawabata, and R. Ichikawa (2012). High-order Sampling Techniques of Aliased Signals for Very Long Baseline Interferometry. *Publications of the Astronomical Society of the Pacific*, 124(920), 1105–1112. DOI: 10.1086/668232.

Tang, G., J. Sun, X. Li, S. Liu, G. Chen, T. Ren, and G. Wang (2016). APOD Mission Status and Observations by VLBI. *IVS 2016 General Meeting Proceedings*. (Johannesburg, South Africa). Edited by D. Behrend, K. D. Baver, and K. L. Armstrong. International VLBI Service for Geodesy and Astrometry, 363–367.

Tesmer, V. and H. Kutterer (2004). An Advanced Stochastic Model for VLBI Observations and its Application to VLBI Data Analysis. *IVS 2004 General Meeting Proceedings*. Edited by N. Vandenberg and K. D. Baver. NASA/CP-2004-212255. International VLBI Service for Geodesy and Astrometry, 296–300.

Tesmer, V., P. Steigenberger, M. Rothacher, J. Böhm, and B. Meisel (2009). Annual deformation signals from homogeneously reprocessed VLBI and GPS height time series. *Journal of Geodesy*, 83(10), 973–988. ISSN: 1432-1394. DOI: 10.1007/s00190-009-0316-3.

Teunissen, P. J. K. and O. Montenbruck, editors (2017). Springer Handbook of Global Navigation Satellite Systems. Springer International Publishing AG. ISBN: 978-3-319-42928-1. DOI: 10.1007/978-3-319-42928-1.

Thaller, D., R. Dach, M. Seitz, G. Beutler, M. Mareyen, and B. Richter (2011). Combination of GNSS and SLR observations using satellite co-locations. *Journal of Geodesy*, 85(5), 257–272. ISSN: 1432-1394. DOI: 10.1007/s00190-010-0433-z.

Thaller, D., M. Krügel, M. Rothacher, V. Tesmer, R. Schmid, and D. Angermann (2007). Combined Earth orientation parameters based on homogeneous and

continuous VLBI and GPS data. *Journal of Geodesy*, 81(6), 529–541. ISSN: 1432-1394. DOI: 10.1007/s00190-006-0115-z.

Thaller, D., K. Sośnica, R. Dach, A. Jäggi, G. Beutler, M. Mareyen, and B. Richter (2014). Geocenter Coordinates from GNSS and Combined GNSS-SLR Solutions Using Satellite Co-locations. *Earth on the Edge: Science for a Sustainable Planet*. Edited by C. Rizos and P. Willis. Berlin, Heidelberg: Springer Berlin Heidelberg, 129–134.

Thompson, A. R., J. M. Moran, and G. W. Swenson (2017). Interferometry and Synthesis in Radio Astronomy. Cham: Springer International Publishing. ISBN: 978-3-319-44431-4. DOI: 10.1007/978-3-319-44431-4.

Tingay, S. J., W. Alef, D. Graham, and A. T. Deller (2009). Geodetic VLBI correlation in software. *Journal of Geodesy*, 83(11), 1061–1069. DOI: 10.1007/s00190-009-0324-3.

Titov, O., V. Tesmer, and J. Böhm (2004). OCCAM v.6.0 Software for VLBI Data Analysis. *IVS 2004 General Meeting Proceedings*. Edited by N. Vandenberg and K. D. Baver. NASA/CP-2004-212255. International VLBI Service for Geodesy and Astrometry, 267–271.

Tornatore, V., R. Haas, S. Casey, D. Duev, S. V. Pogrebenko, and G. M. Calvés (2014). Direct VLBI Observations of Global Navigation Satellite System Signals. Edited by C. Rizos and P. Willis. Berlin, Heidelberg: Springer Berlin Heidelberg, 247–252. ISBN: 978-3-642-37222-3. DOI: 10.1007/978-3-642-37222-3_32.

Tregoning, P. and T. van Dam (2005). Effects of atmospheric pressure loading and seven-parameter transformations on estimates of geocenter motion and station heights from space geodetic observations. *Journal of Geophysical Research: Solid Earth*, 110(B3). DOI: 10.1029/2004JB003334.

Tuccari, G., W. Alef, A. Bertarini, S. Buttaccio, G. Comoretto, D. Graham, A. Neidhardt, P. R. Platania, A. Russo, A. Rov, M. Wunderlich, R. Zeitlhöfler, and Y. Xaing (2010). DBBC2 Backend: Status and Development Plan. *IVS 2010 General Meeting Proceedings*. Edited by D. Behrend and K. D. Baver. International VLBI Service for Geodesy and Astrometry, 392–395.

Tuccari, G., W. Alef, S. Buttaccio, S. Casey, A. Felke, M. Lindqvist, and M. Wunderlich (Aug. 2014). DBBC3: An EVN and VGOS All-inclusive VLBI System. *IVS 2014 General Meeting Proceedings*. Edited by D. Behrend, K. D. Baver, and K. L. Armstrong. International VLBI Service for Geodesy and Astrometry, 86–90.

Tuccari, G., W. Alef, S. Dornbusch, R. Haas, K.-Å. Johansson, H. Rottmann, A. Roy, and M. Wunderlich (2018). New Observing Modes for the DBBC3. *IVS 2018 General Meeting Proceedings*. (Longyearbyen, Norway). Edited by K. L. Armstrong, K. D. Baver, and D. Behrend. NASA/CP–2019-219039. International VLBI Service for Geodesy and Astrometry, 47–49.

Urschl, C., W. Gurtner, W. Hugentobler, S. Schaer, and G. Beutler (2005). Validation of GNSS orbits using SLR observations. *Advances in Space Research*, 36(3). Satellite Dynamics in the Era of Interdisciplinary Space Geodesy, 412–417. ISSN: 0273-1177. DOI: 10.1016/j.asr.2005.03.021.

Vennebusch, M., A. Nothnagel, and H. Kutterer (2009). Singular value decomposition and cluster analysis as regression diagnostics tools for geodetic applications. *Journal of Geodesy*, 83, 877–891. DOI: 10.1007/s00190-009-0306-5.

Visser, P. (1999). Gravity field determination with GOCE and GRACE. *Advances in Space Research*, 23(4), 771–776. ISSN: 0273-1177. DOI: 10.1016/S0273-1177(99)00154-4.

Watkins, M. M. and R. J. Eanes (1997). Observations of tidally coherent diurnal and semidiurnal variations in the geocenter. *Geophysical Research Letters*, 24(17), 2231–2234. DOI: 10.1029/97GL52059.

Whitney, A. (2000). How Do VLBI Correlators Work ? *IVS 2000 General Meeting Proceedings*. (Kötzting, Germany). Edited by N. R. Vandenberg and K. D. Baver. NASA/CP-2000-209893. International VLBI Service for Geodesy and Astrometry, 187–205.

Whitney, A. (2004). The Mark 5B VLBI Data System. *IVS 2004 General Meeting Proceedings*. Edited by N. Vandenberg and K. D. Baver. International VLBI Service for Geodesy and Astrometry, 177–181.

Whitney, A., R. Cappallo, W. Aldrich, B. Anderson, A. Bos, J. Casse, J. Goodman, S. Parsley, S. Pogrebenko, R. Schilizzi, and D. Smythe (2004). Mark 4 VLBI correlator: Architecture and algorithms. *Radio Science*, 39(1). DOI: 10.1029/2002RS002820.

Whitney, A., R. J. Cappallo, C. A. Ruszczyk, J. SooHoo, and G. B. Crew (2014). Mark 6 16-Gbps Next-Generation VLBI Data System. *IVS 2014 General Meeting Proceedings*. Edited by D. Behrend, K. D. Baver, and K. L. Armstrong. International VLBI Service for Geodesy and Astrometry, 86–90.

Whitney, A., M. Kettenis, C. Phillips, and M. Sekido (2010). VLBI Data Interchange Format (VDIF). *IVS 2010 General Meeting Proceedings*. (Hobart, Australia). Edited by D. Behrend and K. D. Baver. International VLBI Service for Geodesy and Astrometry, 65–69.

Whitney, A., C. Lonsdale, E. Himwich, N. Vandenberg, H. van Langevelde, A. Mujunen, and C. Walker (2002). VEX File Definition/Example. Technical report 1.5b1. URL: www.vlbi.org/vex/docs/vex%5C%20definition%5C%2015b1.pdf.

Whitney, A., A. E. E. Rogers, H. F. Hinteregger, C. A. Knight, J. I. Levine, S. Lippincott, T. A. Clark, I. I. Shapiro, and D. S. Robertson (1976). A very-long-baseline interferometer system for geodetic applications. *Radio Science*, 11(5), 421–432. DOI: 10.1029/RS011i005p00421.

Williams, J. G., S. G. Turyshev, D. H. Boggs, and J. T. Ratcliff (2006). Lunar laser ranging science: Gravitational physics and lunar interior and geodesy. *Advances in Space Research*, 37(1), 67–71. DOI: 10.1016/j.asr.2005.05.013.

Williams, S. D. P. and N. T. Penna (2011). Non-tidal ocean loading effects on geodetic GPS heights. *Geophysical Research Letters*, 38(9). DOI: 10.1029/2011GL046940.

Witasse, O., J.-P. Lebreton, M. K. Bird, R. Dutta-Roy, W. M. Folkner, R. A. Preston, S. W. Asmar, L. I. Gurvits, S. V. Pogrebenko, I. M. Avruch, R. M. Campbell, H. E. Bignall, M. A. Garrett, H. J. van Langevelde, S. M. Parsley, C. Reynolds, A. Szomoru, J. E. Reynolds, C. J. Phillips, R. J. Sault, A. K. Tzioumis, F. Ghigo, G. Langston, W. Brisken, J. D. Romney, A. Mujunen, J. Ritakari, S. J. Tingay, R. G. Dodson, C. G. M. van't Klooster, T. Blancquaert, A. Coustenis, E. Gendron, B. Sicardy, M. Hirtzig, D. Luz, A. Negrao, T. Kostiuk, T. A. Livengood, M. Hartung, I. de Pater, M. Ádámkovics, R. D. Lorenz, H. Roe, E. Schaller, M. Brown, A. H. Bouchez, C. A. Trujillo, B. J. Buratti, L. Caillault, T. Magin, A. Bourdon, and C. Laux (2006). Overview of the coordinated ground-based observations of Titan during the Huygens mission. *Journal of Geophysical Research: Planets*, 111(E7). DOI: 10.1029/2005JE002640.

Wu, X., J. Ray, and T. van Dam (2012). Geocenter motion and its geodetic and geophysical implications. *Journal of Geodynamics*, 58, 44–61. ISSN: 0264-3707. DOI: 10.1016/j.jog.2012.01.007.

Xu, M. H., R. Heinkelmann, J. M. Anderson, J. Mora-Diaz, M. Karbon, H. Schuh, and G. L. Wang (2017). The impacts of source structure on geodetic parameters demonstrated by the radio source 3C371. *Journal of Geodesy*, 91(7), 767–781. ISSN: 1432-1394. DOI: 10.1007/s00190-016-0990-x.

Zheng, W., Y. Huang, Z. Chen, G. W. Wang, Q. Liu, F. Tong, and P. Li (2014). Realtime and High-Accuracy VLBI in the CE-3 Mission. *IVS 2014 General Meeting Proceedings*. (Beijing, China). Edited by D. Behrend, K. D. Baver, and K. L. Armstrong. Science Press, 466–472. ISBN: 978-7-03-042974-2.

Zhou, H., H. Li, and G. Dong (2015). Relative position determination between Chang'E-3 lander and rover using in-beam phase referencing. *Science China Information Sciences*, 58(9), 1–10. DOI: 10.1007/s11432-015-5363-1.

Zhu, R., Y. Wu, and J. Li (2016). Progress on the VLBI Data Acquisition System of SHAO. *IVS 2016 General Meeting Proceedings*. (Johannesburg, South Africa). Edited by D. Behrend, K. D. Baver, and K. L. Armstrong. International VLBI Service for Geodesy and Astrometry, 163–165.